Title
Lung Surveillance Revealed by Two-Photon Live Imaging

Author
Thornton, Emily Elizabeth

Publication Date
2012

Lung Surveillance Revealed by Two-Photon Live Imaging

by

Emily E Thornton

DISSERTATION

Submitted in partial satisfaction of the requirements for the degree of

DOCTOR OF PHILOSOPHY

in

Biomedical Sciences

in the

GRADUATE DIVISION

of the

UNIVERSITY OF CALIFORNIA, SAN FRANCISCO

[redacted]

Acknowledgements

First I would like to thank my mentor, **Max Krummel** for his years of guidance and teaching. The relationship between graduate student and PI can be a tricky one, but I have always felt that Max had my back and genuinely wanted me to succeed. His optimism and excitement about science is unmatched by any other scientist I have met. It is easier to get up and go to lab in the morning when you know someone else will be excited about and appreciate your work. I have learned how to think like a scientist while in Max's lab, and my future career in science will forever be influenced by my time working with Max.

With Max as my final science teacher, I need to thank a few that helped me along the way. I have always liked science, but it was **Mrs. Bunting's** 4th grade class (the year after she visited Costa Rica) that showed me how exciting, diverse, and endlessly interesting biology can be. **Mr. Boyle**, my 7th grade science teacher, went a step further by making science a cool class. He offered a reprieve from the middle school students' scorn for learning. The final, and most influential on my decision to go to grad school and pursue a career in science, was **Professor Kevin Kinney** at DePauw University. Professor Kinney taught me general biology, physiology, and immunology. He managed to squeeze more material into my brain than any other professor, and I enjoyed every minute of it. I hope to some day become an educator of his caliber.

I owe all of the immunology faculty at UCSF a huge debt of gratitude. Faculty participation in journal club and the graduate program is remarkable and made me feel like a participant in the scientific community from day one. In particular, I need to thank **Dean Sheppard** and **Rich Locksley** for their participation on my thesis committee. Our

meetings were always a fun, friendly endeavor that resulted in different ways to think about immunity and more experiments to do. I would also like to thank **Mark Looney**, my co-author and partner on the *Nature Methods* paper. Mark showed me the value of perseverance, having clear goals, and teamwork in science.

The Krummel lab has been like a big family to me. I owe my success to all of the members of the Krummel lab, but there are a few I need to thank individually. Max is the head of the household. When I was brought into the family, I already had several older siblings that had plenty to teach me. I got to watch **Rachel Friedman** transition from a grad student to a post-doc and then to a PI. She taught me almost everything I know about imaging and demonstrated how to be a successful woman in science. **Jordan Jacobelli** showed me that hard work and long hours can really pay off. **John Engelhardt** is very even keeled about science and the lab. He is capable of putting setbacks in perspective, and that may be one of the most important lessons of grad school. **Julia Gilden** introduced me to the best things the Bay Area has to offer, especially in the cheese department, and demonstrated that a life separate from lab can be healthy. **Pete Beemiller** is a great teacher and scientist, and I have benefited from all of his skills by working near him. **Audrey Gerard** has managed to keep reasonable hours while being a great mom and scientist, which seems nearly impossible if you haven't seen her in action. **Debasish Sen** and **Oishee Bose** have been particularly helpful to me, especially when experiments get overwhelming. **Mark Headley** came into the lab as a bona fide lung expert and showed me how little time I actually spend in the lab. **Efrat Lelkes** showered me with love and affection, filled me with physical fitness, and made me respect clinician-scientists. Finally, **Caitlin Sorensen** played a pivotal role in my

time at UCSF. She was my Krummel lab partner in crime (and crosswords) from the start. Any time lab got too stressful we could always go outside to watch cars park.

I would like to thank the BMS staff from the bottom of my heart, especially **Lisa Magargal** and **Monique Piazza**. Without their help, this thesis would have been delayed by several of my paperwork mistakes. Besides helping with the actual work of completing a PhD, they are a source of comfort to every stressed out grad student. If I had a dollar for every time I said, "Lisa can help," I wouldn't need a job after grad school.

I am confident that my BMS class is the best group of graduate students that anyone could hope to study with. There was never a sense of competition between us, and I'm sure we will all be great colleagues if not good friends in the future. **Jan Lui** is the smartest guy and best hugger on campus. The girls' book club, **Kristen Coakley, Emily Elliot, Renee Vander Laan, Sarah Gierke, Alison Coady, Lauren Herl Martens, Kegan Warner Donlan, Linda Lee**, **Kate Stewart**, and (honorary classmate) **Kelly Kruze**, have been the best support system a girl could hope for. It was fun sharing hardships, celebrations, and wine, but it will be even more fun to see what becomes of us all. What a wonderful group of talented, strong women. I am so proud to know you all.

The second year of grad school I moved in with **Alison Coady** and **Emily Elliott** so we could get cats. Living with the two of them was probably the best decision I made in grad school. The kitties were a comfort, but nothing could compare to the joy of having roommates who understood exactly what I was going through. We got a little crazy during quals time, but we made it through together. When Ali moved out, **Stephanie Redmond** joined the apartment. I couldn't have hoped for a kinder, happier

roommate. As we grow up and move away, I will always miss the way things were.

My family was only a phone call away, and when things were at their toughest, they were the ones I turned to. My mom, **Kathy Rybak,** and dad, **Tom Thornton**, have always made me feel completely loved and supported. Their love of learning and knowledge has guided me down this path. I owe my mom for every trip to the zoo and my dad for every science article he has clipped for me over the years. They learned to ask how papers were going and then learned to ask more infrequently. My siblings **Elliot**, **Lydia**, and **Anna** have always been so much cooler and more creative than me. I haven't visited as much as I should have, but that doesn't mean I haven't missed them all the time that I'm away.

Finally, and most importantly, I would like to thank my partner, and now husband, Andy Lauder. I would not have made it through graduate school without the unwavering support he has provided. Andy has shown me how one person can embody knowledge and creativity in the same instance. I should take better care of you.

Contribution of co-authors

Chapters I and IV of this dissertation were written by me.

The text of Chapter II is a reprint of the material as it appears in Nature Methods as Stabilized Imaging of Immune Surveillance in the Mouse Lung. I conceived and designed the experiments, validated and implemented the technique, collected and analyzed data and wrote the manuscript. Mark Looney conceived and designed the experiment, validated and implemented the technique, collected and analyzed data and wrote the manuscript. Debasish Sen implemented the technique and collected and analyzed data. Wayne Lamm and Robb Glenny conceived and designed the experiment and edited the manuscript. Matthew Krummel conceived and designed the experiment, provided administrative and financial support and wrote the manuscript.

Chapter III is based on a manuscript submitted for publication. I designed and performed the experiments, collected and analyzed data, and wrote the manuscript. Mark Looney, Oishee Bose, and Debasish Sen performed experiments and collected data. Dean Sheppard and Rich Locksley participated in conception of experiments and edited the manuscript. Xiaozhu Huang performed experiments. Matthew Krummel designed and performed experiments, provided administrative and financial support, and wrote the manuscript.

Abstract

The lung is a complex mucosal organ with the responsibility of oxygenating blood for the entire body. The large surface area of the lung allows for efficient exchange of oxygen in a large blood volume but also causes vast numbers of immune cells to constantly circulate through the organ. The high tidal volumes of air inhaled results in the introduction of particles, pathogens, and allergens into this delicate system. Because of the intimate relationship between the immune cells and the lung, a delicate balance must be maintained in order to sustain life. The goal of this thesis was to develop techniques to study interactions between the environment and the immune system with a particular focus is on the mechanisms and sites of uptake and presentation of antigens in the unchallenged lung and in a mouse model of asthma.

Real-time imaging of cellular and subcellular dynamics in vascularized organs requires image resolution and image registration to be simultaneously optimized without perturbing normal physiology. This problem is particularly pronounced in the lung. Here we report video-rate, two-photon imaging of a physiologically intact preparation of the mouse lung that is stabilizing and nondisruptive.

Asthma pathogenesis is focused around conducting airways. The reasons for this focus have been unclear since it was impossible to track the sites and timing of uptake or subsequent antigen presentation to T cell effectors. Two-photon microscopy of the lung parenchyma revealed early uptake of model antigens in alveoli giving rise to the asthma-specific CD11b+ DC and antigen retention in the airway region. A hyper-reactive lung thus results from selective retention of allergen-presenting cells in airway-adjacent interaction zones, not variation in the abilities of individual cells to survey the lung.

This study elucidates the pathway of antigen from inhalation to presentation to antigen-specific T cells. These techniques can be used to study other lung diseases and can be applied to other peripheral organs. Further study and development of ways to inhibit the different steps along this pathway may lead to therapies that could be used to treat many immune related diseases.

Table of Contents

List of Figures

Chapter II:

Chapter III:

Chapter 1: Introduction

Global Impact of Asthma

Atopic asthma is a chronic disease associated with airway hyperresponsiveness, mucus overproduction, increased IgE, and eosinophilia. Asthma currently affects over 300 million people worldwide (Masoli et al., 2004). In 2011 the medical costs for treatment of adults with asthma in the US reached $18 billion(Sullivan et al., 2011b). Despite ever increasing expenditures, asthma is estimated to be the cause of 1 out of every 250 deaths worldwide(Masoli et al., 2004). In addition to direct medical costs and loss of life, asthma exerts a strong cost on society by causing loss of work and school for the families of those afflicted(Masoli et al., 2004).

Current treatments include inhaled corticosteroids and beta-agonists, which can keep most cases of asthma under control. These treatments act on the airway smooth muscle to prevent hyper responsiveness and decrease local inflammation(Jackson et al., 2011); however, some drug combinations can be associated with severe asthma attacks. Within the pool of individuals that suffer from asthma there is also a small population who suffer from refractory asthma, which is not treatable by any currently available medications(Proceedings of the ATS workshop on refractory asthma: current understanding, recommendations, and unanswered questions. American Thoracic Society., 2000). In order to provide new treatments for these individuals and improve long term care for this chronic disease, it is necessary to understand the underlying immune dysfunction that leads to pathogenesis.

Recent studies have examined the heterogeneity of disease in asthma patients with the goal of segmenting the population for specialized treatment. The previous understanding and data from mouse models supported the hypothesis that asthma is stereotypically a Th2 driven disease. When patients with mild to moderate asthma were studied, only half of the patients exhibited Th2 gene signature expression(Woodruff et al., 2009). Recent work has shown that many of the most severe cases of asthma are associated with a Th17 signature(Al-Ramli et al., 2009). New biologics that target members of the Th2 pathway may only be helpful for up to half of patients suffering from asthma. More importantly, even in the Th2 disease, the cellular surveillance mechanisms that lead antigens to be presented to T cells are not well characterized. By studying the cellular events that contribute to initiation and persistence of this chronic disease we may be able to provide treatments that affect multiple subsets of the patient pool.

Mouse models of Asthma

In order to study the pathogenesis of asthma, researchers have developed several mouse models of the disease. Because different models mimic specific portions of the disease, it is important to choose the model that best represents the pathway of interest. The oldest and most commonly used model is the acute model that relies on OVA as the antigen and alum as an adjuvant. This model is useful for the study of Th2 immunity in the context of the lung(Corry et al., 1998). The OVA/alum model mimics all of the hallmarks of asthma, and the availability of TCR transgenics allows for the study of antigen specific responses. Despite advantages of this short-term model, OVA/alum does

not cause human allergy, and it cannot be used to study airway remodeling, which occurs over time in people with asthma(Boyce and Austen, 2005).

Another acute model, which has the advantage of using a common human allergen, is the house dust mite (HDM) model. Asthma caused by repeated inhalations of HDM may more faithfully mimic human disease because house dust mite can in fact cause disease in humans. The complexity of the organism leads to activation through many distinct pathways. This may complicate the study of individual components of the disease. The development of a TCR transgenic against Derp1 does provide a more tractable model for studying allergen specific T cells during the response to an intact allergen(Jarman et al., 2005). Despite these advantages, acute models of asthma resolve over time and therefore cannot accurately mimic what is a chronic disease in man.

Some of the weaknesses of acute models are solved by chronic challenge models. In many of these systems, mice are sensitized with antigen and adjuvant and then challenged over the course of many weeks to simulate human disease. Use of complex allergens such as HDM abrogate the need for sensitization with adjuvant(Nials and Uddin, 2008). The use of a single mouse strain with a single allergen, despite the advantages of each system, cannot capture the complexity of human disease and therefore should be studied in the context of a wider research program.

Sentinel cells in the lung

The lung contains several types of immune sentinel cells that patrol the tissue to fight infection and maintain organ homeostasis. Innate cells such as neutrophils, macrophages, dendritic cells, mast cells, basophils, and eosinophils react immediately

when triggered and can cause acute respiratory symptoms. While these sentinel populations are associated with different types of immune responses, they are all present in the lungs of asthmatics. Dendritic cells play a critical role in the connection of the innate and adaptive immune response. We hypothesize that understanding how sentinel cells interpret signals from their environment and interact with each other can shed light on the roles these cells play in disease.

Innate sentinel cells

At any given time, the lungs contain about 9% of the body's blood. In a healthy adult, there are $2.5–7.5 \times 10^9$ neutrophils per liter of blood in 5 liters of circulation(Cowburn et al., 2008) indicating 2.25×10^9 neutrophils present in the lungs. These cells must circulate through the lungs prepared to respond to pathogens but without causing damage. In some cases, such as acute lung injury (ALI), neutrophils play a critical role in the disease(Looney et al., 2006); however, their role in asthma is somewhat unclear(Bhakta and Woodruff, 2011). Neutrophils have been associated with the late phase response in some asthma patients(Al-Ramli et al., 2009), but this disease phenotype has not been born out by most mouse models of the disease. In order to understand the role of these potent inflammatory cells in asthma, new mouse models that reflect the non-Th2 subset of asthma patients must be developed.

Eosinophils are recruited to the lungs of asthmatics and are measured as a major read-out of the disease. The binding of allergen specific IgE to their FceRI makes them potent sensors of allergen. Once triggered, they release large quantities of IL-4 and IL-13(Voehringer et al., 2006). Despite their presence in large numbers in both mice and

patients with asthma, their direct role in disease is unclear. Mast cells also express the high affinity Fce receptor. When triggered, mast cells release histamine, cytokines, proteases, and other immune mediators leading to direct effects on airway smooth muscle and the surrounding immune cells(Amin, 2012). Basophils have been proposed to play a role in the innate and adaptive sides of Th2 immunity. The recent development of tools to study these enigmatic cells have given mixed results. Despite several papers to the contrary(Perrigoue et al., 2009; Sokol et al., 2009; Yoshimoto et al., 2009), basophils do not appear to act as antigen presenting cells for T cells(Sullivan et al., 2011a; Hammad et al., 2010), but they do play an important role in immunity against helminths(Voehringer, 2011)

Alveolar macrophages play an important role in the uptake and destruction of inhaled pathogens and particles that reach the alveoli. Positioned in the air space of the alveolus and making up 95% of cells in normal bronchoalveolar lavage fluid (BAL), they play a crucial role in homeostasis of the organ. When AMs are depleted from the lung, mice suffer increased susceptibility to infection(Broug-Holub et al., 1997), but their role in asthma has been debated. Depletion of AMs with chlodronate loaded liposomes leads to increased asthma associated cytokine production and immune cell recruitment(Bang et al., 2011). However, alternative activation associated with Th2 responses may lead to exacerbation of the ongoing immune response in the lung(Gordon, 2003). Despite their important role in clearing inhaled material from the lung, AMs have been shown to be poor stimulators of adaptive immune responses and therefore likely function in regulation rather than propagation of the immune response associated with asthma(Belz et al., 2004).

Dendritic Cells: Linking innate and adaptive immunity

Dendritic cells are present in much lower numbers than AMs in the lung, but they are believed to be the predominant antigen presenting cells. As in other mucosal tissues, the lung contains CD11b+ and CD103+ dendritic cell subsets, which play important roles in stimulating CD4 and CD8 T cells, respectively (Jakubzick et al., 2008a). The CD103+ DCs have been demonstrated to be important for protection from viral infection and in the clearance of apoptotic cells(Desch et al., 2011), but the division of labor in allergen uptake and presentation is unclear. Compared with the other sentinel cells of the lung, DCs have been shown to play a clear role in the pathogenesis of asthma. Depletion of DCs with CD11c-DTR results in loss of the hallmarks of asthma(van Rijt et al., 2005).

Adaptive immune responses in asthma

Adaptive immune responses in the lung begin with antigen uptake and traffic to the draining lymph node. Once antigen arrives in the lymph node, cognate T cells can be activated, skewed, proliferate, and then traffic back to the lung to carry out their effector functions. The adaptive phase of the immune response contributes to life-threatening lung inflammation that can last days after the initial exacerbation.

Antigen uptake and trafficking by DCs

Adaptive immune responses generally begin with DC activation and traffic to the draining lymph node. Understanding where uptake of allergen occurs is important because aerosolized particles of different sizes end up in different regions of the lung. If the goal is to develop a therapeutic agent to target this step in the immune response, the drug must be able to reach its target. For example, if uptake of allergens occurs deeper in the lung, particles of 1-5mm would be appropriate; however, if sampling occurs in the upper airways, particles 5-10mm in size may be more appropriate(Carvalho et al., 2011). According to current thinking, DCs present at the airway are responsible for sampling inhaled antigens through the airway epithelium(Lambrecht and Hammad, 2009).

Dendritic cells have been strongly implicated in the pathogenesis of asthma and are required for the development of the hallmarks of this disease. Studies in the trachea and nasal mucosa have shown DCs sampling the airway lumen, across the epithelial barrier(Takano et al., 2005; Hammad et al., 2009). Despite extensive studies of upper airways and traffic to the lymph node, it remains unclear whether antigen uptake occurs in the conducting airways and/or alveoli.

While DCs sample antigen from the environment, the surrounding milieu is important to give context to the antigen. DCs are very adept at sensing patterns from pathogens and tissue damage, but they can also be instructed by the surrounding tissue and other resident immune cells. Airway epithelium can produce many cytokines, including thymic stromal lymphopoietin (TSLP) and IL-25, which help to instruct the immune response. For example, TSLP can directly activate DCs(Soumelis et al., 2002). The other cells in the alveolus, mainly AMs, may also secrete cytokines to affect the activation status of DCs, especially during an ongoing infection.

Once antigen uptake has occurred, DCs must leave the alveolus in order to present their cargo to T cells. Previous studies have described steady state migration of DCs to the draining lymph node carrying tracers(Vermaelen et al., 2001), but a study using genetic marking of monocyte decendents has drawn the concept of large amounts of steady state migration into doubt(Jakubzick et al., 2008b). Despite the controversy over steady-state traffic, DCs have been shown to carry particulate or soluble antigen from the lung to the mediastinal lymph node after allergen challenge(Xia et al., 1995; Jakubzick et al., 2006). Activated DCs express CCR7 making them responsive to CCL19 and CCL21 from the lymph node(Randolph et al., 2008). The CD11b+ DC subset of DCs has been shown to be more capable of carrying soluble antigen and therefore stimulating CD4 T cells. In contrast, CD11b- DCs were more successful at carrying latex beads and subsequently stimulated CD8 T cells(Jakubzick et al., 2008a). Because asthma is thought to be a CD4 mediated disease, this data points to the importance of CD11b+ DCs.

T cell activation and trafficking

Once antigen reaches the lymph node, DCs can present it to antigen-specific naive T cells. As with DCs, T cells have been shown to be required for the hallmarks of disease in mouse models of asthma(Corry et al., 1998). When exposed to IL-4 during activation, T cells differentiate into Th2 helper T cells. During the initiation of the immune response it is not clear which cell type or cytokine drives differentiation toward the Th2 axis. Basophils were proposed as APC and IL-4 source for T cells that become Th2 cells(Perrigoue et al., 2009; Sokol et al., 2009; Yoshimoto et al., 2009), but these studies have largely been refuted(Sullivan et al., 2011a; Hammad et al., 2010). The

CD103+ DC subset was proposed to skew naïve cells toward Th2, but no mechanism for this action has been shown(Nakano et al., 2012).

Once activated, Th2 cells require chemokine receptor CCR4 to traffic to the lung(Mikhak et al., 2009). Th2 cells may be attracted by CD11b+ myeloid cells present in the tissue that produce CCL17 and CCL22, CCR4 ligands(Medoff et al., 2009). CD11b+ DCs have also been shown to accumulate in the lung after allergen challenge and produce and secrete chemokines more efficiently than the CD103+ subset (Beaty et al., 2007), possibly indicating their importance in this step in the response to allergen. Because many cell types in the inflamed tissue produce chemokines, redundant pathways may exist.

Effector Functions within the Tissue

After activation and traffic to the tissue, T cells can exert their effector functions. Th2 differentiated T cells produce many cytokines that feed back on the innate and adaptive immune cells associated with asthma. In the lymph node, T cells making IL-4 and IL-13 can instruct B cells to produce IgE, which in turn coats FcepsilonRI on mast cells and basophils(Barnes, 2008). IL-4 produced by Th2 cells can also help skew other naïve T cells as they are activated. IL-5 produced by Th2 cells enhances the differentiation and survival of eosinophils, increasing the number of these cells within the tissue. IL-13 can directly cause goblet cell hyperplasia and excess mucus production. Despite the obvious role of T cells in asthma, all of these cytokines can be produced by other cells within the tissue so the orchestrating role of Th2 cells remains somewhat

unclear. Observing which cells Th2 cells interact with in the tissue may hold the key to how this keystone cell type functions during disease.

T cell reactivation

After initial sensitization, asthma sufferers often come in contact with an allergen that triggers an asthma exacerbation. In these cases, innate immune cells are quickly activated, resulting in an early asthmatic response. The early response can begin within 10 minutes, peaks after 30 minutes, and resolves after about an hour. Once antigen is captured and processed for presentation, the adaptive immune response kicks in resulting in a late-phase asthmatic response. The late response begins after 4 hours, peaks around 8 hours, and resolves over the course of 24 hours to several days(Robertson et al., 1974). Current belief is that DCs must traffic to the lymph node in order to present antigen to T cells for reactivation(Medoff et al., 2008); however, the small amount of time between inhalation and activation draws this assumption into question.

Groups of immune cells have been described in experimental models of asthma(Huh et al., 2003); however, the nature of these cell clusters has not been carefully characterized. Cell groupings within the tissue may allow for fast reactivation of allergen specific T cells. Reactivation of T cells within the lung tissue has been inferred during viral infection(Chapman et al., 2011), but where activation occurs and where the activated T cells act in the tissue have not been addressed.

During chronic immune responses or after strong inflammatory stimuli, tertiary lymphoid organs can develop within tissues. In the lung, the tertiary lymphoid organ associated with the airways is known as bronchus associated lymphoid tissue (BALT).

BALT is the accumulation of T cells, B cells, and DCs into structures that resemble the lymph node. BALT formation occurs after viral infection and other forms of strong TLR signaling (Moyron-Quiroz et al., 2004; Halle et al., 2009; Rangel-Moreno et al., 2011); however, the cell types and signals required for BALT initiation are still in dispute (Rangel-Moreno et al., 2011; Fleige et al., 2011). DCs have been implicated in the maintenance of BALT in the lung after viral infection(Halle et al., 2009) and may therefore play a role in maintaining cell groupings in asthma. Patients with asthma have increased BALT compared to control patients(Elliot et al., 2004). The presence of BALT in asthmatic lungs may allow for a shorter delay between allergen inhalation and the activation of antigen specific T cells.

Understanding Immunity through Live Imaging

In order to understand how immune responses are elaborated *in vivo* it is important to understand which cells are present, what they are doing, and how they are interacting with each other. Techniques such as FACS and imaging of fixed tissues can give insight into the first two parameters, but some phenomena will only occur in their native environment. Two-photon imaging has been used to track the behavior of lymphocytes in lymph nodes for a decade(Cahalan and Parker, 2008). These studies have shed light on the series of interactions required for T and B cell activation; however, only recent studies have looked before and after T cell activation to visualize antigen uptake and effector functions in the tissue. Imaging of mucosal tissues is of particular interest because of the complex interactions that occur between immune cells and the

environment. Both gut and skin imaging have shown the importance of resident DCs for sampling the environment(Chieppa et al., 2006; Sen et al., 2010).

Asthma is an over activation of the immune system in response to harmless antigens. Somewhere after inhalation, an inappropriate signal is being transmitted from cell to cell. These uptake and interaction questions can only be addressed by live imaging. The lung provides a distinct challenge because the tissue must constantly be in motion for the health of the tissue. Because only one study has examined the behavior of immune cells in the lung(Kreisel et al., 2010), there are a large number of questions still to be answered regarding lung immunity. This study focuses on how antigen is handled within the tissue from uptake to presentation.

Chapter II: Stabilized Imaging of Immune Surveillance in the Mouse Lung

Abstract

Real-time imaging of cellular and subcellular dynamics in vascularized organs requires image resolution and image registration to be simultaneously optimized without perturbing normal physiology. This problem is particularly pronounced in the lung, in which cells may transit at speeds >1 mm s^{-1} and in which normal respiration results in large-scale tissue movements that prevent image registration. Here we report video-rate, two-photon imaging of a physiologically intact preparation of the mouse lung that is stabilizing and nondisruptive. Using our method, we obtained evidence for differential trapping of T cells and neutrophils in mouse pulmonary capillaries, and observed neutrophil mobilization and dynamic vascular leak in response to stretch and inflammatory models of lung injury in mice. The system permits physiological measurement of motility rates of >1 mm s^{-1}, observation of detailed cellular morphology and could be applied in the future to other organs and tissues while maintaining intact physiology.

Introduction

The lung is a unique organ with an air-liquid interface exposing it to the environment and to a large volume of blood that transits the organ each minute. The lung microcirculation is also distinctive with a rich network of capillary segments with diameters as small as a few micrometers, which requires many leukocytes to deform their shape to pass through(Wiggs et al., 1994). In fact, as compared to systemic vascular beds, the initial sequestration of neutrophils in the lung microcirculation is more dependent on mechanical forces than adhesion-mediated rolling along the endothelial surfaces(Burns et al., 2003). Any perturbation to the integrity of the lung's air-liquid interface can have devastating consequences, resulting in lung vascular leak and compromised gas exchange. Furthermore, the nature of the collaboration between immune cells and structural elements of the lung has been inaccessible for real-time analysis.

The uniqueness of the lung requires direct imaging, but this demands fast, high-resolution and penetrant imaging methodologies as well as demonstrable maintenance of intact physiology. The lung provides a particular challenge as it propagates motion resulting from cardiac contractions, pulsatile blood flow and overall movements during the inhalation-exhalation cycle(Wagner, 1969). Compared to the sub-micrometer resolution demanded by analysis of deformability, these movements are on the scale of millimeters when measured at the pleural face of the lung. Previous protocols for imaging in the lung have relied on methods such as isolation and reperfusion of the lung *ex vivo*(Kiefmann et al., 2008), clamping of ventilation(Hasegawa et al., 2010) or capturing images at the end of lung expiration (end-expiration) or after cessation of mechanical ventilation(Tabuchi et al., 2008). Although each of these approaches has been useful for

lung imaging, an improvement was needed to study high-speed, three-dimensional cellular dynamics under physiological gas exchange and blood flow.

We addressed these issues via an optimized, resonant-scanning, two-photon platform(Bullen et al., 2009). In our method we adopted point-scanning multiphoton imaging, which provides excellent depth penetration. The depth (*z* dimension) resolution across many air-liquid alveolar interfaces severely influences the coherence of light at the focus. Multiphoton excitation, with its inherent requirement for high-photon densities, is resistant to image degradation, compared to single-photon approaches. Resonant scanning permits acquisition at or exceeding video rate(Nguyen et al., 2001), thus providing high temporal resolution over large cross-sectional areas. Finally, and most importantly, we optimized a gentle stabilization system, which limits tissue motion, even while permitting intact blood flow at predicted rates and providing continuous access to inhaled gases. We used this system to describe immune cell circulation and cellular movement under steady-state physiology and in lung inflammation and injury models. Our results suggest surveillance of the alveolar-capillary interface from the bloodstream.

Results

Experimental setup and stabilization

To stabilize the lung for imaging in a live animal with minimal disruption of ventilation or circulation, we constructed a thoracic window(Wagner, 1969; Lamm et al., 2005), modified for the mouse with a 4-mm internal diameter (**Fig. 1A,B**). An important feature of this device is its loose adherence to the lung surface via 20–25 mm Hg of reversible vacuum spread over a large local area allowing for gas to enter and expand the lung but limiting the associated movement in the *x, y* and *z* dimensions. The vacuum in this device circulates through grooves adjacent to the imaging area and gently pulls the tissue into a shallow conical region facing an imaging-grade coverslip. The vacuum also effectively sets the cover slip in a small groove along the outside dimension of the device.

For the surgical preparation, we anesthetized the mice and performed a tracheotomy to facilitate mechanical ventilation. Then we placed mice in the right, lateral decubitus position and resected three left anterior ribs revealing the left, anterior lung surface (**Fig. 1C**). We positioned the thoracic suction window, attached to a rigid strut and a micromanipulator, immediately above the left lung and applied 20–25 mm Hg of suction to gently immobilize the lung throughout the respiratory cycle (**Fig. 1D**). We chose the least amount of suction that allowed the lung to enter the thoracic window and remain stablilized for visualization throughout the respiratory cycle. Although the applied suction is an increase above the negative pleural pressures in the intact thorax of spontaneously breathing mice(Hoffman et al., 2010), we expected this pressure to dissipate in areas further away from the window itself, thus providing limited effects well within the range of two-photon excitation. Then we lowered the objective onto the 12-

mm glass coverslip for imaging with our two-photon microscope (**Supplementary Fig. 1A**) in the central region of this preparation to minimize any effects of suction transmitted to the edges. We tested for any damage to the lungs from mechanical ventilation or thoracic suction using the gravimetric method to measure lung edema formation. We found no increase in lung edema after 2 h of continuous ventilation and thoracic suction (**Supplementary Fig. 1B**).

To determine whether there was still motion associated with inhalation-exhalation, we imaged alveolar inflation and deflation under suction window conditions (**Supplementary Video 1**); this confirmed that ventilation was maintained in the portion of lung in the thoracic window. One of the important advantages of two-photon microscopy is tissue penetration beyond what is achievable with single-photon confocal approaches. We tested the tissue imaging depth range of our method by injecting Texas Red– dextran intravenously and scanning along the *z* axis. We captured images at different depths down to 125 μm **(Supplementary Fig. 1C**), which allowed us to completely visualize the capillary bed above and under the subpleural alveoli (**Fig. 1E**).

We next tested the stability of images captured from our imaging system. Using mice that ubiquitously expressed CFP (actin-CFP), ventilated at 120 breaths per minute (bpm), we captured images at 30 frames per second (fps) of inspiration, expiration and inspiration again; overlay images from three subsequent time points revealed that the alveolar and microvascular structures were stable with our imaging technique (**Fig. 1F** and **Supplementary Video 2**). Based on the limited movement of vessels even during respiration, we estimate that we reduced overall motion to ~5–10 μm in all dimensions.

To quantify the stability and the deflections induced by mechanical ventilation captured at 30 fps, we used the Pearson's coefficient to compare images between frames (**Fig. 1F**). This revealed that exactly four frames per breath are disrupted owing to ventilation (120 bpm), but that the image reliably returned to a stable baseline after each respiratory cycle, thus yielding 20 fps with exceptional 'colocalization' of tissue. Time-averaging (15 integrated video-rate frames) of our image acquisition also effectively averaged out the four out of sync frames owing to breathing (**Fig. 1G** and **Supplementary Video 3**), producing low-noise images. An alternative approach to improve image stability was to remove the four frames in which breathing was occurring in postprocessing (**Supplementary Fig. 1D**). We also injected intravenous Texas Red dextran (molecular weight 70,000 Da) into wild-type mice to visualize the lung microcirculation. Our system stably captured these blood vessels and slow-moving cellular shadows within them (**Supplementary Video 4**).

Perfusion and cellular behavior with thoracic suction

We next examined blood flow velocities in the lung contained in the thoracic window by intravenously injecting fluorescent microspheres (1-μm beads) into actin-CFP–expressing mice and tracking movement of the beads inside microvasculature using fast acquisition rates (30 fps). We tracked an individual red fluorescent microsphere during its transit through the imaging field of an 8–15 μm blood vessel (**Fig. 2A**). We quantified the microsphere perfusion velocities by calculating instantaneous (frame to frame) and average (mean over entire observation period) track speeds (Online Methods); the majority of beads transited lung microvasculature at fast flow rates (109 ± 12 μm s^{-1},

mean ± s.e.m.; **Fig. 2B**) through this small-sized blood vessel (**Fig. 2A** and **Supplementary Video 5**). We also calculated bead speeds through a larger vessel (30 μm in diameter), which yielded faster flow rates of 280 ± 53 μm s^{-1} (**Fig. 2B** and **Supplementary Video 6**). Our calculated perfusion velocities in these blood vessels are similar to those in previous reports in the lung and in systemic microvasculature not using stabilized window methods(Popel and Johnson, 2005; Waisman et al., 2006).

An important advantage of intravital imaging in the mouse is the availability of fluorescent reporter strains to facilitate cellular imaging, and we sought to couple our method with these to understand how specific cell types behave as they transit the lung. Most notably, it has not been possible to assess the extent to which neutrophils or T cells may 'patrol' the vasculature, given the extremely tight constrictions during their transit. We tracked the movement of endogenous LysM-$EGFP^+$ (also known as LysM-GFP^+) or Cfms-GFP^+ neutrophils in both small capillary segments (10–15 μm average diameter) and in larger vessels (30 μm average diameter) (**Fig. 2C**), and we calculated the individual transit velocities of these cells (**Fig. 2D**). We collected sequential images of neutrophils transiting a medium-sized blood vessel into which we also injected 1-μm red fluorescent beads (**Fig. 2C** and **Supplementary Video 6**). $EGFP^+$ neutrophils transited at 1.42 ± 0.16 μm s^{-1} in capillary segments and at 97 ± 38 μm s^{-1} in vessels that were roughly twice as large (**Fig. 2D**). In medium-sized vessls, we observed a bimodal distribution of neutrophil perfusion velocities, with one population of neutrophils transiting at speeds just below the rate of 1-μm beads and another population transiting much more slowly and rolling and even arresting along the endothelial surface (**Fig. 2E** and **Supplementary Video 6**). Some individual neutrophils remained trapped for long

periods and moved much more slowly even in larger-sized blood vessels, compared to the flow as calculated by the movement of much smaller beads. The heterogeneity of neutrophil transit velocities has been previously documented in the canine pulmonary circulation(Gebb et al., 1995). This suggests both trapping in narrow capillaries but also continuous scanning of the lung vasculature under rapid flow.

We next tested the contribution of cell size or activation state to intravascular cell velocities in the lung, and we observed a general trend in which larger and more activated cells move more slowly than naive ones: naive T cells (CD2-RFP) injected into the jugular vein moved with a velocity of 2.48 ± 0.49 μm s^{-1} compared to T cells that had been activated for 4 d with their cognate antigen and with interleukin-2 (blasts), which transited at less than 0.5 μm s^{-1} (**Fig. 3A**). With the 0.6-μm resolution capacity of our two-photon microscope, we also detected that small (naive) T cells did not evidently adopt elongated 'amoeboid' characteristic morphology (**Fig. 3B**), even while they surveyed the capillary (**Supplementary Video 7**). In contrast, larger, stimulated T cells were not only characteristically amoeboid but also made multiple projections, likely down two vessels at a junction (**Fig. 3B**). Furthermore, when we intravenously injected naive T cells into mice, we detected entry of T cells into the capillary segments of the lung, whereas T cell blasts were restricted to larger blood vessels and largely did not enter the capillary segments (**Fig. 3C,D** and **Supplementary Video 7**). This differences in size of these two cell types likely explain the observed distribution (**Fig. 3E**).

Neutrophil dynamics in lung inflammation and injury

An important value in our system is that the lung continues to receive ventilation as it normally would and is under normal physiological blood flow, allowing for the direct examination of events when inhaled or intravascular agents first enter the lung. We used our imaging technique to examine, under different pathologic conditions, the cellular changes that occur as inhaled material enters the lung (**Fig. 4**). We imaged LysM-GFP mice injected with Texas Red–dextran before and after intratracheal challenge with the neutrophil chemokine, macrophage inflammatory protein-2 (MIP-2; 5 μg; **Fig. 4A**). As we predicted based on still images from killed mice, we observed a large influx of GFP^+ neutrophils after chemokine challenge (**Fig. 4B** and **Supplementary Video 8**). In control experiments when LysM-GFP mice were continuously ventilated under suction window conditions for 75 min, there was no artificial recruitment of neutrophils over time (**Fig. 4C**). Intratracheal challenge with MIP-2 produced a dynamic scrum of cells; we observed neutrophil crawling in the intravascular compartment, with individual cells rapidly changing their leading and trailing edges (**Fig. 4D** and **Supplementary Video 9**). Additionally, we identified mobile, extravascular neutrophils with rounded morphologies after chemokine challenge (**Fig. 4E** and **Supplementary Video 10**). As this model provides global chemokine, it is perhaps not unexpected to see such active behaviors or intra-alveolar entry of cells. To examine a more physiological insult, we used a model of acute lipopoly saccharide (LPS) inflammation and injury, and identified similar neutrophil swarming after intratracheal LPS challenge (5 mg kg^{-1}; **Fig. 4F,G** and **Supplementary Video 11**).

We also examined the dynamic leakage of dextran into the extravascular compartment, which is indicative of the increased lung vascular permeability characteristic of acute lung injury (**Fig 4h** and **Supplementary Video 12**). We quantified the average progressive increase in dextran leakage after intra tracheal LPS; this revealed a differential rate of vascular leakage across the imaged alveoli (**Fig. 4i** and **Supplementary Video 12**). This observation could not be made with common endpoint mea surements (for example, bronchoalveolar-lavage protein mea surements) of global lung vascular permeability.

Finally, we examined a model of ventilator-induced lung injury, an important contributor to excess mortality in critically ill individuals(Oba and Salzman, 2000). We visualized and quantified dextran leakage into the interstitial and alveolar spaces in mice challenged with lung stretch compared with normal tidal volumes (**Fig 4J,K** and **Supplementary Video 13**). Again, we observed heterogeneity in the rates of vascular leak among the imaged alveoli.

Discussion

Our method does not involve interruption of ventilation with the attendant pulmonary vasoconstrictor response(Hasegawa et al., 2010) or artificial perfusion or removal of the organ from the host. Isolated, perfused lung preparations have been widely used in pulmonary research with great success and with the advantage of manipulating flow velocities and shear stresses(Presson et al., 2002; Kuebler et al., 1999; Bhattacharya and Staub, 1980). However, this technique does not retain lymphatic flow, circulation is interrupted so that recruitment of cells from the bone marrow or lymphatic system is not possible, and perfusion through an artificial circulation may have unintended consequences on cellular behavior.

Our technique preserves both ventilation and perfusion. The rates of blood flow were similar to values presumed from other organs, and there was visible evidence of ventilation, but this did not prevent imaging because the system reliably returns to the same location after a ventilatory cycle. Imaging throughout the respiratory cycle is an important technical advance over prior intravital lung preparations in which imaging either occurred with the interruption of ventilation or was timed for capture at only end expiration(Tabuchi et al., 2008). Finally, our approach is durable with no detectable injury to the stabilized lung, and we routinely imaged for up to 3 h, which is the longest duration of imaging that we have attempted thus far.

Neutrophils uniquely traverse the lung compared to other tissues(Gebb et al., 1995), yet much of the studies of neutrophil rheology using intravital techniques have come from nonpulmonary organs, which may not accurately reflect the dynamics of the pulmonary microcirculation(Zarbock and Ley, 2009). Neutrophil-mediated lung diseases,

such as acute lung injury(Looney et al., 2006), can now be studied directly. Our approach also permitted us to observe capture of multiple cell types and to measure dwell times for lymphocytes that reach the small capillary segments. This stalling effect may provide ample opportunity for both surveillance and also for lung-remodeling factors to be deposited; these details are now open to investigation using our approach. Our method should enable the study of both the onset of adaptive immune responses and the homing of metastatic tumors to the lung. Breast tumor metastases and normal breast ductal cells may establish residency in the lung(Podsypanina et al., 2008); our method will enable the study of this process and possibly allow researchers to identify the supporting cells of the metastatic niche.

The limitations of our system include (i) imaging under positive pressure ventilation and not during spontaneous breathing, and (ii) imaging of only subpleural blood vessels and alveolar units, although we imaged up to 125 μm below the pleural surface, and the subpleural and deeper parenchymal microvascular networks are generally thought to be similar in terms of vascular regulation(Short et al., 1996). A recent study(Kreisel et al., 2010) in which the authors used glue to fix the lung surface to a coverslip is a possible alternative method that may have similar benefits to those presented here, but the physiologic integrity of that preparation has yet to be established. Although our system substantially improves upon existing approaches, there is room for improvements. For example, adaptive optics has recently been used to overcome the distortions associated with changes in refractive index as two-photon light enters the target tissue(Ji et al., 2010). Such an approach would undoubtedly be beneficial in the lung, where light transverses many such interfaces at the surface of each subsequent air-

filled alveolus. Advances in miniaturization, such as the use of gradient index lenses(Barretto et al., 2009) or miniaturized lens elements, should also be possible, which may result in even less-invasive approaches that are possibly suitable for diagnostic thoracic imaging in humans.

Figures

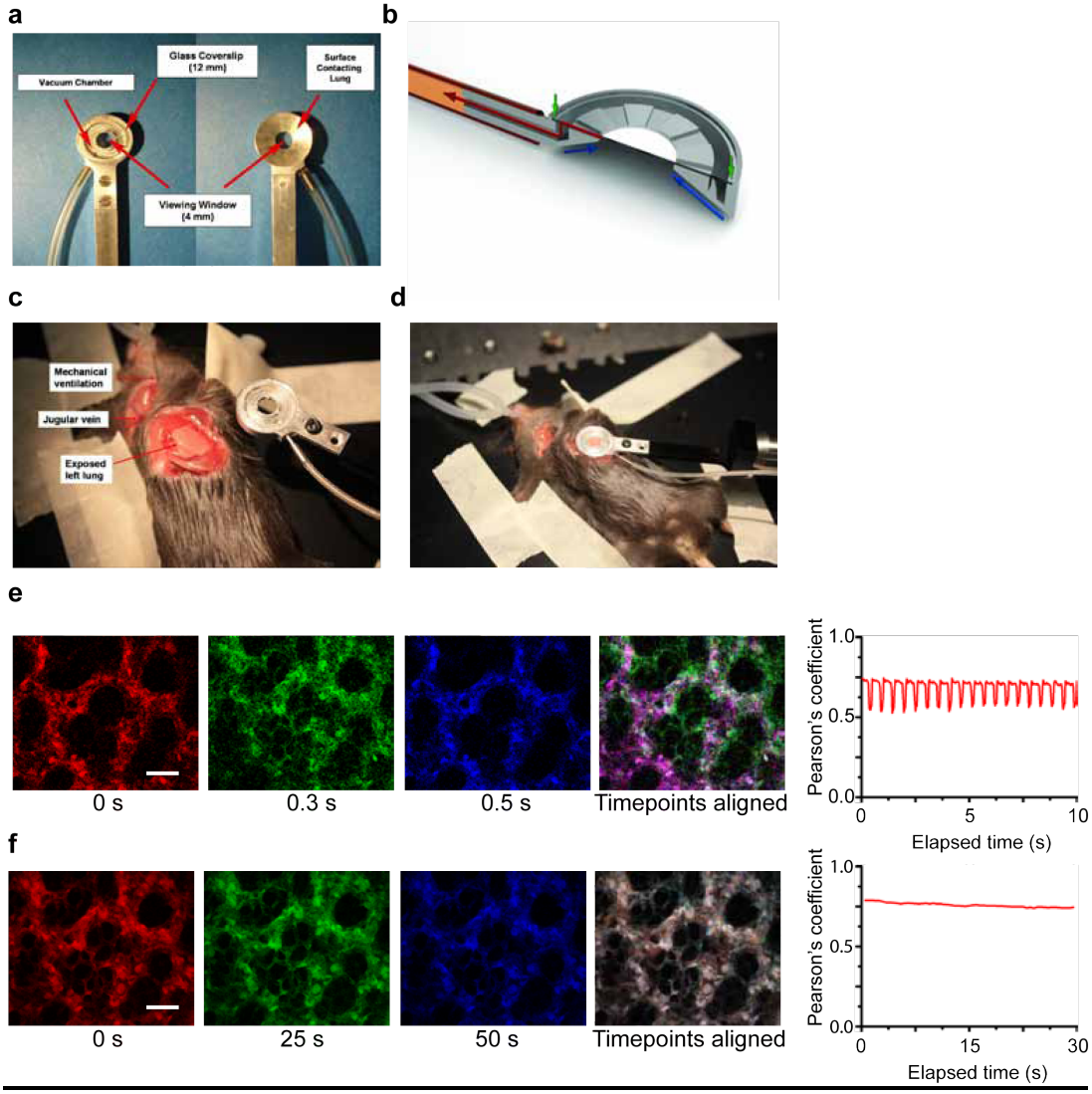

Figure 1. Experimental setup and image stability for intravital imaging of the mouse lung. (**a**) Anterior and posterior views of the thoracic suction window fitted with a coverslip. (**b**) Side-view rendering of the suction window showing suction chamber, cover slip (green arrows) and vacuum flows (blue arrows near tissue, red arrows toward suction regulator). (**c**) Surgical preparation of left thorax with exposed left lung. (**d**) Suction window *in situ*. (**e**) Representative images at the indicated depths in a mouse injected with Texas Red dextran, showing the capillary bed above and below the subpleural alveoli (left to right). Scale bar = 50 μm (**f-g**) Still images of CFP fluorescence

in an actin-CFP mouse lung at three time points, coded respectively as red, green and blue. Images were captured at 30 fps; in (**f**) each timepoint from (**g**) is aligned to produce a merged image. The plot shows the Pearson's coefficient from a 30 fps video over time. See also Supplementary Movie 2. (**g**), each frame represents 15 integrated images that are then merged (timepoints aligned). Scale bar = 50 μm. The plot shows the Pearson's coefficient over time from a video taken using the 15 integrated image acquisition. See also Supplementary Movie 3.

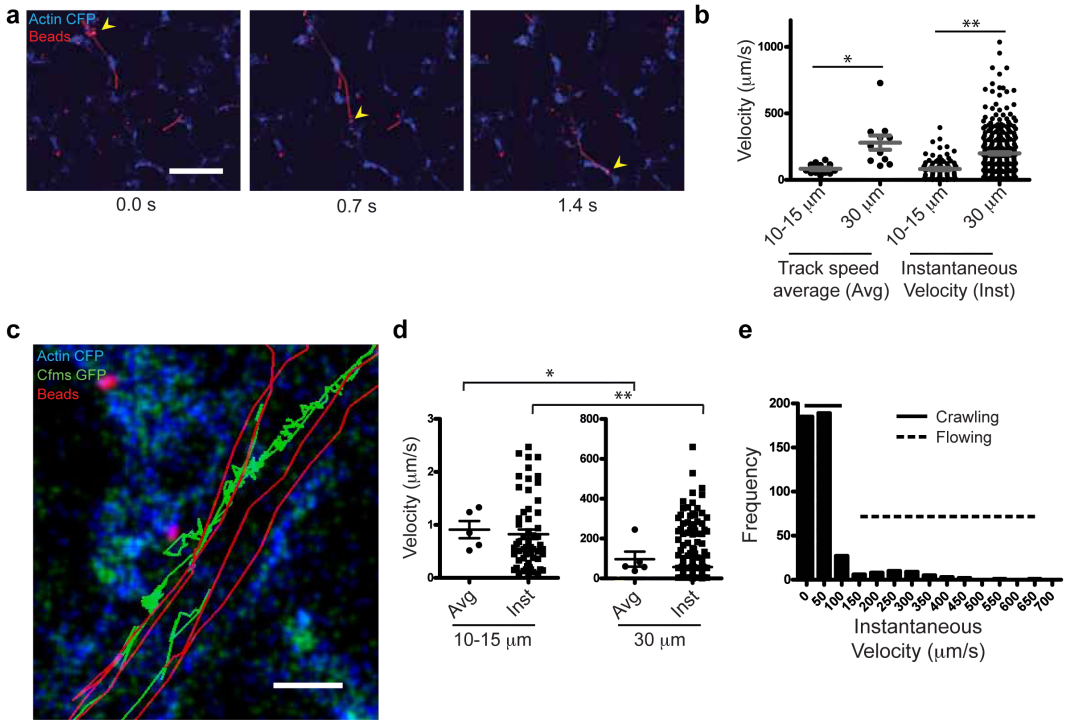

Figure 2. Perfusion velocities of beads and neutrophils in the lung. (**a**) The micrographs show sequential images of individual beads traversing the lung microcirculation (yellow arrow heads), in actin-CFP mice injected i.v. with red fluorescent microspheres and then imaged at 30 fps. Time elapsed after the first frame is indicated. Scale bar = 50 μm. See also Supplementary Movie 5. (**b**) The plot shows perfusion velocities of individual beads in small (109 ± 12 μm/s, mean ± s.e.m., n = 14) and medium-sized blood vessels (280 ± 53 μm/s, mean ± s.e.m., n = 11, $P < 0.001$). Instantaneous = instantaneous bead speeds. Average = average speed of individual beads. (**c**) The micrograph shows four representative tracks of neutrophils (green) and beads (red) inside a vessel of an Actin-CFP/*c-fms*+ mouse injected with fluorescent microspheres and imaged at 30 fps. Scale bar = 10 μm. (**d**) The plots show the average and instantaneous speed of neutrophils in small (0.91 ± 0.16 μm/s, mean ± s.e.m., n = 5) and medium-sized (96.5 ± 37.8 μm/s,

mean ± s.e.m., $n = 5$, $P < 0.05$) blood vessels. (**e**) Histogram of neutrophil perfusion velocities in a medium-sized blood vessel. See also Supplementary Movie 6.

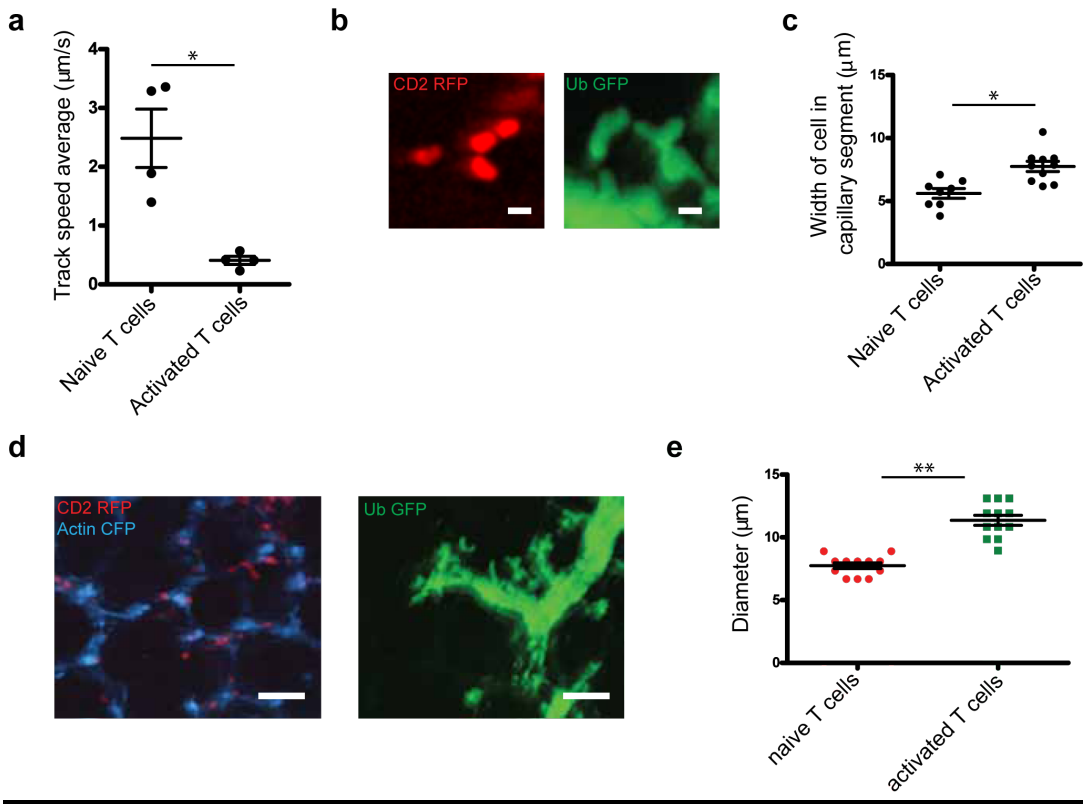

Figure 3. Perfusion velocities of T cells in the lung. (**a**) Track speed averages of naïve (2.48 ± 0.49 μm/s, mean ± s.e.m., $n = 4$) and activated T cells (0.41 ± 0.07 μm/s, mean ± s.e.m., $n = 4$, $P < 0.01$) injected into the jugular vein of actin-CFP mice are plotted. See also Supplementary Movie 7. (**b**) Representative images showing the morphology of naïve T cells (CD2 RFP) and T cell blasts (ubiquitin-GFP). Yellow arrows indicate a T cell blast with two leading edges, likely extending into two vascular branches. Scale bar = 10 μm. (**c**) Width of the capillary segments containing naïve (5.61 ± 0.39 μm, mean ± s.e.m., $n = 8$) and activated T cells (7.75 ± 0.41 μm, mean ± s.e.m., $n = 12$, $P < 0.01$) are plotted. (**d**) Still images showing the sizes of intravascular naïve (left panel) and activated (blasts; right panel) T cells. Scale bar = 50 μm, 40 μm Z stack. (**e**) Average diameters of naïve (7.74 ± 0.23 μm, mean ± s.e.m., $n = 12$) and activated T cells (11.36 ± 0.40 μm, mean ± s.e.m., $n = 12$, $P < 0.0001$).

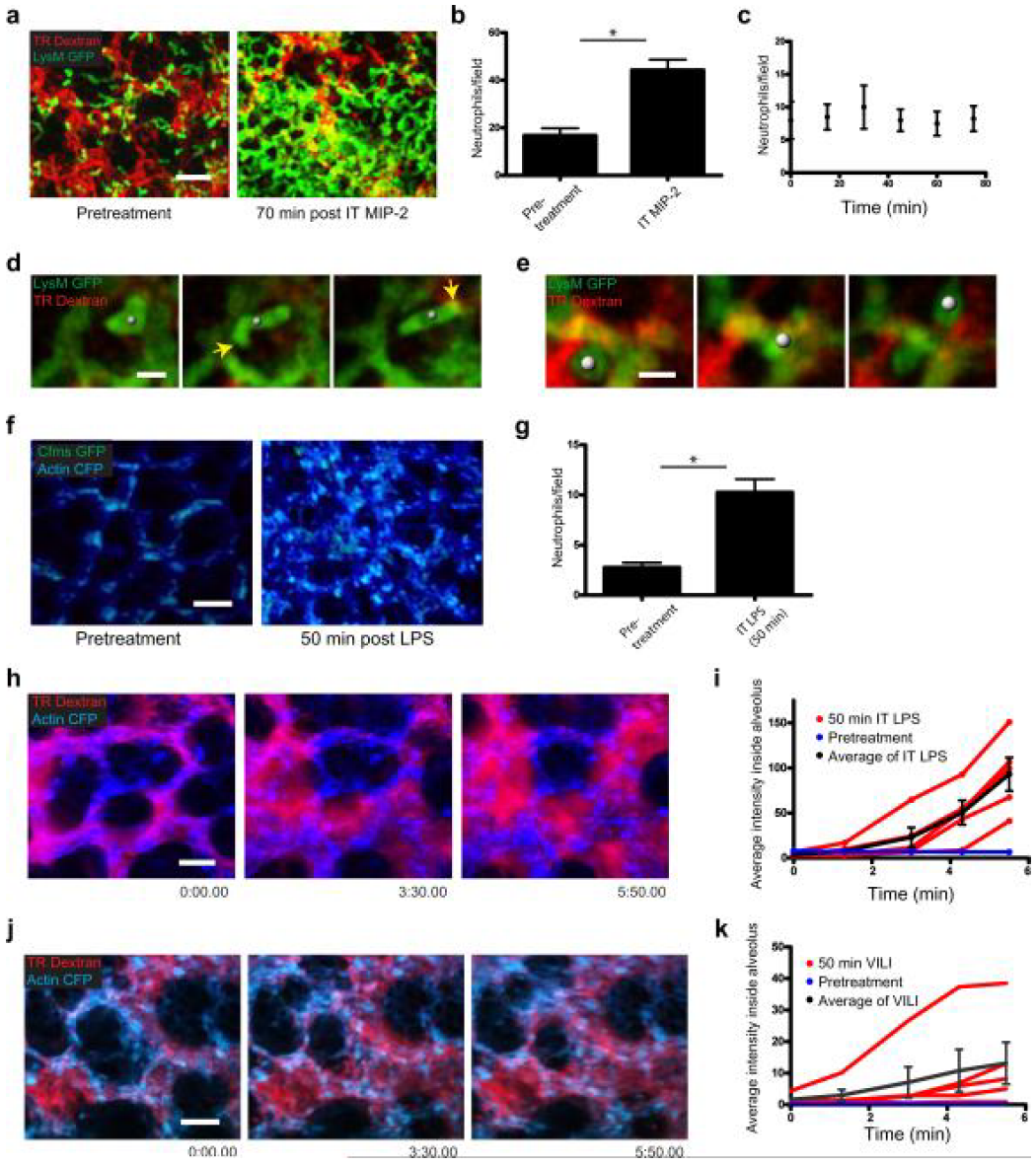

Figure 4. Imaging inflammation and injury-induced neutrophil dynamics in physiologically intact lungs. (**a**) Images of the lung of a LysM-GFP mouse injected with Texas Red dextran and imaged before (left panel) and after (right panel) intratracheal instillation of MIP-2. Scale bar = 50 μm, 40 μm z stack. See also Supplementary Movie 8. (**b**) Number of GFP+ neutrophils in the imaging field before (16.75 ± 3.06 cells, mean ± s.e.m., $n = 4$) and after MIP-2 (44.25 ± 4.42 cells, mean ± s.e.m., $n = 4$, $P < 0.01$)

instillation. (**c**) Number of GFP+ neutrophils in the lung vasculature under continuous suction (n = 4 for each timepoint). (**d**) Representative images of an intravascular GFP^+ neutrophil. Scale bar = 10 μm, single z plane at 5:20, 6:40 and 9:20 min:sec. (**e**) Representative images of a GFP^+ neutrophil moving within alveoli. Scale bar = 10 μm, single z plane at 0:40, 5:40 and 9:00 min:sec. See also Supplementary Movie 10. (**f**) Images of the lung of an actin-CFP/*c-fms*-GFP mouse before and after intratracheal instillation of LPS. Scale bar = 50 μm, 40 μm z stack. See also Supplementary Movie 11. (**g**) Number of neutrophils per field before (2.75 ± 0.48, mean ± s.e.m., n = 4) and after LPS instillation (10.25 ± 1.32, mean ± s.e.m., n = 4, $P < 0.01$). (**h, j**) Images of the lung of an actin-CFP mouse injected with Texas Red dextran and either challenged with intratracheal LPS for 50 minutes (**h**) or subjected to ventilator-induced lung injury for 60 minutes (**j**). Scale bar = 50 μm, 40 μm z stack. See also Supplementary Movie 12, 13. (**i, k**) The plots shows the average intensity of fluorescent dextran in the alveolar space at the indicated times after LPS treatment (**i**) or ventilator-induced lung injury (**k**). Blue lines are the pre-treatment average (n = 3 alveoli), red lines are individual alveoli measured post-treatment, and black lines are the post-treatment average (n = 5 alveoli).

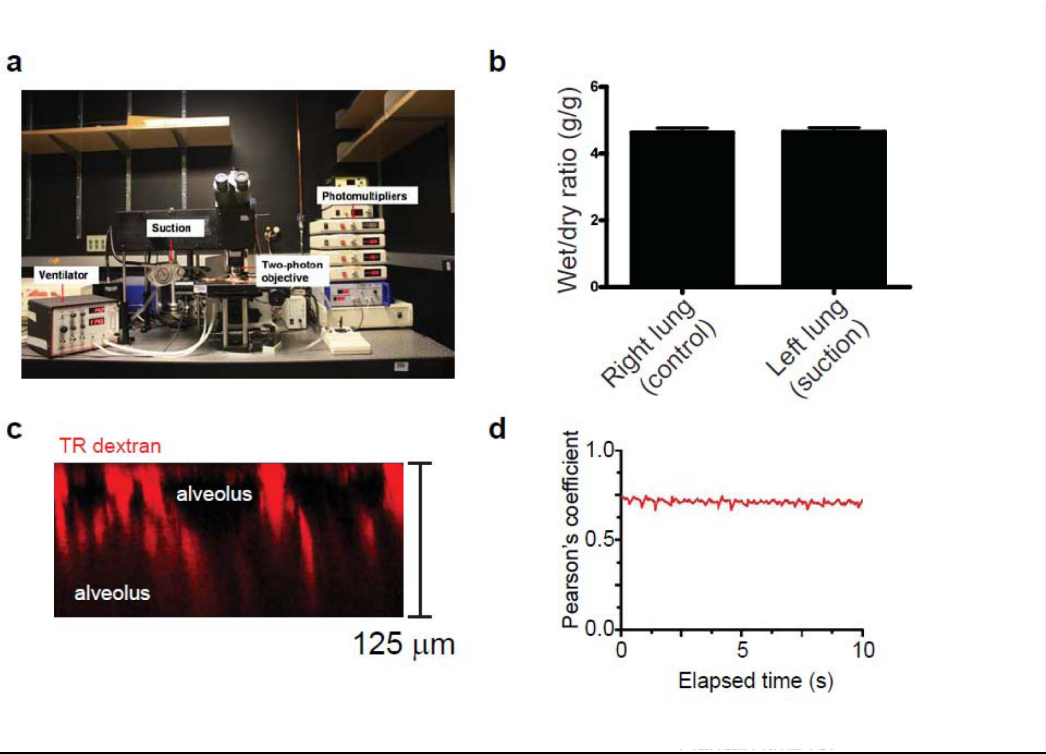

Supplementary Figure 1. Imaging set-up, lung edema measurements, z-depth imaging, and image stability. (**a**) Imaging set-up with mechanical ventilator, suction manipulator, and two-photon excitation and detection systems. (**b**) Lung wet-to-dry weight ratio (g/g) in the right and left lungs of mice (n = 4) under continuous anesthesia, mechanical ventilation, and thoracic suction (left lung). (**c**) x-z rendering of a lung vasculature filled with Texas Red dextran and imaged to a depth of 125 µm. (**d**) Pearson's coefficient of a timelapse after removal of four frames out of fifteen, which represent ventilation.

Materials and Methods

Mice

The following mice were used in our experiments: C57BL/6 wild-type (Charles River); *c-fms*-GFP(Sasmono et al., 2003) in which EGFP is driven under the CSF-1R promoter (highlights neutrophils, monocytes, and macrophages and were provided by Z. Werb (University of California San Francisco)); actin-CFP(Hadjantonakis et al., 2002) have the CFP transgene ubiquitously expressed and were obtained from I. Weissman (Stanford University); CD2-RFP (expressing RFP in all T cells and a small subset of NK cells), OT-II TCR transgenic (OVA-specific Class II restricted), and ubiquitin-EGFP (EGFP expression in all cells) were obtained from The Jackson Laboratories. LysM-EGFP mice (EGFP expression in monocytes, macrophages and neutrophils) were obtained from E. Robey (University of California, Berkeley)(Faust et al., 2000). All experiments involving mice were approved by the Institutional Animal Care and Use Committee at the University of California, San Francisco.

Reagents

The reagens used were Texas Red–dextran (70,000 molecular weight; Invitrogen); 1 μm, red fluorescent microspheres (Invitrogen); lipopolysaccharide (LPS) (from *Escherichia coli* O55:B5; Sigma-Aldrich); and MIP-2 (R&D Systems).

Thoracic suction window

We adapted a custom, thoracic suction window based on previously published designs(Lamm et al., 2005), by miniaturizing to a 4 mm internal diameter, and we fitted this with a 12 mm glass coverslip.

Surgical preparation

Mice were anesthetized with Ketamine (80 mg kg^{-1}) and Xylaxine (12 mg kg^{-1}) i.p. and placed on a custom, heated microscope stage. PE-90 tubing was inserted into the trachea and sutured into place to facilitate mechanical ventilation with a rodent ventilator (Kent Scientific). Mice were ventilated with pressure control ventilation (inspiratory pressure = 12–15 centimeters of water (cmH_2O), a respiratory rate of 120 breaths per minute, a fraction of inspired oxygen of 0.5–1.0 and a positive-end expiratory pressure (PEEP) of 3 cmH_2O. Isoflurane was continuously delivered at 1% to maintain anesthesia and mice were given an i.p. bolus of PBS (1 ml) before the thoracic surgical procedure. The mice were then placed in the right lateral decubitus position and three left anterior ribs were resected and the left lung was carefully exposed. The thoracic suction window attached to a micromanipulator on the microscope stage was then placed into position and 20–25 mm Hg of suction was applied (Amvex Corporation) to gently immobilize the lung. The two-photon microscope objective was then lowered into place over the thoracic suction window and a 12 mm coverslip. For intravenous injections, the right jugular vein was cannulated with a 30 gauge needle attached to PE-10 tubing for injections of cells or intravascular dyes.

Two-photon microscopy

A custom resonant-scanning two-photon instrument(Bullen et al., 2009) contains a four-photomultiplier tube detector (R5929 Hamamatsu), collects data at video rate, and uses an Olympus XLUMP FL20XW (numerical aperture (NA) 0.95) objective with an overfilled back aperture with a fill-factor of approximately 1. Samples were excited with a 5-W MaiTai TiSaphire laser (Spectra-Physics) tuned to a wavelength of 910 nm, attenuated via a variable neutral density wheel to ~25–40% of power (0.175–0.28 W) and using emission wavelengths of 440/40 nm (for CFP), 505/20 nm (for EGFP), and 605/70 nm (for beads or dextran) were collected. A custom, four-dimensional acquisition module in VideoSavant digital video recording software (IO Industries) or in Micromanager was used for image acquisition. For time-lapse acquisition, each *x-y* stack spans 240 μm × 288 μm at an x-y resolution of 0.6 μm per pixel. For *z*-stacks, we collected data at a *z*-dimension resolution of 2 μm. *z*-dimension distances and averaged frames are indicated for each individual experiment.

Blood flow velocity experiments

Red, fluorescent microspheres (1 μm; Invitrogen) were injected into the right, jugular vein and imaged using a fast acquisition mode at 30 fps. To measure cellular velocities, individual fluorescent protein-labeled mice were used. Imaris spot detection was used to locate the centroid of cells or beads, and the tracking function was used to determine instantaneous velocities (between time points) or average track speeds (average of instantaneous velocities for the entire observation period). All additional analyses were performed using Metamorph (Universal Imaging), Imaris (Bitplane Inc.) and Photoshop (Adobe Inc.) software.

Lung stretch injury

Lung stretch injury (ventilator-induced lung injury) was initiated by increasing the pressure controlled ventilation to 30 cmH_2O and decreasing the PEEP to 0 cmH_2O. Mice were also injected with Texas Red dextran (70,000 MW) via the jugular vein for the imaging of lung vascular leak.

MIP-2 and LPS-induced lung injury

Mice were intratracheally challenged with MIP-2 (5 μg; R&D Systems) or LPS from *Escherichia coli* O55:B5 (Sigma-Aldrich) at 5 mg kg^{-1}.

Quantifying lung vascular permeability

Alveolar spaces were defined by the absence of Actin CFP. Isosurfaces were drawn in the alveolar space using Imaris (Bitplane, Inc) manual surface creation tool. The relative amount of dextran within the space was determined by calculating the average red (Texas Red–dextran) intensity in the airspace.

Quantifying lung edema

The gravimetric method was used to measure the lung wet-to-dry weight ratio (grams/grams) as previously described(Looney et al., 2006; Faust et al., 2000). The right and left lungs were separately removed, weighed, placed in a drying oven at 55 °C for 48 h, and then weighed again to calculate the wet-to-dry weight ratio.

T-cell experiments

Activated ubiquitin-EGFP T cells were generated by incubating splenocytes and lymph node cells from an ovalbumin-specific T-cell receptor transgenic (OTII) × Ub-EGFP mouse with ova peptide SIINFEKL (Sigma-Aldrich) and supplemented with recombinant mouse IL-2 (BD-Biosicences). They were transferred after 4 or 5 d of culture. Naïve CD2-RFP OTII cells were isolated and used immediately. A single cell suspension was isolated from lymph nodes and spleens of CD2 RFP/OTII TCR transgenic mice. Naive CD4 T cells were purified using the Stemsep CD4 negative selection kit. T cells were transferred into actin-CFP mice via the jugular vein.

Statistics

Data is presented as mean ± s.e.m. *P* values were determined by performing a two-tailed *t*-test. To determine the stability of the imaging setup, Pearson's correlation coefficient of actin-CFP fluorescence intensity was measured for every frame with respect to the first frame, using the 'co-localization' function in Imaris.

Chapter III: Spatiotemporally Separated Alveolar Antigen Uptake and Airway Presentation of Allergens in the Lung

Abstract

Asthma pathogenesis is focused around conducting airways. The reasons for this focus have been unclear since it was impossible to track the sites and timing of uptake or subsequent antigen presentation to T cell effectors. Two-photon microscopy of the lung parenchyma revealed accumulation of CD11b+ DCs around the airway after allergen challenge but very limited access of these airway-adjacent DCs to the contents of the airspace. In contrast, we observed prevalent transepithelial uptake of particulate antigens by alveolar dendritic cells (DCs). These distinct sites are temporally linked with early uptake in alveoli giving rise to the asthma-specific DC and antigen retention in the airway region. A hyper-reactive lung thus results from selective retention of allergen-presenting cells in airway-adjacent interaction zones, not variation in the abilities of individual cells to survey the lung**.** The location and function of these zones in allergy, sites that also attract and reactivate T cells, may be similar to the more profound bronchial-associated lymphoid tissue (BALT), generated in response to pathogens.

Introduction

The tissue of the lung is a complex filigree, supporting gas exchange and presenting a large surface for antigen surveillance and uptake. This interface provides a classic example of the challenges of mucosal immunity; responses to environmental antigens need to be minimized while the exposure to pathogens requires rapid local responses. The dominant symptoms of asthma, airway constriction and mucus accumulation, are the results of immune responses near airways. A rich body of literature has identified lung dendritic cells (DCs) and alveolar macrophages (AMs) as predominant phagocytic populations, both in the steady state and in disease(McWilliam et al., 1996; Grayson et al., 2007; Holt, 2005; Robinson et al., 1992; van Rijt et al., 2005; Hammad et al., 2010; Garnier et al., 2005; Belz et al., 2004; Sung et al., 2006). While it is clear by depletion protocols that lung DCs play a major role in airway pathogenesis(van Rijt et al., 2005; Lambrecht et al., 1998), the spatial dynamics that define how and where they sample material and when and where they present antigen has not been assessed.

DCs in the lung, in contrast to AMs, are very effective at generating T cell responses(Belz et al., 2004) and are also instrumental in initiating and perpetuating T cell hyperresponsiveness associated with asthma(van Rijt et al., 2005; Hammad et al., 2010). CD103+ and CD11b+ subsets have been proposed to activate CD8 and CD4 responses respectively(Jakubzick et al., 2008a). CD103+ have been shown to play important roles in viral responses(Ballesteros-Tato et al., 2010) and apoptotic cell uptake(Desch et al., 2011), but the localization and uptake capacity of these cells has not been addressed in the lung. Increased numbers of DCs are found in bronchoalveolar lavage (BAL) fluid of asthmatic patients after allergen challenge(Robinson et al., 1992; van Rijt, 2002),

suggesting their increase is associated with disease. In mice, upon Ova challenge in an Ova/alum mouse model of asthma, lung tissue associated DCs also increase in number and increase expression of co-stimulatory molecules(van Rijt et al., 2005). After depletion of DCs and macrophages with the CD11c driven diphtheria toxin receptor, Ova treated mice lose the hallmarks of asthma(van Rijt et al., 2005). Despite the large amount of data indicating the importance of DCs in allergic responses in the lung, their functions within the tissue have remained unclear.

Despite the wealth of studies on the trafficking of DCs from the lung taken from end-point analyses, less is understood about the initial competition for antigens with the more populous AMs; specifically, how *in situ* movement and surveillance by DCs and AMs influences the fate of inhaled materials. The specific handling of antigens by DCs in the entire lung has largely been inferred from studies of tracheal preparations. These have revealed DCs that project dendrites into but not through the tight junctions of epithelial cells(Jahnsen et al., 2006). Similar studies highlighted tracheal DCs as interlinked sheets lining the mucosal surface(Lambrecht et al., 1998). The uptake of fluorescent particulate antigens and macromolecules that are too large to cross the epithelial border by lung DCs suggested that these cells have mechanisms to reach across into the airspace(Byersdorfer and Chaplin, 2001; Vermaelen et al., 2001). A prominent proposal is that breakdown in the epithelium, perhaps in response to TLR ligands, underlies pathogenesis(Lambrecht and Hammad, 2009). Increased DC motility has been observed in tracheal sections in response to epithelial recognition of TLR4 ligands(Hammad et al., 2009), and occasional dendritic extensions in tracheal DC preparations have been reported although it is not clear that these are present under

normal conditions(Hammad and Lambrecht, 2008). These extensions mimic similar dendrites that protrude(Rescigno et al., 2001), increasingly following injury or TLR signaling, into the lumen of the gut(Chieppa et al., 2006). In vitro studies using lung airway epithelium cultures have suggested that, though their cell bodies are often beneath the epithelium, DCs may protrude through epithelial tight junctions(Vermaelen et al., 2001; Blank et al., 2007) although the relevance of this to the whole lung remains undescribed.

It is well established that the majority of particulate antigen transport to the draining lymph nodes is done by dendritic cells, and not by passive carriage of antigen via the flow of afferent lymph. Diptheria toxin-mediated depletion of lung dendritic cells reduces antigen traffic to the lymph node(Vermaelen et al., 2001), and DC homing depends on CC-chemokine receptor 7(Jakubzick et al., 2006; Hammad and Lambrecht, 2007; Wikstrom and Stumbles, 2007). Particle-bearing DCs that traffic to the lymph node can subsequently elicit T cell responses to proteins borne on the particulate(Byersdorfer and Chaplin, 2001). The late (adaptive) phase of asthma exacerbations begins only eight hours after antigen inhalation, which would provide little time for antigen traffic to the lymph node and T cell traffic back to the lung(Wenzel et al., 2007). How and where these allergens are presented to T cells to generate airway-localized inflammatory responses is not clear.

Two-photon imaging has previously been used to track the dynamic behavior of lymphocytes in lymph nodes(Miller et al., 2002) and provides the possibility to assess cells deep within their native and complex tissues(Cahalan and Parker, 2008; Germain et al., 2006). For lymph nodes, both intravital as well as organ explant models have been

described, and the comparisons of these two has provided insight into when each is applicable. The use of two-photon microscopy for lung has previously been demonstrated with viable lung slices for the study of smooth muscle functions(Bergner and Sanderson, 2002), but the behavior of the immune system during allergy in these preparations has not been formally assessed. Recently, stabilized and ventilated intravital lung imaging has also become possible. Using this method, airflow and blood flow remain intact, and alveolar imaging is possible(Looney et al., 2011; Kreisel et al., 2010). Under such a preparation, tissue remains demonstrably viable and without evidence of immune infiltrate induced by the preparation(Looney et al., 2011).

Here we have applied two-photon live imaging of viable lung slices and intravital stabilized lung to discover the antigen surveillance and presentation dynamics in lung. We tested the hypothesis that surveillance changes at the cellular level after allergen challenge. Using CD11c-EYFP mice(Lindquist et al., 2004) which, by two-photon imaging, mark DCs and mark AMs only after allergen challenge, we were able to differentially track the behavior, antigen uptake, and cell-cell interactions of CD11b+ DCs in viable lung tissue. We compared these activities on a per-cell basis, both in the steady state and in the widely studied Ova model of allergic lung disease. While other mucosa has demonstrated evidence of changes in motile behavior of DCs during insult, neither acute allergy induction nor treatment with bacterial LPS significantly changed their surveillance behaviors within the lung tissue. We also found that alveoli are unexpectedly the sites of the most robust DC air surveillance in the steady state with highly dynamic dendrites that project across epithelial barriers. We captured examples of DCs ingesting particles directly from an alveolar atrium and found that DCs are

extremely effective at phagocytosis of particulate antigens from this location. Airway DCs, which exhibit greater center-of-mass motility than parenchymal DCs, rarely send processes across the airway epithelium. We have been unable to detect either breakdown of the epithelium leading to dendritic cell access or increased extension after allergen challenge. However, antigen-bearing DCs accumulate near airways after allergen challenge. Concurrently, activated T cells accumulate in the same regions. Thus, accumulation of antigen-bearing DCs near airways, rather than changes in alveolar APC phagocytic function during surveillance, generates a local presentation mechanism. This represents the dominant varation in antigen handling and a likely driver of pathogenesis in allergic airways disease and asthma.

Results

CD11b+DCs Accumulate Near Allergic Airways

In order to understand the nature of antigen processing for presentation to T cells as it occurs on and in the lung mucosa during asthma, it was necessary to firmly establish the details of AM and DC populations as well as a system for marking these cells for imaging. We opted to perform all of these studies in the context of the highly studied OVA-challenge model of allergic lung disease, representing a subset of the features of some forms of human asthma(Blyth et al., 1996). The system is primarily based upon a standard immunization strategy with ovalbumin (OVA) in Alum (**Fig. 1A**) followed by inhalation of OVA in the 'recall' phase which routinely results in robust responses including eosinophil infiltration (data not shown), airway hyperresponsiveness(Voehringer et al., 2006), and goblet cell hyperplasia(Blyth et al., 1996). In contrast, saline (Sal) inhalation does not result in significant changes in the lung.

In order to track AM and DC populations in real-time, we took advantage of transgenic mice in which EYFP expression is driven under the control of the CD11c locus (CD11c-EYFP)(Lindquist et al., 2004). FACS analysis showed that CD11b+ DC numbers increase in the lungs of allergic mice (**Supplementary Fig. 1A-E**) but showed also that CD11c-EYFP was expressed on all DC populations and AMs after allergen challenge (**Supplementary Fig. 1H-M**). Whereas CD11b+ DCs, CD103+ DCs and AMs expressed similar levels of Class II prior to allergen challenge, both DC populations upregulate Class II expression after allergen challenge. This is consistent with the ability to prime or reactivate T cells within the lung (**Supplementary Fig. 1F, G**). With

understanding of the CD11c-EYFP marker expression profile and this in situ maturation, we turned towards imaging to segregate DCs spatially and to use image-analysis to deconvolve these populations.

We developed a technique for live cell imaging in the lung adapted from previous work of Sanderson(Bergner and Sanderson, 2002). Briefly, lungs were filled with agarose, removed from the mouse, and sectioned into 300μm sections using a vibratome (**Supplementary Fig. 2A**). Lung sections are maintained at 36°C in oxygenated media for imaging. Under these conditions, PI staining 4 hours after imaging shows only modest cell death, confined to the cut face and distant from the sites of our imaging, which always began at least 50mm beneath the cut site and proceeded downward (**Supplementary Fig. 2B**). Cell autonomous behaviors and viability were evident from ciliary beating in the large airways (**Supplementary Video 1**), which has been documented to be maintained under these conditions for 10 days(Bergner and Sanderson, 2002).

Tiling of large 3-dimensional volumes obtained in this way confirms and highlights the dramatic expansion of CD11c-EYFP^{hi} cells that we observed using flow cytometry and allowed us to spatially assign this to regions of the alveolar spaces and airways (**Fig. 1B**). However, as would be predicted from the CD11c^{hi} gate in the flow analysis, dendritic cells are the dominant cells imaged under control conditions whereas both DCs and AMs are visualized with this marker in the allergen challenge condition (Supplementary Figure 1). In order to resolve this, we took advantage of the distinct morphologies of these two cell types to separate them using automated image analysis. The AMs were distinguishable because of their very round shape, which is associated

with a sphericity measure of >0.75, shown as the second peak of sphericity in the histogram representing the CD11c-EYFP population (**Fig. 1C**). Side-by-side analysis of Siglec-F, a marker closely linked to AMs but not DCs, confirmed that this sphericity corresponded well to AM:DC distinction (**Supplementary Fig. 2C**). This morphological criterion in turn allowed us to separate these two cell types within images (**Fig. 1E**) and ultimately to confirm that the majority of the DC accumulation observed by FACS was accounted for in the airway-adjacent DC populations with much less variation in the alveolar populations (**Fig. 1D and F**).

Because the lung contains subpopulations of DCs, we also wanted to determine which subpopulations we were examining in our imaging system. By staining live lung sections from CD11c-EYFP mice with CD11b APC antibody, we were able to visualize the CD11b+ and CD11b- DC populations (**Fig. 1G**). Quantification of the resulting images shows that the DCs that accumulate near the airway are CD11b+; however CD11b+ and CD11b- DCs are not otherwise strictly segregated by location within the lung (**Fig. 1H**). In sum, this analysis indicated that inflammation during allergen challenge was largely associated with increased numbers of CD11b+ DCs retained in the airway-adjacent region, where the pathology of asthma is most evident.

DCs in Lung Subregions Behave Differently

While this imaging system provided much-needed clarity about phagocyte accumulation after allergen challenge, the method also provided a route to directly analyze the behaviors of those cells *in situ*. By acquiring time-lapse movies of these viable lung slices, we were able to track these potential APCs. Using both the EYFP

marking and the sphericity measures of Figure 1, we found that DCs exhibit significant center-of-mass motility near airways, moving non-directionally just below the surface of the epithelium. In contast (with the exception of the rare CD11c-EYFP cell that moved within the lung parenchyma and was perhaps targeted toward lymphatics) there was generally very little motility in alveolar regions (**Fig. 2A** and **Supplementary Video 2**).

Quantification of the motility of many cells (as defined by the movement of the weighted center of their cell bodies) revealed speeds of approximately 2.5mm/min near the airway surface, which was not appreciably altered under allergen challenge. In contrast to the more motile airway-adjacent DCs, DCs located near the alveoli were typically more stationary (mean velocity of 1-1.5 mm/min) under both conditions, possibly indicating different functions for DCs at the two locations. AMs, by contrast, only moved at very slow speeds after allergen challenge (less than 1mm/min; **Fig. 2B**). This slow motility of AMs was also similar in control animals, as assessed using a different marking strategy (**Supplemental Fig. 2D,E** and **Supplementary Video 3**); however, this data does not preclude the possibility of different behavior in the case of infection. Speed analysis is sometimes confounded by possible 'jitter' of cells accounting for an apparent center-of-mass movement and so we performed analysis of the tracks of airway and alveolar associated DCs. This confirmed that airway DCs displace over time where alveolar DCs largely do not (**Fig. 2C**). However, further analysis of a large number of DCs observed over a long period of time revealed that a trafficking fraction of alveolar DCs displaced more than 5 mm in 30 minutes (**Fig. 2D**).

Airway DCs are motile and send few processes through the airway

Airway DC were motile in the airway-adjacent regions (**Fig. 3A** and **Supplementary Video 4**). However, these aggregate descriptions do not give an accurate view of individual cells. For example, we occasionally observed slow DC circling, potentially providing surveillance of a fixed area of epithelium or representing a cell under the influence of a local chemoattractant (**Fig. 3B** and **Supplementary Video 5**). By using mice expressing CFP under the actin promoter to mark all cells (Actin-CFP(Hadjantonakis et al., 2002)) crossed to CD11c-EYFP, we also sought to determine whether airways DCs send processes across the epithelium, as has been shown for tracheal DCs. A small fraction of DCs observed were clearly situated just below the airway epithelium while sending projections toward and possibly between the epithelial cells (**Fig. 3C** and **Supplementary Video 6**). However, only 3 percent of airway DCs generated processes in this way when observed over 30 minute periods in saline treated or allergen challenged mice (**Fig. 3D**), and comparing the Actin-CFP marking, we were unable to ever observe a dendrite extend past the outermost epithelium and into the lumen.

Because previous data suggested DC sampling and/or motility was augmented by TLR stimulation in the trachea(Hammad et al., 2009) and gut(Chieppa et al., 2006), lung sections were treated with LPS to measure changes in DC behavior. Up to three hours after treatment, airway DC speed remained unchanged (**Fig. 3E**), and we observed no change in sampling behavior or frequency (data not shown). Since the previous findings of changes in DC behavior were mediated by epithelial TLR4 it was tempting to hypothesize that, in comparison, the lung epithelium may not induce the requisite

changes to augment DC scanning. Staining of collagenase-digested lung and trachea confirmed that the population of TLR4 expressing cells in the trachea was 10 times that of the lung, possibly accounting for differences in DC responses at these sites (**Supplementary Fig. 3A, B**). We thus conclude that, within this short time-scale, prior to LPS induced major lung injury, DC surveillance in the airway remained confined to the interstitium.

Alveolar DCs Send Dendrites into Airspace

While DC center-of-mass motility was limited in the alveoli (Fig. 2C), analysis of time-lapses demonstrated that the dendrites of these cells were quite active. This was evident under steady-state as well as for allergen challenged DCs (allergen challenged: **Fig. 4A** and **Supplementary Video 7**). As with airway DC, intercrosses with Actin-CFP mice provided sufficient contrast to analyze whether dendrites were transepithelial and, in contrast with airway DCs, alveolar DCs demonstrated extending and retracting dendrites moving along the mucosal face of alveolar epithelial cells (unchallenged mouse: **Fig. 4B** and **Supplementary Video 8).** DCs extending and retracting multiple dendrites were also observed to extend into multiple alveoli at the same time. Surprisingly, quantification of both the number of extended dendrites and the total surface area (a value that increases as dendritic projections increase in number or size) shows no difference in the phenotype of cells after control or allergen challenge (**Fig. 4C,D**). As was shown in airway cell behavior, treatment with LPS did not increase DC motility or change morphology (**Fig. 4D** and **Supplementary Fig. 3C,D**). The efficacy of our LPS was shown by its ability to induce 48-hour lung-injury in studies using the same reagent (data not shown).

DCs are very responsive to tissue stressors and so we considered it possible that our section method may have induced behaviors in these cells that are not present in normal, intact lung. As we also wished to broadly test the validity of the slice model for supporting normal lymphocyte behaviors, we adopted a newly described intravital live-imaging method(Looney et al., 2011). Alveolar projections along the mucosal face of alveolar epithelial cells in CD11c-EYFP Actin-CFP lungs were again observed in control conditions (**Fig. 4F** and **Supplementary Video 9**). The number of projections was both similar to that observed using the slice method and was also conserved between control and allergen challenge conditions (**Fig. 4G**). Because AMs reside in the alveolar airspace, it is possible that filling the lung with agarose could impede their motility; however, the live imaging system also showed that AMs in mechanically ventilated lungs also demonstrate very little migration (**Fig. 4H**).

Alveolar but not airway DCs sample antigen

The position and morphological characteristics of DCs in the alveoli was consistent with an active role as phagocytes in this setting. We modified our Ova challenge protocol to include the intranasal administration of both labeled OVA (to prime immune responses) and highly fluorescent 1mm polystyrene beads at the last intranasal challenge prior to sacrifice to assess their ability to directly capture model antigens from the airspace (**Fig. 5A**). When assessed within 1 hour of antigen administration, we were able to directly observe the dendrites capturing the microspheres and retracting, bringing the antigen into the cell body (**Fig. 5B** and **Supplementary Video 10**). In this example, a subsequent dendrite projecting from the same region of the DC that did not carry the bead

outwards again during this projection, indicated that the bead had been transported into the cell body. 3-dimensional rendering confirmed that the bead was within the volume of the labeled cell (data not shown). As noted previously, we only observed this uptake in alveolar DCs but have not observed similar transepithelial bead capture by airway-adjacent DCs. In contrast, when we imaged lungs 24 hours after bead inhalation, we now also observed motile DCs within the non-alveolar interstitium, bearing beads near the airways. (**Fig. 5C** and **Supplementary Video 11**). This sequence of events strongly suggests a predominance of at least initial uptake in the alveoli followed by release and trafficking of DC into the airway-adjacent region.

In order to quantify these dynamics from images, we gated our analysis upon DCs and determined the percent of airway-adjacent DCs (defined as being 0-75μm from the airway border) versus alveolar DCs(>75 μm from the airway border) that were carrying model particulate antigen immediately after and 48 hours after bead inhalation(**Fig. 5D,E**). Because of the architecture of the lung, it is impossible to objectively define an airway-adjacent region that completely excludes alveoli. The arbitrary 75μm border was chosen to prevent bias in image analysis. We expressed the percent of bead-bearing DCs as a normalized percentage (see methods), and we only analyzed data that had bead densities within 2-fold ranges to minimize any effects due to overall density of beads (data not shown). As assessed in this way, the percent of alveolar DCs with antigen was 10% at 2 hours after inhalation, and this was very similar with allergen challenge (12%). The percent of DCs bearing beads in alveoli increased at 48 hours to 39% suggesting additional alveolar uptake and retention of some antigen-bearing cells. Again, there was

no statistically significant difference between the saline and allergen challenged mice in terms of rate of uptake, consistent with our observations of their scanning behaviors.

In contrast, DCs within 75μm of airways at 2 hours in control and allergen challenge were 6% and 0% bead-positive, respectively (**Fig. 5E**). This suggested a significant defect in the ability of these cells to ingest antigens, and we noted that the majority of the few cells that became bead positive likely had access to alveoli that lay within this cutoff distance. In saline treated control mice, this level of bead-bearing DC in the control treated condition remained low (3%) 48 hours later, showing that few antigen-bearing cells accumulated there over continuous exposure. However, in OVA allergen challenged animals, DCs bearing particles represented 18% of airway-adjacent DCs by 48 hours (**Fig. 5D,E**). One explanation for this profound rise would be that DC that ingested antigen in the alveoli and migrated toward the airway were specifically recruited and retained there in allergen challenge conditions. Alternatively, the airway DCs may capture antigens more efficiently over time and then stay within that region. While we rarely observed airway DCs to send processes across the epithelium more consistent with the former hypothesis, we sought to address the dynamics of antigen partitioning to address these possibilities.

We therefore adopted a system where saline or OVA challenged mice were given two rounds of beads with a 2-day interval between to compare immediate uptake with equilibrated pools. Mice received blue beads intranasally after their third challenge (day 23; '2-day equilibration') and red beads 48 hours later (day 25; 'immediate uptake') (**Fig. 6A**). Mice were then immediately analyzed by imaging to determine where each pool of

beads was localized. **Fig. 6B** shows airway regions in control and OVA challenged mice and demonstrates the near 1:1 accumulation of equilibrated (blue) and immediate (red) beads in control lungs but an increased prevalence of the blue equilibrated beads (13:5 ratio blue:red in the images) in allergic lungs. Quantification of the ratios of equilibrated and immediate beads by region demonstrates that airways favor 'equilibrated' beads over 'immediate' beads most prominently in allergen challenged airways (**Fig. 6B**,**C**). In control lungs, there was no specific retention of the 'equilibrated' beads at either site.

In Figure 1, we demonstrated that the majority of DCs that accumulate near the airways are CD11b+. However, several studies have shown that CD103+ DCs, which occur in very small numbers in the lung after allergen challenge, are important for traffic to the draining lymph node in other disease models. We sought to independently confirm that the retention we observed was specific to the lung airway in comparison to the lymph nodes. For this, mice inhaled a single color of bead and mediastinal lymph nodes (MLN) were analyzed after 48 hours. In contrast to the airway region, CD11b+, CD103+, and LN resident DCs were present in similar proportions in the lymph node of saline and allergen challenged mice (**Fig. 6D**) showing that, under 'sterile' allergen challenge (i.e. without overt pathogen), these cells continue to populate the draining lymph node with similar dynamics. When all beads in the lymph nodes at 48 hours were enumerated by flow-cytometry and assigned, using surface markers, to the DC subset that bore them, CD103 were represented 45% out of proportion to their frequency amongst all DC (20%) consistent with a more active trafficking role (**Fig. 6E**). In contrast with the airway, all three subsets of lung draining DCs bore model antigen at similar frequencies under control versus challenge conditions. This therefore suggests that allergic lungs

specifically retain antigen-bearing DCs within the airway-adjacent region without evidently altering lymph node trafficking. Although allergens are frequently particulate and therefore this form of uptake is possibly most relevant, we also compared these populations for uptake of a soluble fluorescent OVA conjugate via FACS. While percentages of cells were largely the same and percentages amongst phagocytes again mostly mirrored relative abundance, CD11b+ DCs were notably better at soluble antigen uptake (**Supplementary Fig. 4**). This may be a result of the enhanced access of this form of antigen to permeate the sub-airway region coupled with the overall higher frequency of this cell type (Fig. 1).

DC-T cell interactions occur near allergic airways

The use of ovalbumin as a model allergen permitted us to study the dynamics of retained DCs relative to antigen specific T cells and the degree to which interactions might be confined to this site. By transferring naïve, CD2-RFP labeled OTII T cells(Veiga-Fernandes et al., 2007) before a single IP allergen senstization, these antigen specific cells were expanded. They were subsequently recruited to the lung and mediastinal lymph node during the allergen challenge phase (**Supplementary Fig. 5A,B**). Antigen-specific T cells accumulate near airways after allergen challenge and interact with airway-adjacent DCs (**Fig. 7A, B, Supplemental Video 12** and **Supplementary Fig. 5C**). We observed T cells that move from one DC to another; however, on average, airway-adjacent T cells were in contact with at least one DC for greater than 90 percent of the time observed, thus providing ample opportunities for continued stimulation. In contrast, the few T cells that were present near alveoli were

very rarely in contact with DCs (**Fig. 7C**). We then adopted pre-activated OTII or control SMARTA (LCMV gp-specific) T cells during the challenge period to compare activities of allergen-specific and non-specific cells. Interestingly, velocities of previously activated airway-associated antigen specific OTII T cells (mean velocity = 5.1μm/min) were similar to the previously activated non-specific SMARTA T cells (mean velocity = 5.7μm /min)(**Fig. 7D**). Since previously activated cells are recruited to this space, this data implies that this airway region serves as a meeting ground where recently activated T cells may meet up with DCs that recently sampled the alveolar airspace and that neither entry nor motility are antigen-regulated. Instantaneous velocities of these cells fluctuate between nearly stopped and moving rapidly, indicating serial interactions with DCs (**Supplementary Fig. 5D**). These data suggest that the airway-adjacent region attracts activated T cells and antigen-loaded DCs in allergic lung disease where they are more likely to interact. To determine whether the serial interactions of these previously activated cells result in activation (as measured by calcium flux), activated OTII cells were labeled with Fluo-4 and CMTMR before transfer. This demonstrated that allergen-specific T cells signal upon even these transient interactions with airway-associated DCs (**Fig. 7E, F** and **Supplementary Video 13**). This data highlights that T cells and DCs are dynamically engaging in contact rather than assembling as stable static structures, giving rise to a continuously evolving microenvironment that affects the ongoing immune response.

Discussion

An important finding of this work is the regional segregation of DC behaviors resulting in separated antigen surveillance and presentation within the lung despite no changes in sampling behavior after allergen challenge. Importantly, the behavior of DCs in the lung is not well represented by what was previously observed in the trachea, which has been the site of choice for analysis of DC phenotype, morphology and dynamics(Jahnsen et al., 2006; Lambrecht et al., 1998). The alveolar regions of lung favor uptake, with almost every DC visualized having dendrites into the surfactant layer. In contrast, the airway is a site of antigen-bearing DC accumulation and T cell activation.

Alveoli: A Competitive Landscape for Antigen Capture

Alveolar macrophages, as professional phagocytes, account for approximately 95% of bronchoalveolar lavage (BAL) leukocytes and are therefore considered as the sentinel phagocytic cells of the respiratory tract(Martin and Frevert, 2005). Yet, DCs appear to be the primary cells to carry antigens for presentation to T cells, particularly in asthma(van Rijt et al., 2005; Vermaelen et al., 2001; McWilliam et al., 1996). Our study generates a vivid picture of the varied uptake strategies of these cell types. In both intravital and lung-slice imaging, AMs are immotile within alveoli and likely require antigens to come to them. In contrast, alveolar DCs actively scan and take up antigens as they 'sweep' the alveolar air space. Both of these cell types likely benefit from the surfactant layer providing a medium for the collection of inhaled particles or pathogens, reducing the distance DCs must travel into the alveolus in order to sample its contents.

The uptake capacity of alveolar DCs was clearly shown by the active uptake of inhaled particulate antigen from the alveolar air space.

A further competition likely occurs between DC subsets. Recent studies have emphasized the distinction between CD103+ and CD11b+ DCs in traffic and presentation capacities within the barrier tissues of the body. In the lung, CD103+ DCs have been shown to play an important role in immunity to viral infection(Lukens et al., 2009) and carry apoptotic cell debris to the draining lymph node(Desch et al., 2011). The location and sampling behaviors of these DCs have not been reported in the lung nor have changes during non-pathogenic allergen responses been compared. Here we describe that the few CD103+ DCs in the lung are distributed throughout the tissue while CD11b+ DCs are present throughout the lung and accumulate near the airways after allergen challenge. The presence of CD11b+ DCs in greater numbers and near the airways suggests the importance of CD11b+ DCs instead of CD103+ DCs in the ongoing pathogenic immune responses that are associated with asthma.

Because recruited CD11b+ DCs have been proposed to arise from inflammatory monocytes(Lambrecht and Hammad, 2009), it is possible that recruited monocytes also compete for antigen within the lung. Monocytes might be predicted to extravasate into the interstitium or into the surfactant layer. There, they may ultimately differentiate into one of the other DC cell types and contribute to the accumulations we observe. The role that they play as phagocytes prior to such differentiation is not yet clear but may reveal additional mechanisms and sites for antigen uptake.

Despite having a very low average speed, analysis of many cells identified a motile population of alveolar DCs. These slow but migratory DCs likely contribute to

antigen trafficking and the accumulation of DCs at the airway after allergen challenge. While we did not discern directional migration towards airways for DCs located more than 75μm from the airways (data not shown), those located near the airways were largely retained in the clusters there. This would suggest two steps in the recuitment of DCs to the airway after allergen challenge; one that leads to release of DC in the alveoli and a second, likely chemokine, that captures the cells when they are sufficiently close to the chemokine source. Future studies identifying the factors that elicit these cells to leave their positions in the tissue or those that capture them into the DC clusters may allow for the process to be perturbed for theraputic means.

Regional Segregation of Antigen Surveillance and Presentation in the lung

Cellular projections into airspace have been reported across human nasal mucosa of allergic rhinitis in situ, where dendrites penetrate beyond well-developed epithelial tight junctions(Takano et al., 2005). Similar findings were reported in a rat tracheal model in which 1–5% of intraepithelial dendritic cells were observed to extend projections into the airway lumen, both under steady-state conditions and during inflammation(Jahnsen et al., 2006). The airways, fundamental sites of asthma responses, were notably sparse with these projections. And, while we routinely confirmed that our protocol reproducibly generated eosinophilia and airway hypersensitivity (data not shown), it did not lead to increased dendritic probing at the airway. This highlights the differences between nasal epithelium, trachea, large airways, and alveoli.

Another level of regional difference is evident because dendritic projections in the alveoli are largely independent of allergen or TLR challenge. This differs from the

reports of transepithelial surveillance by DCs in the gut where TLR stimulation leads to increased surveillance(Chieppa et al., 2006). While fixed tracheal sections have demonstrated that DCs are capable of making projections there(Jahnsen et al., 2006), live imaging of TLR-dependent changes have focused on increased motility of DCs in sub-epithelial regions. This increased mobilization was shown to be dictated by TLR signaling in epithelial cells rather than in the DCs themselves(Lambrecht and Hammad, 2009). As we demonstrate, TLR4 expression is vastly different between trachea and lung. It is therefore likely that regional differences in the epithelia play a key role in determining responses to inhaled material at distinct sites.

One possible model from this data is that pathogenic microbes detected in the trachea or nasal mucosa could generate a 'danger' response leading to DC uptake, trafficking and generation of active immune responses. In contrast, the distinct absence of these projections in airways may ultimately protect the delicate and critical conducting airways from all but the most dangerous pathogens that make it deep into the lung or breach the epithelium. At the deepest levels, alveolar DCs may exist to sample for fulminate bacterial or helminth infections. These DCs may be capable of both priming a response in the lymph node and, through an as-yet-undiscovered mechanism, be successfully retained to boost effector responses near the affected airway. Asthma, in this model, may result from the over-retention of antigen-bearing DCs near the airways, which activate the already-primed Th2 T cells from the circulation.

Regional retention of CD11b+ DCs near airways is the basis for a new model DC contribution to the pathogenesis of asthma (**Supplementary Fig. 6**). Lymph node CD11b+ DCs have been shown to play an important role in CD4 T cell

priming(Jakubzick et al., 2008b). Activated T cells are recruited to the areas of DC accumulation and swarm along the surface of these DCs, without arresting in order to signal. Calcium fluxes observed in these motile airway-associated T cells likely reflect the lower activation threshold of previously activated T cells, making the airway a site for antigen specific re-priming. While this data points to DC re-priming of CD4 T cells, there may be additional maturation of DC that is a consequence of this interaction. Indeed we note that DCs from allergen challenged lungs have higher Class II expression. Although methods do not exist to test this prediction, it is interesting to speculate that the T-APC clusters we visualize may also represent the precursor to bronchus-associated lymphoid tissue (BALT) and that similar foci may form at these sites in response to infections.

Dynamic Imaging in the Lung

Two-photon imaging has been successfully applied to immune cells in multiple sites including lymph nodes, spleen, brain and gut. This study provides insight into the nature of immune cell dynamics in lung airways and alveoli. While the lung slice model(Bergner and Sanderson, 2003) has been previously established as a suitable model for studying smooth muscle contractility, it was not established that this slice method would preserve the behaviors of immune cells. Our demonstration that DCs, whose behaviors are thought to be very sensitive to tissue damage, function similarly in the slice model as compared to intravital imaging provides validation for its use in future experiments. Future investigators will want to be wary of the pitfalls of the slice model that include cell death near the cut site and the absence of incoming cells via the blood or

egress via the lymph. However, the method avoids challenging surgeries and tissue stabilization procedures(Looney et al., 2011), provides an ideal mechanism by which to perfuse in reagents or cells, is amenable to higher throughput, and allows observation of airways distant from the lung surface. A similar side-by-side comparison of T cell motility in excised lymph node as compared to intravital lymph node imaging(Miller et al., 2002; 2003) has provided the basis for many exceptional studies using the organ model. It will be important for each subsequent study to assess the validity of observations in slice-models using criterion specific to the questions being addressed.

Further implications for Lung Immunity

It is important to note that pathogens may compound and alter the DC recruitment that we observed with allergen challenge. For example, increases in DC number in the lung, particularly along the trachea are also seen in viral infection(McWilliam et al., 1996). Infection with *Mycoplasma pulmonis* leads to increases in lung DCs even more pronounced than that seen after acute allergen challenge (EET, unpublished observation). Bacterial, viral, and mycoplasma infections have also been associated with exacerbations of asthma(Tan, 2005; Martin et al., 2001; Kraft et al., 1998), and lung DCs have been shown to stimulate T cells after viral infection(Hamilton-Easton and Eichelberger, 1995).

One interpretation of these previous findings in the context of our observations is that a pathogen-mediated accumulation of DCs in the lung results in more antigen uptake and presentation by these inflammatory DCs within the lung. Pathogens can also cause an increase in DC activation state due to TLR signaling mediated by the pathogen and thus exacerbate responses to allergens. It remains to be determined if these multiple insults

might also lead to variations in the site and timing of interactions between antigen-loaded DCs and naïve or effector T cells. Specifically, in settings where different DC subsets appear to play dominant roles (i.e. CD103+ in viral and CD11b+ in asthma responses) it will be important to understand which cells dominate and how they affect the subsequent responses. The interactions between T cells and DCs seen in peri-airway regions likely allow for adaptive immune responses to allergens to occur quickly, without the need for cells to traffic to the draining lymph node. These data correlate with the late phase of the asthma response, which is an adaptive response but begins only 8 hours after allergen inhalation(Wenzel et al., 2007).

This study sheds light on several steps in the immune response to an allergen that may be targeted for therapy. Antigen uptake, DC accumulation, and T-DC interactions occur sequentially and may therefore be targeting separately or concomitantly for effective therapy. Since we have shown the importance of alveolar uptake, it is important to consider the ability of therapeutic agents to reach the distal portions of the lung. Future studies should address possible mechanisms to target antigen away from CD11b+ DCs and toward a possibly tolerogenic pathway. Our data examines a "naked" model antigen, but antigens coated with biologically relevant molecules may represent a prospect for therapy if they can be targeted away from airway-retained populations. Conversely, targeting depleting agents to these cells may also block the pathogenic immune response. In that respect, previous studies have shown preferential uptake of bacteria by AMs(Pedroza-González et al., 2004). More study is also required to address the factors that lead to the accumulation of antigen-bearing DCs and previously activated T cells in the airway-adjacent region. Blocking antigen traffic and/ or T cell recruitment may

prevent productive T cell activation and delay or prevent the onset of severe symptoms at the airway.

Figures

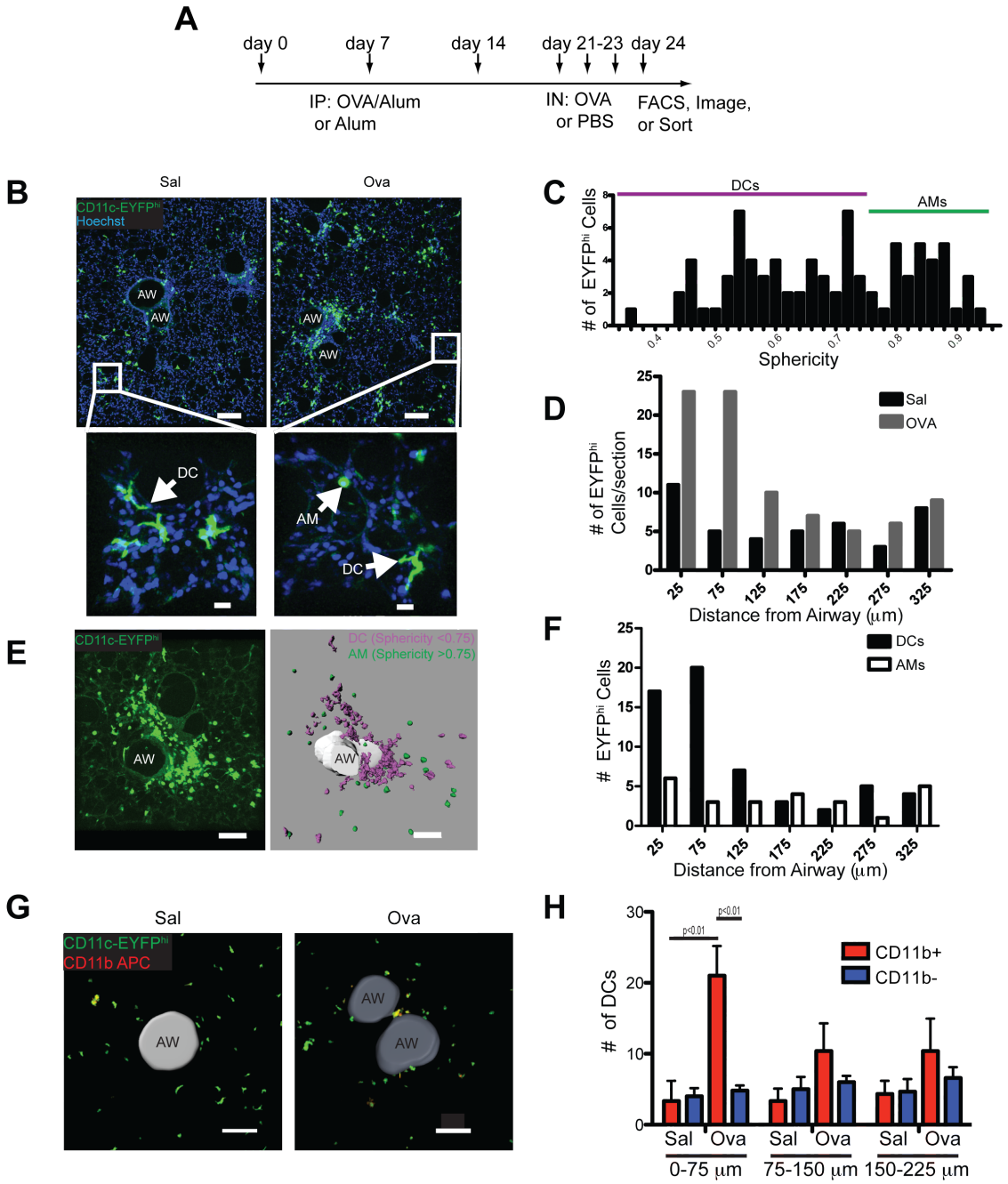

Figure 1. Specific accumulation of CD11b+DC near allergic airways.

(A) Method for inducing allergic airway inflammation involving three intraperitoneal (IP) sensitizations with Ova/Alum followed by three intranasal (IN) administrations of either Ova or Saline. **(B)** Large-scale 3D surveys of >300 mm slices from CD11c-EYFP mice

stained with Hoechst (blue) shows DC and AM distribution in control and Ova allergen challenged mice obtained by two-photon microscopy with 910 nm excitation. Insets provide a zoomed in view of the two distinct morphologies. Scale bar represents 100μm for large panels. Scale bars represent 10μm for zoomed sections. **(C)** Measurement of sphericity allows for separation of DCs (purple line) from AMs (green line) with AMs having a sphericity greater than 0.8. **(D)** Quantification of data from an allergen challenged mouse shows accumulation of CD11c-EYFP+ cells near the airways. **(E)** When images are subdivided by sphericity, the data shows that DCs but not AMs account for the accumulation within 75μm of the airway post allergen challenge. **(F)** Color-coding of localization based on sphericity with bulk CD11c-EYFP data shown on the left and subdivided data (DCs purple, AMs green, airway white) on the right from an ova allergen challenged mouse. Scalebar represents 100μm. **(G)** Example images from CD11c-EYFP sections (gated on EYFP+ sphericity <0.75) stained with CD11b APC. Scale bar represents 150μm. **(H)** Quantification of CD11b+ and CD11b- DCs distance from the nearest airway for saline and Ova challenged mice. Graphs represent at least 5 mice per group from at least 3 independent experiments. Images are representative data from at least 3 independent experiments.

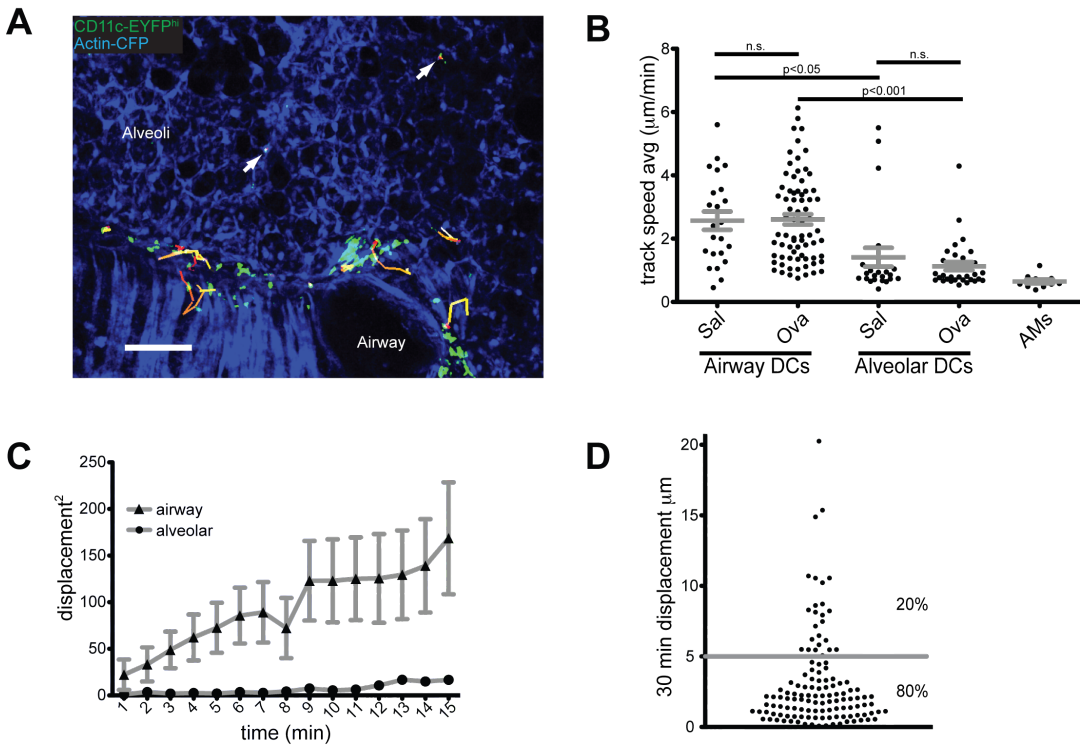

Figure 2. Airway and alveolar DCs exhibit different behaviors.

(A) Detailed image with overlaid tracks of cell motility at airway surfaces and alveolar spaces over the course of two hours. The top half of the image is mostly alveoli while the bottom is mostly airway. Arrows indicate alveolar DCs. Scalebar represents 100μm. **(B)** Track speed averages calculated by Imaris for CD11c-EYFP DCs and AMs separated by airway and alveolar location and saline and Ova allergen challenge conditions. **(C)** Mean squared displacements as a function of time for alveolar (circles) or airway-adjacent (triangles) DC from control mice. **(D)** 30 minute displacement for alveolar DCs from allergen challenged mice. Data is from at least 3 independent experiments.

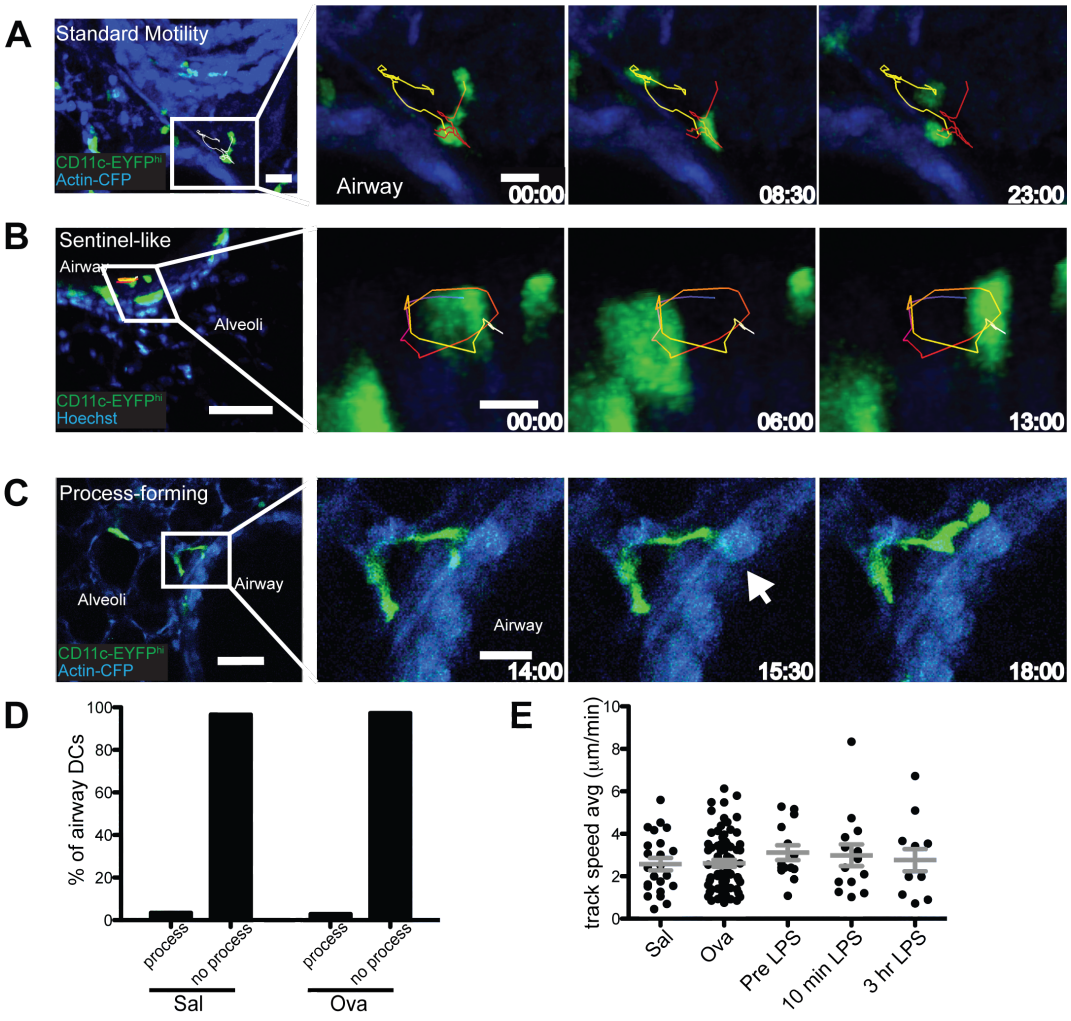

Figure 3. Airway DCs are motile but send few processes through the epithelium

(**A**) Example representative motility of airway-adjacent DCs. Entire field for orientation (left) followed by zoomed images from relevant regions, collected at indicated times. Scale bars represent 25mm for initial image. Scale bars represent 15mm for following images. (**B**) 'Sentinel'-like Motility of CD11c-EYFP cells on the inner surface of an airway obtained using two-photon microscopy and rendered in Imaris. Scale bars represent 50mm for initial image. Scale bars represent 10mm for following images. Time stamp min:sec. (**C**) DCs marked by CD11c-EYFP in Actin-CFP background uses a process (indicated by arrow) to probe airway epithelium. Scale bars represent 50mm for

initial image. Scale bars represent 15mm for following images. (**D**) Quantification of processes from airway DCs across airway epithelium in saline treated or allergen challenged mice (3% of DCs in both cases). (**E**) Track speed averages of airway DCs from saline control, Ova allergen challenged, before LPS treatment, after 10 min of LPS treatment, and 3 hours of LPS treatment. Images are representative images from over 12 mice per group. Quantification of track speed averages are combined data from three separate experiments.

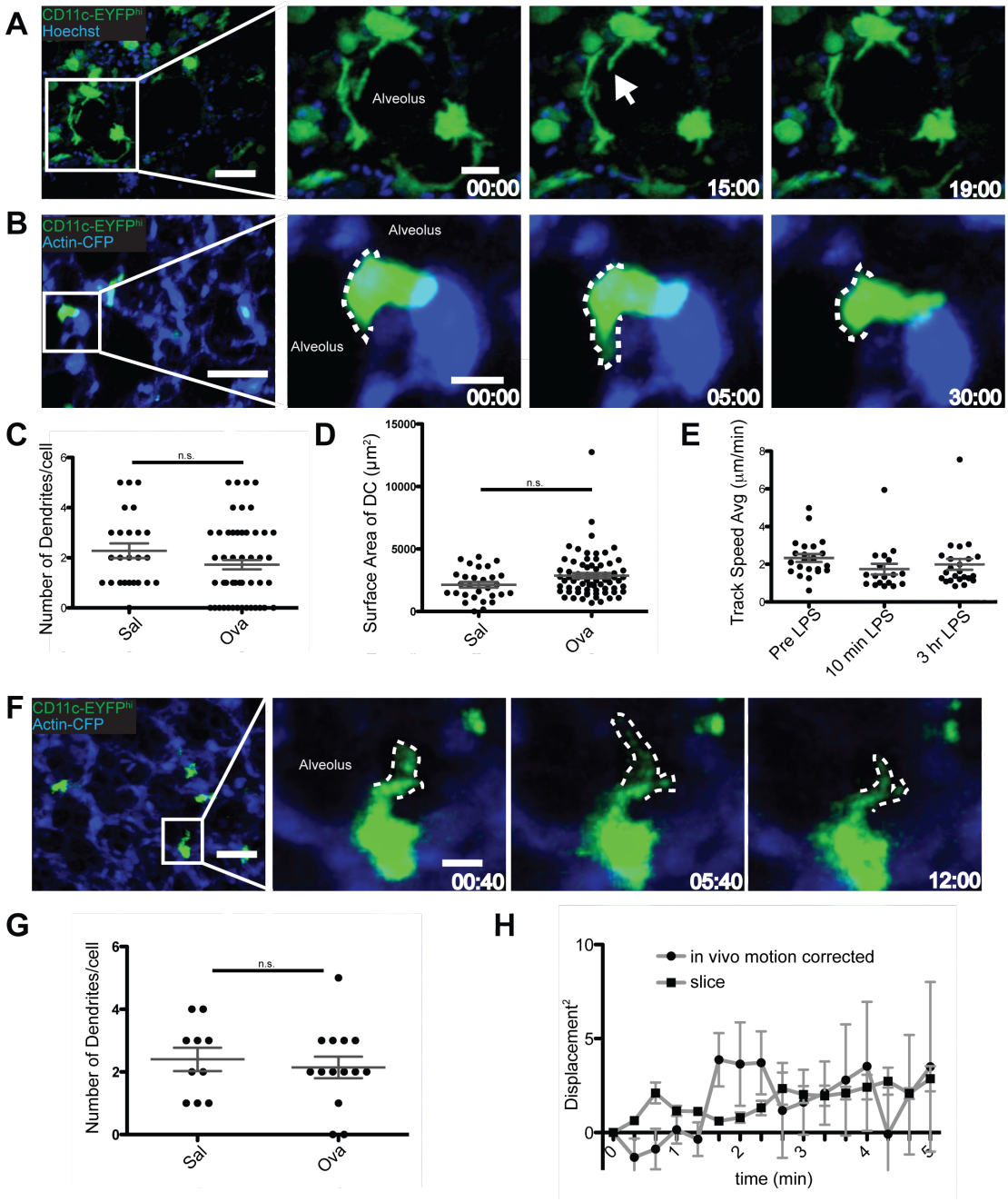

Figure 4. DCs sweep the alveolar air space using transepithelial dendrites.

(A) Motility of CD11c-EYFP DCs in the alveolus of an Ova challenged mouse stained with Hoechst (blue). Scale bars represent 50µm for initial image and 20µm for following images. **(B)** Alveolar motility of a CD11c-EYFP DC in a saline treated Actin-CFP mouse. Dotted line traces dendrite surface. **(C)** Quantification of dendrite numbers per

DC for saline and Ova allergen challenged lungs. **(D)** Surface area of DCs from saline and Ova challenged mice calculated using isosurface tool in Imaris. **(E)** Track speed averages of alveolar DCs before LPS treatment, after 10 min of LPS treatment, and 3 hours of LPS treatment. **(F)** Intravital *in vivo* motility of a CD11c-EYFP DC in the alveolus of an Actin-CFP mouse that is anesthetized, ventilated, and imaged with two-photon microscopy. Scale bars represent 50μm for the initial image and 10μm for following images. Dotted line traces dendrite surface. **(G)** Quantification of intravital *in vivo* dendrite numbers per DC for saline and OVA challenged lungs. **(H)** Mean squared displacements as a function of time for AMs from *in vivo* lungs corrected for breathing artifacts with type II epithelial cells versus sectioned lungs. Images are representative images from over 12 mice per group for slice and 4 mice per group for live imaging. Quantification of dendrites, surface area, and track speed averages are combined data from three separate experiments.

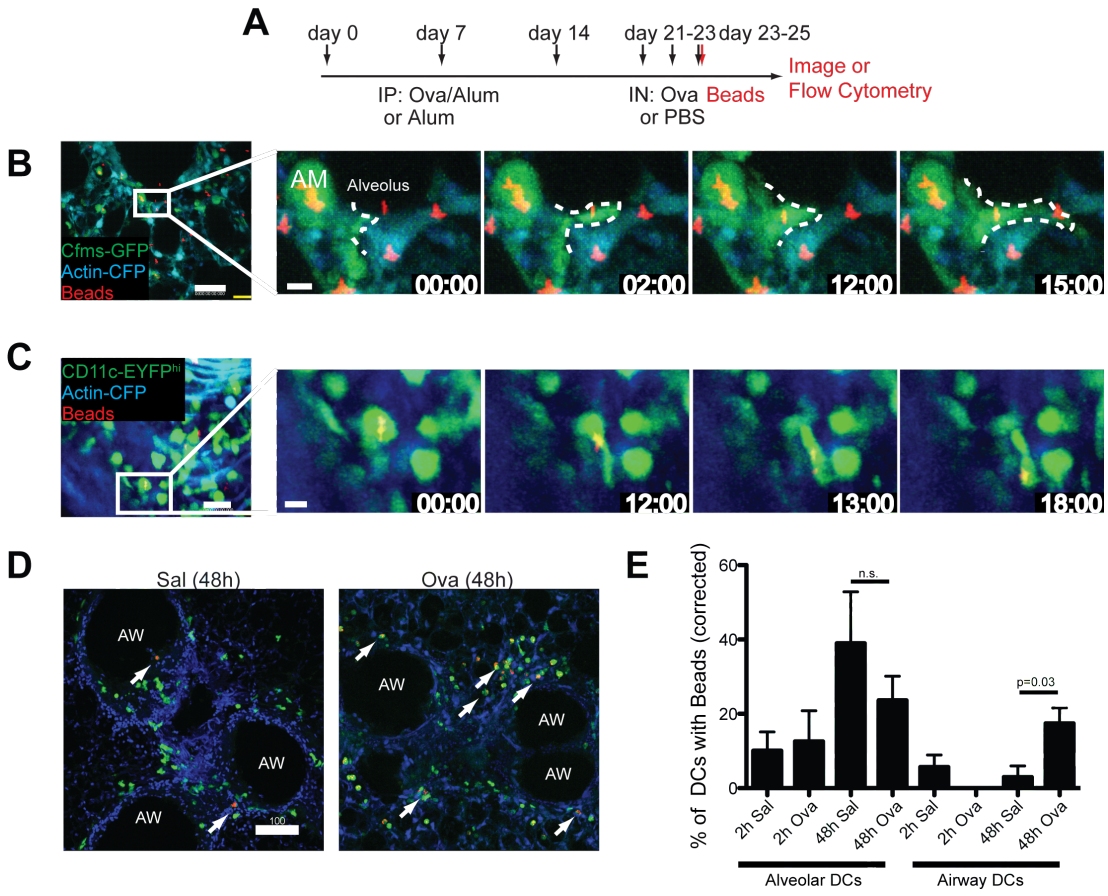

Figure 5. DCs directly phagocytose inhaled antigens and accumulate model antigen in airway-adjacent regions.

(A) Scheme for allergen challenge includes three intraperitoneal injections of OVA/Alum and three intranasals of OVA (black arrows) followed by an intranasal of labeled antigen (red arrow). **(B)** Stills of a movie from a *c-fms*-EGFP (green) Actin-CFP (blue) mouse 1hr after intranasal with 1 mm fluorescent polystyrene beads (red). Note extension, uptake, retraction and re-extension of indicated DC. Also note round AM to the left of the DC, within the alveolus. **(C)** Migration of CD11c-EYFP cells just below the surface of an airway of an Ova treated lung stained with hoechst (blue) 24 hrs after bead (red) inhalation. **(D)** Representative image of airway associated, antigen bearing DCs in saline and Ova allergen challenged mice. Arrows indicate DCs with beads. Scale bar represents

100μm. **(E)** Quantification of proportion of alveolar and airway associated DCs that contain beads immediately after and 48 hours after bead inhalation. All images are representative of at least 4 mice per group from four independent experiments. Quantifications include data from 4 independent experiments.

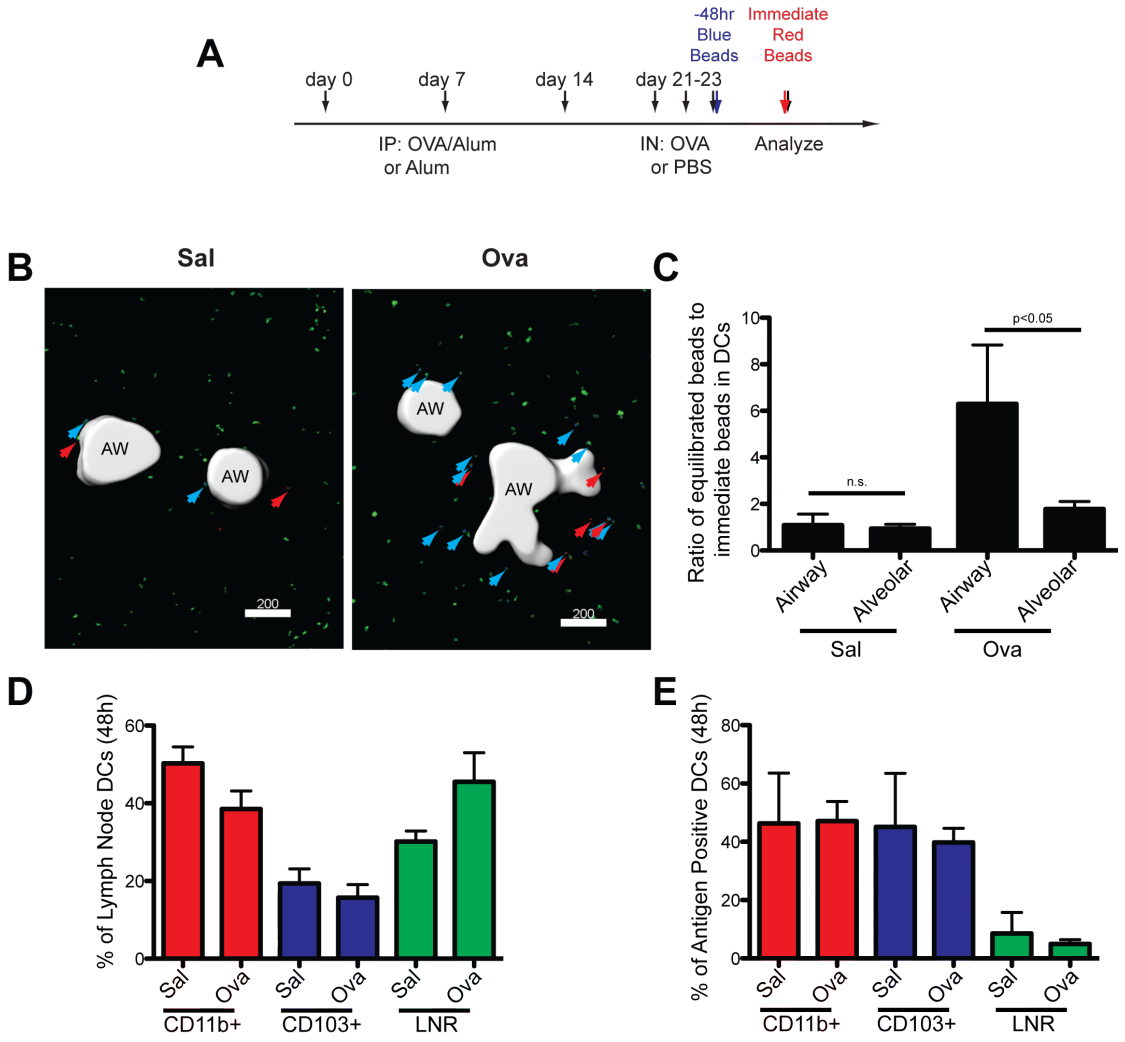

Figure 6. DCs carry model antigen to airway-adjacent regions as well as lymph nodes. **(A)** Scheme for allergen challenge includes three intraperitoneal injections of OVA/Alum and three intranasals of OVA (black arrows), an intranasal of red beads (red arrow), and an intranasal of blue beads (blue beads) to dissect uptake versus trafficking. **(B)** Example images of beads in CD11c-EYFP DCs. Arrows indicate example beads in DCs. Scale bar represents 200 μm. **(C)** Quantification of beads in CD11c-EYFP DCs. The airway region is defined as 75 mm from the inner airway surface.

(D) CD103, CD11b, and lymph node resident DC populations are compared by FACS after saline or Ova allergen challenge. **(E)** The population of DCs carrying model antigen

to the lymph node is analyzed by phenotype, showing similar numbers of CD103 and CD11b positive DCs with model antigen 48 hours after bead inhalation. All data represents at least 8 mice per group from at least 5 independent experiments.

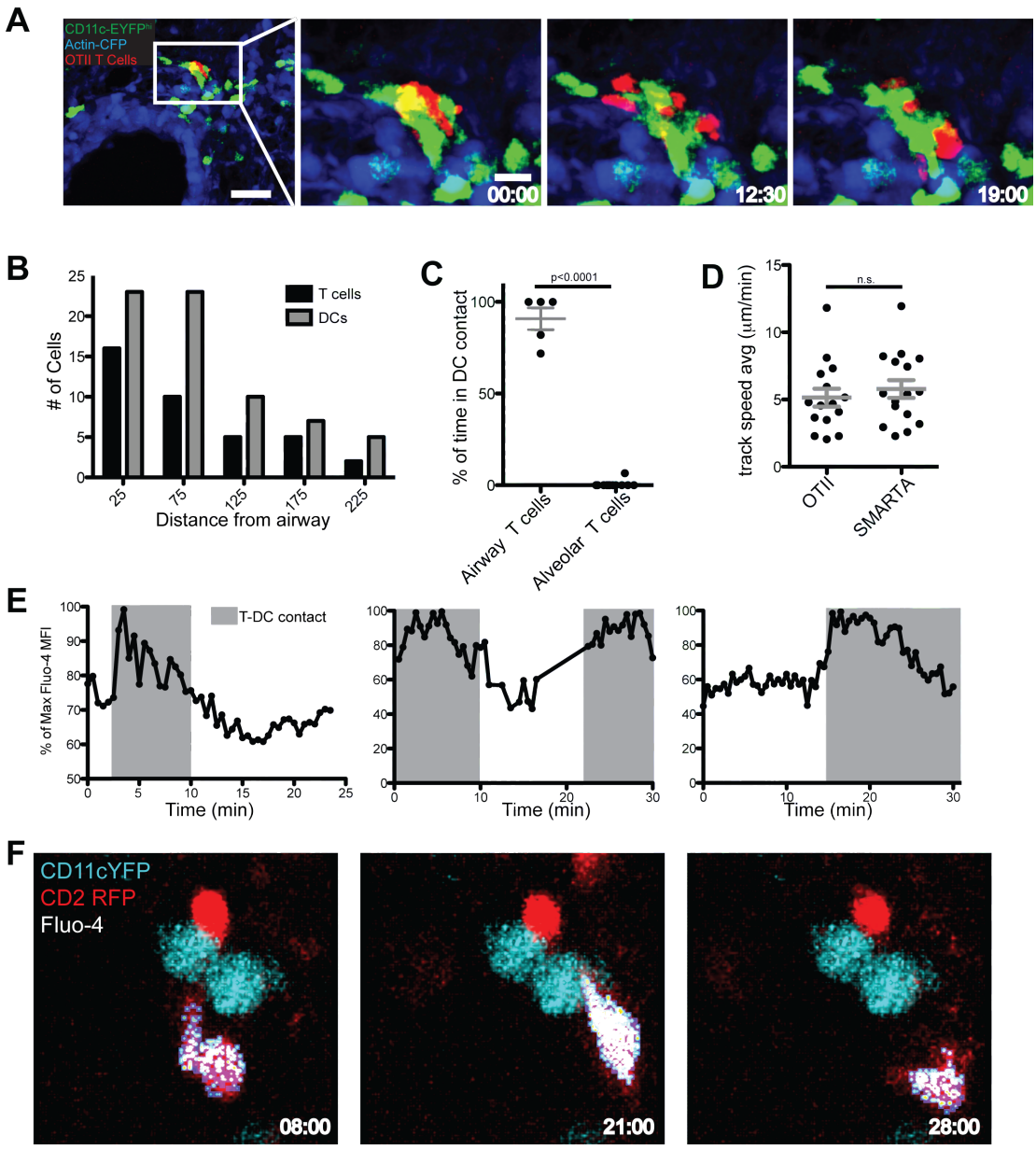

Figure 7. Activated T cells interact with airway-adjacent DCs.

(A) OTII T cell accumulation within 75mm of a representative airway compared with DC accumulation within the same area. **(B)** Interactions of T cells (red) and DCs (green) illustrated by a time course showing T cells swarming over the surface of multiple DCs but always remaining in contact with at least one. Scale bars represent 50μm for the first frame and 15mm for following images. Time stamp min:sec. **(C)** Percent of duration of a

30 minute movie that OTII T cells were in contact with at least one DC in either the airway or alveolar region. **(D)** Track speed averages for previously activated antigen specific (OTII) or non-specific (SMARTA) airway T cells. **(E)** Percent of maximum mean fluorescence intensity of Fluo-4 in previously activated T cells. Grey background indicates the time that T cells are in contact with a DC. **(F)** Transferred T cell stained with CMTMR (red) and Fluo-4 (gated on the CMTMR signal of the cell, pseudocolored) moves toward an airway, transiently interacting with a DC (teal) on the way. Images and quantification are representative of at least 3 mice per group from at least 3 independent experiments.

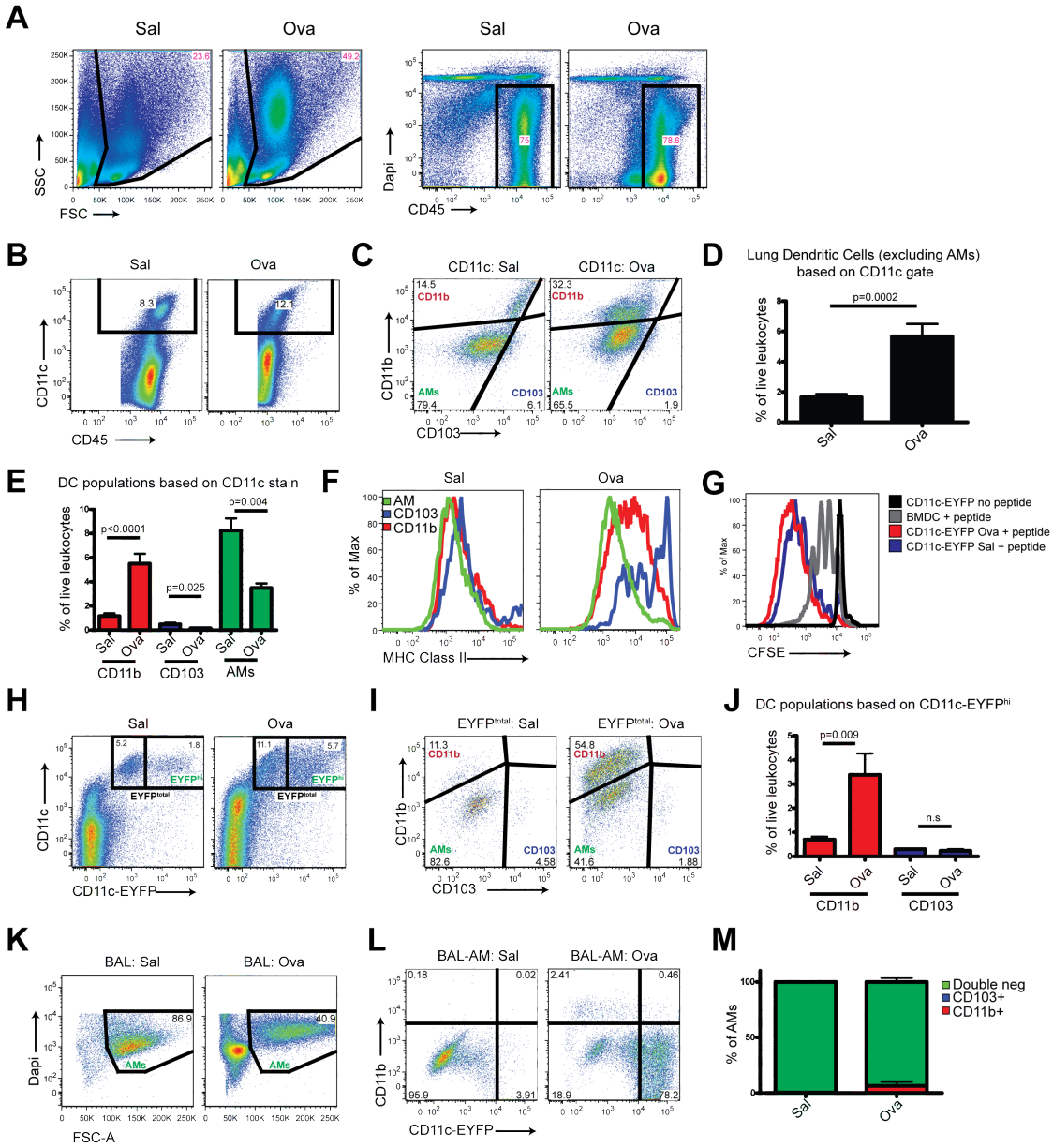

Supplementary Figure 1. CD11b+ DCs accumulate in allergen challenged lungs, and CD11c-EYFP+ cells sorted from the lung can stimulate naïve T cells.

(A) Gating strategy for all FACS experiments shows FSC vs SSC for size exclusion (top). The subsequent gate shows dapi- CD45+ gates for live leukocytes (bottom). **(B)** Enrichment of CD11c positive cells (Dapi- CD45+ gated) in single cell suspensions from lungs following control (Sal:left) and Ova allergen challenge (Ova:right). **(C)**

Predominant expansion of CD11b+ cells within the CD11c+ gated cells from A. Percentages refer to gates that delineate CD11b+ DCs, CD103+ DCs, and alveolar macrophages (AMs) for saline control (left) and Ova allergen challenge (right). **(D)** Quantification of proportion of live leukocytes in the lung from combined CD11b+ and CD103+ DC populations in saline or Ova allergen challenged mice. **(E)** Quantification of CD11b+ DCs (red), CD103+ DCs (blue), and AMs (green) in saline and Ova allergen challenged mice. **(F)** Histograms of MHC class II expression for CD11b DC (red), CD103+ DC (blue), and AM (green) populations from saline and Ova allergen challenged mice. **(G)** CFSE dilution of naïve OTII T cells after 3 days in the presence of sorted CD11c-EYFP cells or bone marrow derived dendritic cells (BMDC). **(H)** CD11c-EYFP transgene expression versus CD11c antibody staining (Dapi- CD45+ gated). Note similarities to panel Supplementary Fig. 1B. **(I)** CD103 versus CD11b plot of CD11c-EYFP^{total} gated cells. Gates delineate CD11b+ DCs, CD103+ DCs, and alveolar macrophages (AMs) for saline control and Ova allergen challenge. **(J)** Quantification of CD11b+ DC and CD103+ DC populations gated on CD11c-EYFP^{hi} cells in saline and Ova allergen challenged mice. Note similarity to Supplementary Fig. 1D. **(K)** Bronchoalveolar lavage (BAL) from saline and ova allergen challenged mice used to gate on alveolar macrophage populations gated as Dapi- and FSC+. **(L)** FACS plots of CD11c-EYFP versus CD11b of AM gated populations taken from J for saline and Ova allergen challenged mice. **(M)** Quantification of CD11b and CD103 expression on AMs in saline and Ova allergen challenged mice.

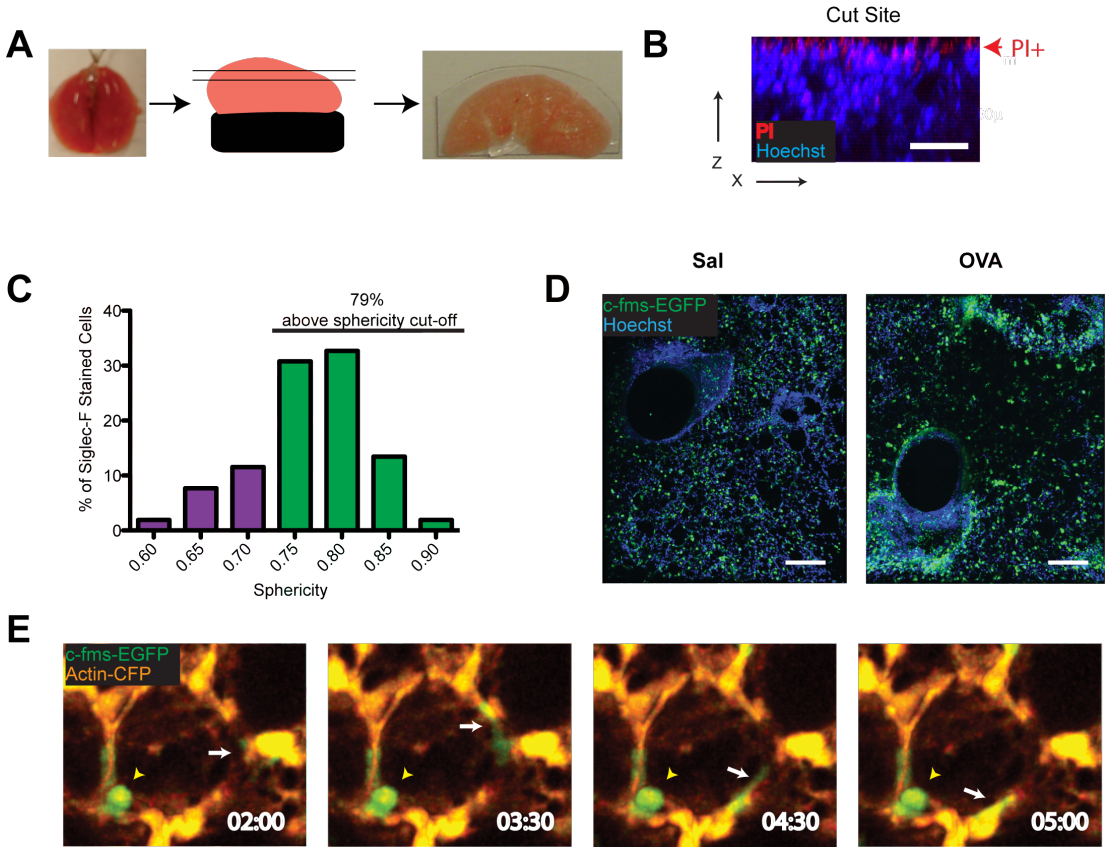

Supplementary Figure 2. Imaging of lung slices stained with antibodies define AMs and DC populations.

(A) Method of lung preparation for live imaging. Lungs were filled with 2% low melting temp agarose, cut into >300mm sections using the vibratome, and affixed to a plastic cover slip. **(B)** Exclusion of PI in lung sections 4 hrs after cutting. Propidium iodide (red) is effectively excluded from cells below the cut site of an Actin-CFP mouse (blue). Scalebar represents 100 μm. **(C)** Imaris was used to make surfaces of Siglec-F+ CD11c-EYFP+ cells from Ova challenged mice. The sphericity of these cells is graphed, showing about 80 percent of Siglec-F staining AMs are captured by the sphericity measurement. **(D)** As an alternative means to mark most cells of the monocytes lineage and to delineate AMs in control mice, we used *c-fms*-EGFP mice in which GFP is expressed from the CSF-1R locus(Sasmono et al., 2003). Monocytes, neutrophils, DCs,

and alveolar macrophages are all marked using this strategy. Surveys of *c-fms*-EGFP (green) lung sections stained with Hoechst (blue) show a population comprised of round putative alveolar macrophages distributed throughout the alveoli, other more-amoeboid neutrophils, as well as a population of the elongated dendritic cells, and monocytes. **(E)** Imaging of *c-fms*-EGFP Actin-CFP alveoli showing nearly immotile AM and rapidly moving amoeboid cell, likely a neutrophil. The yellow arrow indicates the non-motile, round AM in the alveolus. The white arrow indicates a neutrophil or monocyte moving rapidly through a blood vessel.

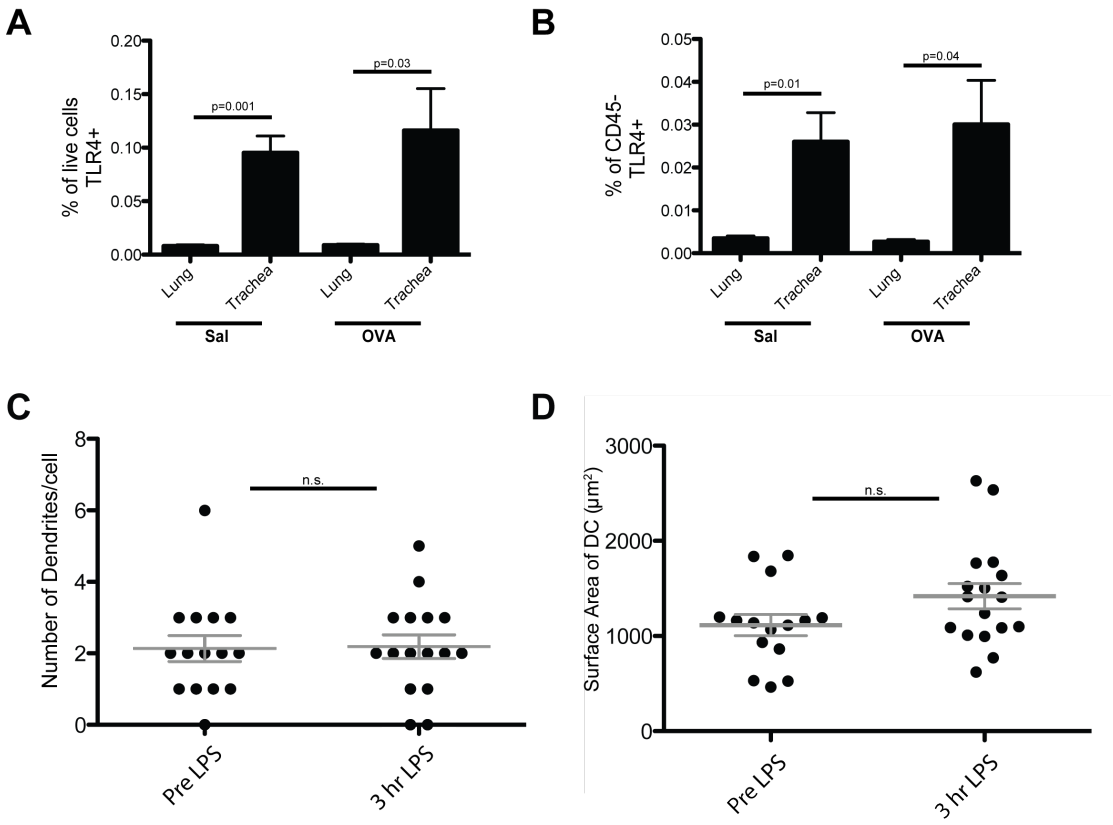

Supplementary Figure 3. TLR4 is more widely expressed in trachea than the lung. **(A)** Percent of total live cells that stain positive for TLR4 shows a greater than 10 fold increase in the trachea compared to the lung. **(B)** The percent of CD45- cells that are TLR4+ is also greatly increase in the trachea compared to the lung. **(C)** Number of dendrites per cell is quantified before and after 3 hrs of LPS exposure. **(D)** Surface area of alveolar DCs is quantified before and after 3 hrs of LPS exposure.

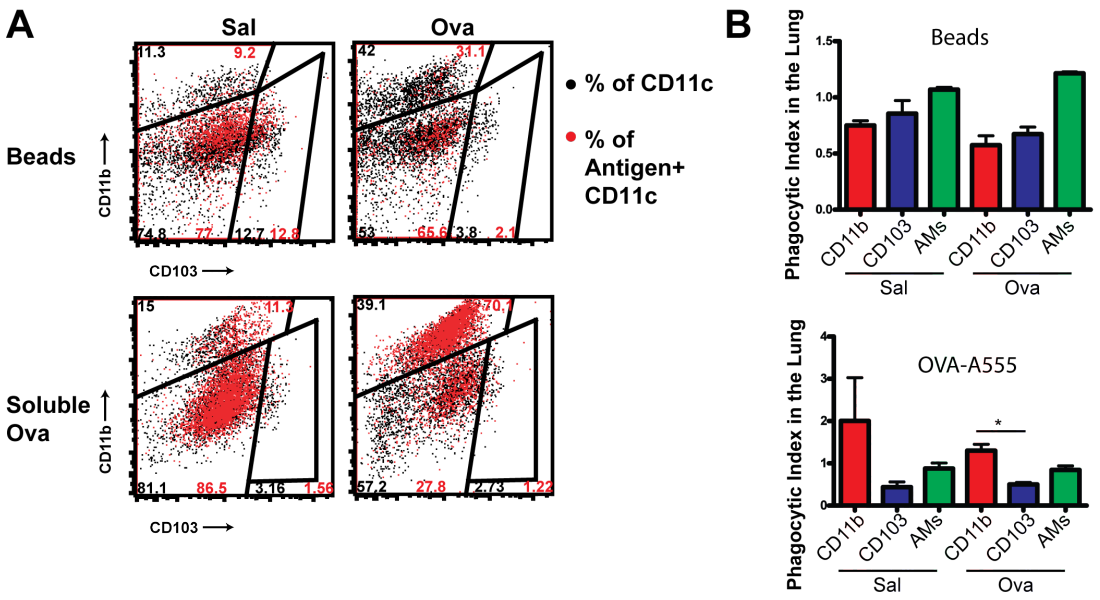

Supplementary Figure 4. Lung DCs efficiently take up antigen before and after allergen challenge.

(A) FACS analysis of gated dapi-CD45+CD11c+ showing CD103 versus CD11b populations. Percent of CD11c population (black dots) is compared with percent of CD11c bearing model antigen (beads above, OVA A555 below) positive cells (red dots).

(B) A phagocytic index generated as the ratio of CD11b, CD103, and AM which are CD11c+model antigen+ cells to CD11b, CD103, and AM which are CD11c+. Note similarity under beads but augmented uptake of Ova by CD11b+ cells, possibly due to the enhanced access of this form of antigen to permeate the sub-airway region. Because another possible reason for the difference between bead uptake and soluble OVA uptake could be the presence of OVA itself, we separately compared uptake of beads that were coated with OVA versus uncoated and obtained identical results indicating that, in this model, antigen-specific uptake was not a primary mechanism (data not shown).

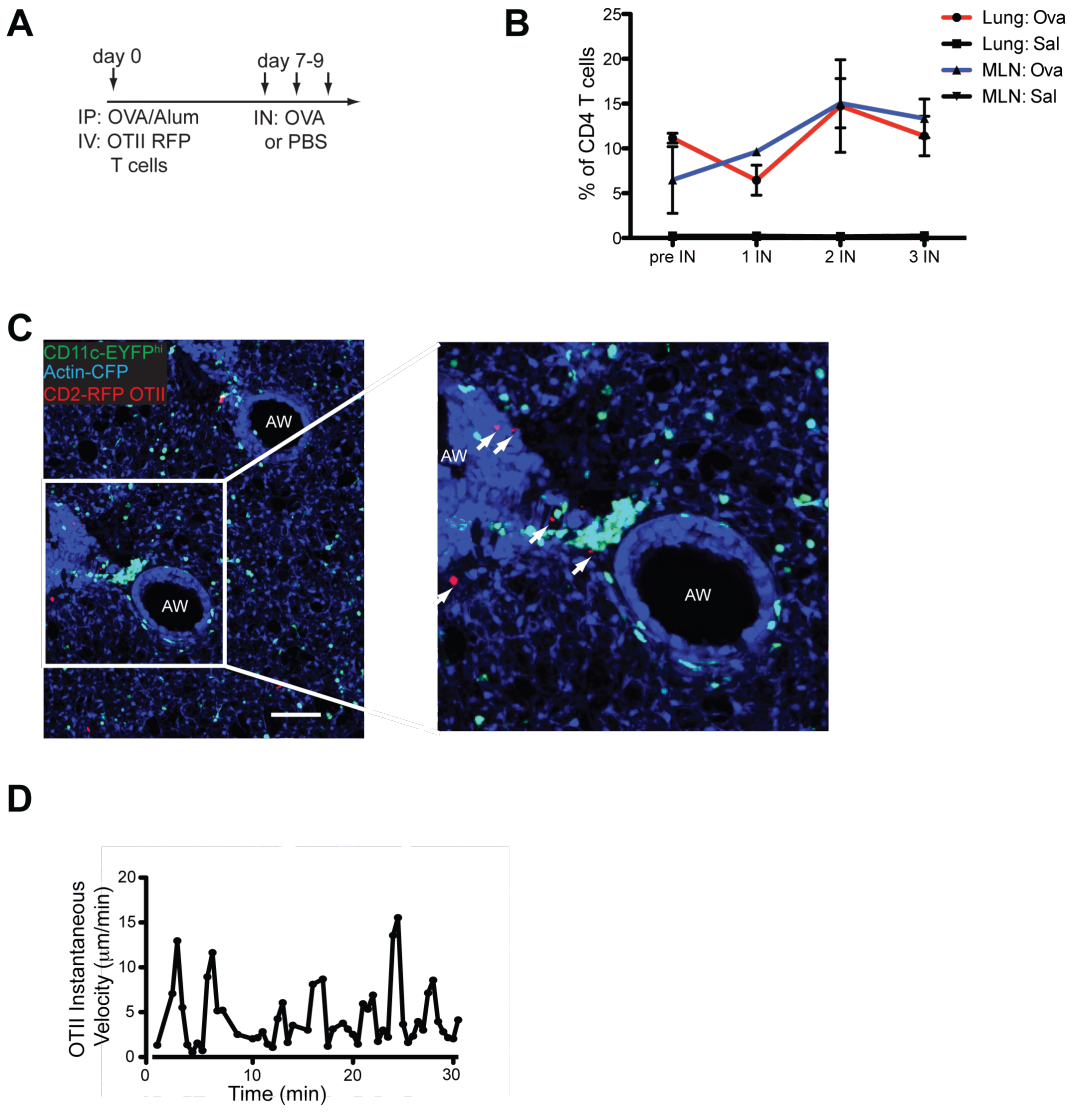

Supplementary Figure 5. T cells accumulate in the lung and mediastinal lymph node (MLN) after allergen challenge.

(A) A shortened protocol was developed for T cell transfer experiments that involves transfer of $1x10^6$ OTII RFP T cell at the time of sensitization followed by three intranasals with Ova. **(B)** FACS analysis of the T cell population in the MLN and lung before and after each of the Ova intranasal administrations. OTII RFP T cells are measured as a percent of total CD4 T cells recruited to the MLN and lung. Antigen

specific cells are specifically recruited to the lung and MLN after antigen challenge, growing to 10% of the CD4 pool. **(C)** Survey image of OTII T cells in the lung with a zoom in to show T cells present around the airway. Scale bar represents 150 μm. **(D)** Instantaneous velocities for an example airway-associated OTII T cell in contact with airway-associated DCs.

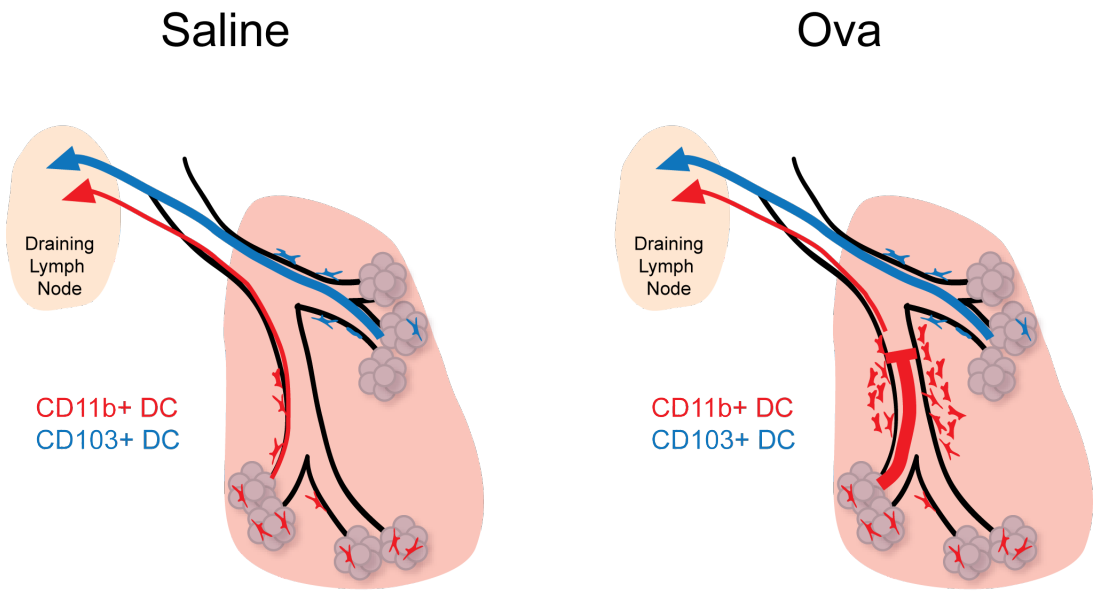

Supplementary Figure 6. Model of antigen uptake and DC traffic after allergen challenge.

A model for CD11b+ and CD103+ DC trafficking in the steady state suggesting increased basal transport of antigen to lymph nodes by CD103+ DC relative to CD11b+ DC. In allergen challenge conditions, little variation in CD103+ antigen trafficking is observed and scanning behaviors at each site remain unchanged. However, CD11b+ DC specifically accumulate in airway-adjacent regions.

Materials and Methods

Mice

All mice were bred and housed in specific pathogen free housing and in accordance with the guidelines of the Lab Animal Resource Center of the University of California at San Francisco (San Francisco, California). All mice were C57Bl/6 background. CD11c-EYFP**(Lindquist et al., 2004)** transgenic reporter mice were provided by Michel Nussenzweig (Rockefeller University), *c-fms*-EGFP transgenic mice**(Sasmono et al., 2003)** were provided by Zena Werb (UCSF). Both CD11c-EYFP and *c-fms*-EGFP mice were crossed to Actin-CFP mice**(Hadjantonakis et al., 2002)** obtained from I. Weissman (Stanford University). OTII TCR transgenic mice were obtained from Jackson labs and CD2RFP**(Veiga-Fernandes et al., 2007)** mice were a kind gift of Mark Coles (University of York).

Antibodies and Flow Cytometry

Antibodies used include CD45 APC-Cy7 (30-F11, BD), CD4 A647 (GK1.5, UCSF Hybridoma Core), MHC class II biotin (N22), CD11c PE-Cy7 (N418, eBioscience), CD11b APC (M1-70, eBioscience), CD103 (2E7, eBiosciences), Siglec-F APC (BD Pharmingen, lightning link APC conjugated, Novus Biologicals) and CD40 PE (3/23, BD). FACS was performed on an LSRII or Fortessa and analyzed using FlowJo software using standard protocols.

OVA sensitization and challenge protocol

We used the murine model of asthma based on ovalbumin and adjuvant administration(Blyth et al., 1996). In brief, endotoxin-depleted Ovalbumin (Sigma)(Aida and Pabst, 1990) (0.25 mg/ml in alum(Sigma), 5 mg/ml) in a total volume of 200 ul was injected intraperitoneally on days 0, 7, and 14. Intranasal challenge with ovalbumin (100 ug in 40 ul of PBS) or PBS alone was performed on days 21, 22, and 23.

Lung and trachea dissection and dissociation

Mice were given a lethal dose of avertin and exsanguinated from the descending aorta before lung dissection. Trachea, heart, lungs, and lymph node were removed from the chest cavity together. Lung lobes and trachea were separated and placed into dissociation medium composed of RPMI with 10% FCS, 400 units/ml collagenase D (Roche), and 0.25 mg/ml DNase I (Boehringer). Lobes and trachea were cut into small pieces with a razor blade and placed at 37° C for 30 minutes with pipetting to dissociate the tissue. Resulting cells were filtered through a 100 μm filter, separated from dead cells and debris with a histopaque (Sigma) gradient, and stained for FACS or Sorting.

Preparation of Lung Sections for live cell imaging in the lung

Lung sections were prepared for culture using methods similar to those used in studying lung smooth muscle contraction(Delmotte, 2006; Bergner and Sanderson, 2003; 2002), extending older methods of thick tissue sections(Dandurand et al., 1993). Mice were given a lethal overdose of avertin and exsanguinated by cutting the descending aorta. The lungs and trachea were exposed by cutting through the diaphragm and chest wall. The mice were intubated by tracheotomy with the sheath from an 18 gauge IV catheter. Lungs

were inflated with 1 ml of 2% low melting temp agarose (BMA) in sterile PBS maintained at 37° C and the solution was solidified by briefly rinsing the inflated lungs with PBS at 4° C. Inflated lungs were then excised from the mouse and placed in a sterile 50 ml conical containing RT RPMI without phenol red (Gibco). The left lobe was isolated, cut into approximately 300μm sections using a vibratome filled with cool PBS, mounted on plastic slides with vetbond (3M) and placed in a dish containing RT RPMI without phenol red prior to imaging.

LPS treatment of lung slices

Lung sections were prepared as listed above. A timelapse was collected before treatment. At t = 0 oxygenated media was replaced with oxygenated RPMI with 1 mg/ml LPS (Sigma). Media with LPS was continuously flowed over the section throughout the experiment. Timelapses were recorded starting at t = 10 minutes and t = 3 hours.

Real-time 2-Photon Imaging

A custom resonant-scanning 2-photon instrument(Bullen et al., 2009) contains a four-photomultiplier tube detector and collects data at video rate. Where indicated, lung sections were stained with Hoechst for 20 minutes at a concentration of 100ng/ml and then maintained at 36°C in RPMI medium bubbled with 95% O2 and 5% CO2 for up to 5 hrs. Health of lung sections was assessed by ciliary movement in large airways. Samples were excited with a 10-W MaiTai TiSaphire laser (Spectra-Physics) tuned to a wavelength of 910 nm, and emission wavelengths of 440/40 nm (for Hoechst and CFP), 505/20 nm (for GFP), 542/27nm (for YFP), and 605/70 nm (for beads) were collected. A

custom four-dimensional acquisition module in VideoSavant digital video recording software (IO Industries) was utilized for image acquisition. Each lung section was first surveyed in a raster scan spanning 1567μm x 1300μm x 175μm in xyz. For time-lapse acquisition, each xy stack spans 313μm x 260μm at a resolution of 0.653μm per pixel spaced 1μm apart for approximately 100μm in z, and 10-20 video-rate frames were averaged.

Live Lung Imaging

Mice were anesthetized with Ketamine (80 mg/kg) and Xylaxine (12 mg/kg) i.p. and placed on a custom, heated microscope stage. Mice were mechanically ventilated with pressure control ventilation. Isoflurane was continuously delivered at 1% to maintain anesthesia and mice were given an i.p. bolus of PBS (1 ml) prior to the thoracic surgical procedure. The left lung was carefully exposed. The custom thoracic suction window attached to a micromanipulator on the microscope stage was then placed into position and 20-25 mmHg of suction was applied (Amvex Corporation) to gently immobilize the lung. The two-photon microscope objective was then lowered into place over the thoracic suction window and a 12 mm coverslip.

Imaris-Based Analysis of Motility and Morphology

Images were analyzed with Imaris software using isosurface with masking and spot tracker applications. Three-dimensional images were rendered by Imaris or Metamorph software and sphericity was calculated by Imaris using the ratio of the surface area of a

sphere (with the same volume as the given particle) to the surface area of the particle. Equation shown below:

$$\Psi = \frac{\pi^{1/3}(6V_p)^{2/3}}{A_p}$$

V_p=volume of particle A_p=surface area of particle

T cell transfers

Naïve CD2-RFP OTII cells were isolated and transferred immediately. A single cell suspension was isolated from lymph nodes and spleens of CD2 RFP/OTII TCR transgenic mice. Naive CD4 T cells were purified using the EasySep CD4 negative selection kit (Stem Cell Technologies). T cells were transferred into CD11c-EYFP Actin-CFP mice via retro-orbital injection.

Statistics

Data is presented as mean ± s.e.m. *P* values were determined by performing a two-tailed *t*-test or an ANOVA as necessary using Prism 5 (Graphpad).

Tissue fixation for static microscopy

Mice were overdosed with avertin, the descending aorta was cut to drain excess blood from the chest cavity, and lungs were filled with 1 ml OCT (Tissue-Tek). The left lobe was tied off and frozen in OCT using liquid nitrogen and stored at-80 C until use. 7 mm sections were cut at -20 C using a cryostat and stained with fluorescent antibodies using TSA amplification kit (Invitrogen). Tissues were examined with a spinning disk confocal microscope (Yokogawa Instruments) and analyzed using Metamorph.

Chapter IV: Conclusion

Summary

The data presented here have introduced and validated new imaging techniques that allow immune cells to be visualized within the lung. We have elucidated the steps of antigen uptake, relocation, and presentation within the lung. Antigen uptake primarily occurs in the alveoli and not the airway, as was previously believed. Antigen bearing CD11b+ DCs and activated T cells accumulate in the airway-adjacent region in allergen challenged mice. T cells are activated through transient interactions with DCs while remaining motile. This study opens the door for future study in all of these areas and elucidates a pathway that may be targeted at several points for therapeutic intervention.

Future questions about DC uptake and trafficking

In this study we have described the standard behavior of DCs sampling the alveoli without much center of mass motility but then moving within the parenchyma of the lung in order to reach the airway-adjacent region and lymph node. Alveolar DCs were observed to send processes into the alveolus under steady-state and allergen challenge conditions. These alveolar DCs compete with AMs for antigen that has made its way into the alveolus. It may be possible to target antigen away from pro-inflammatory DCs and into a possibly tolerogenic AM pathway. Siglec-F is specifically expressed on AMs while CD11b is expressed on most of the DCs after allergen challenge. Coating antigen with targeting antibodies or affixing

them to carriers of different sizes may be a way to coopt this competition step to affect disease outcome.

Because this is the first description of DC traffic from the alveoli, the signals that drive DCs to leave their sampling posts and begin motility have not been defined. TSLP has been shown to increase the cell autonomous migration of DCs in a 3D matrix, but its affect in the tissue has not been examined (Fernandez et al., 2011). It may be that TSLP made by airway epithelial cells simultaneously activates DCs and promotes their motility toward the airway. In the trachea, TLR4 recognition has been shown to affect DC migration(Hammad et al., 2009), but LPS does not seem to have an affect on alveolar DCs over the three hour time period tested. The slice method of lung imaging offers a tractable system to study DC motility, but the loss of other chemokine gradients may affect results. One factor that may contribute to liberation from the tissue may not lead to movement of the DC from its alveolus without other signals.

Once released from the tissue, DCs from allergen challenged mice migrate toward the airway. CCL17 and CCL22 are known to attract T cells to the airway after activation, but these chemokines are produced by myeloid cells(Medoff et al., 2008). For DCs, the airway itself is a likely producer of chemoattractants. In the context of asthma, airway epithelial cells are known to produce many chemokines including CCL2, which can act through CCR2 present on monocytes and DCs(de Boer et al., 2000). After allergen challenge, the area where immune cell aggregation has been established may produce CCR7 ligands similar to the lymph node. Experiments blocking all chemokine receptor signaling with pertussis toxin

followed by specific blocking antibodies or knockout mice could identify the critical factors that recruit DCs to the airway. Arrays and cell specific deletions of the chemokines of interest can determine which cell may be targeted to prevent DC accumulation. Injection of CCR2 and CCR7 deficient DCs along with wildtype DCs would be an easy first step.

Lung tissue architecture may also contribute to DC recruitment to the airway. The parenchyma of the lung consists of thin blood vessels flanked by even thinner epithelial cells. When DCs are liberated from the alveolus, they may have few choices about directionality if the only place with space is "up". Lung lymphatics change during the course of infection(Baluk et al., 2009). It is possible that after allergen challenge lymphatics extend to the alveoli and provide a conduit for DC transport to the airways. Another possibility is that DCs accumulate near the airways and enter lymphatics there to traffic to the draining lymph node. Increased availability of tissue specific transgenics and antibody marking strategies will allow testing of these possibilities.

Future questions about T cell activation near the airway

This study shows that activated T cells are recruited to the airway-adjacent region of the lung where they participate in interactions with airway associated DCs. These interactions occur while T cells scan the DCs without arresting for an appreciable period of time. Previous studies have relied on track speed averages to define functional cognate T-APC interactions(Germain et al., 2008). The calcium imaging provided here demonstrates that T cells can participate in short lived

interactions that result in calcium flux. Previous studies have described T cell signaling without motility arrest(Friedman et al., 2010); however, this is the first description of this phenomenon in a peripheral tissue. The identification of this motile synapse raises the possibility that T cells are activated in this manner on a regular basis at effector sites. Decrease in T cell speed may imply T cell activation, but the absence of this phenomenon does not mean that T cells are not being activated.

T cell reactivation is an open field for study. Work over the past decade has focused on the activation of naïve T cells in the lymph node, but little is known about what factors trigger helper T cells to carry out their effector function at the tissue. In addition to effector cells, memory cells are present within the tissue of asthmatic patients(Medoff et al., 2008). Reactivation of these cells may be possible within the tissue, allowing for a faster adaptive response after allergen inhalation. Future studies into the behavior of tissue-resident memory T cells may demonstrate that the motile synapse is the standard mode of activation for previously activated cells.

Another factor that likely affects T cell activation within the tissue is the surrounding scrum of immune cells. Eosinophils are recruited to the lung in large numbers after allergen challenge. These cells secrete IL-4 and IL-13, which may directly affect airway-associated T cells. In addition to innate cells, the combination of T cell subsets may also affect disease outcome. Th17 cells have been documented in a mouse model of asthma that relies solely on airway instillation of antigen(Wilson et al., 2009). A subset of non-atopic patients with severe asthma have been shown to express higher levels of Th17 cytokines than mild asthmatics or

control patients (Al-Ramli et al., 2009). Because Th2 and Th17 T cells can be present in asthmatic lungs at the same time, they may compete for antigen, interact with each other, or spatially segregate to carry out different roles in disease. Tregs have been shown to interact with antigen presenting APCs to prevent Teffector activation(Tang et al., 2006). During the acute OVA/alum model, antigen specific T cells differentiate into Th2 but not Tregs (EET, unpublished observation); however, future studies with the chronic model and transfer of *in vitro* differentiated Tregs may reveal interactions that could be manipulated for therapy.

Defining the T-DC interaction zone

Tertiary lymphoid organs have been described in many inflamed tissues over the last few years(Carragher et al., 2008). In the lung, bronchus associated lymphoid tissue (BALT) has been demonstrated in several models of lung inflammation(Moyron-Quiroz et al., 2004; Fleige et al., 2011; Halle et al., 2009). The collections of T cells and DCs in the acute model of allergic asthma are not organized enough to be considered BALT, but it is tempting to speculate that they may be a precursor. Further characterization of these foci in the lung may provide a system to study lymphoid tissue inducer cells at work. It would be very interesting to tease out which cells appear first and what signals beget the cascade. IL-17 has been proposed to be an important factor in BALT formation. With the development of Th17 dependent models of asthma, the development of BALT may occur within the timeframe of an acute model of asthma.

Interactions between immune cells other than T cells and DCs have been neglected. With the generation of lymphoid tissue in the lung, there is also the possibility that B cells may also be located much closer to antigen and therefore may be able to be activated and receive help within the target organ. The larger question of whether innate immune cells play a role in skewing cells during activation or reactivation remains to be studied.

Future imaging requirements

Current imaging techniques only allow for imaging 100μm below the surface of the lung in an intact host, which is about the depth of one alveolus. The structure of the lung causes light to scatter going into and coming out of the organ. Imaging through one alveolus requires the light to pass through several layers of epithelium, four layers of endothelium, two surfactant layers, and a large air bubble. All of these materials have different refractive indexes and therefore lead to scattering. This limitation precludes the possibility of watching a DC sample antigen from an alveolus, traffic through the tissue to the airway, and present to T cells. In fact, it is currently impossible to validate any of the airway-associated observations in living mice.

There are a few possibilities to improve imaging capabilities in the lung. In order to image the airway, fiberoptic two-photon probes could be inserted into the lung through the trachea instead of imaging from the outside. The easiest place to image would be the airway branch points or carinas. While this may appear to be a disadvantage, the carinas tend to have associated aggregations of immune cells,

making them a perfect place to study immune cell interactions. Another option is to improve the depth of penetration within the lung. Adaptive optics have been used to image deep into the brain(Ji et al., 2010); however, the challenges of the lung have yet to be resolved by these methods.

Implications for asthma

This study relied almost exclusively on the acute OVA/alum model of allergic asthma. While this is a good starting point to understand the adaptive immune response to an allergen, this model has limitations. Future studies should include complex allergens and chronic asthma models. House dust mites contain a huge number of protein antigens, which would be presented in the context of the response to the whole organism. House dust mites also contain chitin, which on its own can lead to innate immune cell recruitment in the lung(Reese et al., 2007). Using the data from the OVA/alum model, it is tempting to speculate that DCs may also integrate signals from chitin recognition for activation or to skew T cells toward the Th2 phenotype. Other inhaled particulate, such as diesel exhaust, which are small enough to reach the alveoli may be inhaled with innocuous antigens and therefore prime the immune response instead of tolerizing. Chronic models of allergic asthma allow for the study of long term processes such as tissue remodeling that may involve different T cell subsets and innate immune cells.

Viral infections have long been associated with asthma exacerbations(Minor et al., 1974), and infection with RSV as an infant predisposes children to asthma(Tregoning and Schwarze, 2010). While these connections have been made epidemiologically, the changes that occur after infection or once the patient has asthma remain unclear. CD103+

DCs have been shown to be important for dealing with viral infections(Lukens et al., 2009) whereas CD11b+ DCs have been shown to be associated with asthma. As with viruses, atypical bacterial infections are associated with increased asthma exacerbations(Sutherland and Martin, 2007). In the case where both diseases occur simultaneously, which DCs and innate cells are responsible for the pathogenesis? On the other hand, would treatments that inhibit antigen presentation, cell trafficking, or T cell activation for asthma lead to increased risk of viral or bacterial infections?

Expanding paradigms to other diseases

Asthma is a disease that affects millions of people around the world, but the mechanisms of uptake and antigen presentation observed in these studies likely translate to other lung diseases and other tissues. Respiratory viruses affect the immune homeostasis in the lung. RSV is a budding virus that infects the airway epithelium. Infection of the epithelium with any virus may compromise its integrity and allow for DCs to sample across the airway more efficiently. CD103+ DCs have been shown to be important for viral clearance. The CD103+ subset instead of CD11b+ DCs may dominate the airway-adjacent region of the lung during viral infection. Another possibility is that tertiary lymphoid structures could develop elsewhere in the lung, allowing for a different pathway to antigen presentation.

The skin and gut are two other organs that must cope with constant contact with the environment. Inflammation of the gut or skin can result in lymphoid foci that could also develop into tertiary lymphoid organs. Teasing apart these antigen uptake and presentation mechanisms in the lung may provide basis for treatment of

debilitating, chronic diseases such as psoriasis and Crohn's disease. Both tissues have large pools of memory T cells and therefore may rely on a similar method of T cell reactivation for homeostasis and during disease(Sheridan and Lefrançois, 2011). In addition to understanding chronic inflammatory diseases, understanding how to manipulate adaptive immune pools present in peripheral tissues, which encounter antigens first, could improve vaccination strategies and advance treatments for infections.

References

Aida, Y., and M.J. Pabst. 1990. Removal of endotoxin from protein solutions by phase separation using Triton X-114. *J. Immunol. Methods*. 132:191–195.

Al-Ramli, W., D. Préfontaine, F. Chouiali, J.G. Martin, R. Olivenstein, C. Lemière, and Q. Hamid. 2009. T(H)17-associated cytokines (IL-17A and IL-17F) in severe asthma. *J. Allergy Clin. Immunol.* 123:1185–1187.

Amin, K. 2012. The role of mast cells in allergic inflammation. *Respir Med*. 106:9–14.

Ballesteros-Tato, A., B. León, F.E. Lund, and T.D. Randall. 2010. Temporal changes in dendritic cell subsets, cross-priming and costimulation via CD70 control CD8(+) T cell responses to influenza. *Nat. Immunol.* 11:216–224.

Baluk, P., L.-C. Yao, J. Feng, T. Romano, S.S. Jung, J.L. Schreiter, L. Yan, D.J. Shealy, and D.M. McDonald. 2009. TNF-alpha drives remodeling of blood vessels and lymphatics in sustained airway inflammation in mice. *J. Clin. Invest.* 119:2954–2964.

Bang, B.R., E. Chun, E.J. Shim, H.S. Lee, S.Y. Lee, S.H. Cho, K.U. Min, Y.Y. Kim, and H.W. Park. 2011. Alveolar macrophages modulate allergic inflammation in a murine model of asthma. *Exp. Mol. Med.* 43:275–280.

Barnes, P.J. 2008. The cytokine network in asthma and chronic obstructive pulmonary disease. *J. Clin. Invest.* 118:3546–3556.

Barretto, R.P.J., B. Messerschmidt, and M.J. Schnitzer. 2009. In vivo fluorescence imaging with high-resolution microlenses. *Nat. Methods*. 6:511–512.

Beaty, S.R., C.E. Rose, and S.-S.J. Sung. 2007. Diverse and potent chemokine production by lung CD11bhigh dendritic cells in homeostasis and in allergic lung inflammation. *J. Immunol.* 178:1882–1895.

Belz, G.T., C.M. Smith, L. Kleinert, P. Reading, A. Brooks, K. Shortman, F.R. Carbone, and W.R. Heath. 2004. Distinct migrating and nonmigrating dendritic cell populations are involved in MHC class I-restricted antigen presentation after lung infection with virus. *Proc. Natl. Acad. Sci. U.S.A.* 101:8670–8675.

Bergner, A., and M.J. Sanderson. 2002. Acetylcholine-induced calcium signaling and contraction of airway smooth muscle cells in lung slices. *J. Gen. Physiol.* 119:187–198.

Bergner, A., and M.J. Sanderson. 2003. Airway contractility and smooth muscle Ca(2+) signaling in lung slices from different mouse strains. *J. Appl. Physiol.* 95:1325–32; discussion 1314.

Bhakta, N.R., and P.G. Woodruff. 2011. Human asthma phenotypes: from the clinic, to cytokines, and back again. *Immunol. Rev.* 242:220–232.

Bhattacharya, J., and N.C. Staub. 1980. Direct measurement of microvascular pressures in the isolated perfused dog lung. *Science*. 210:327–328.

Blank, F., B. Rothen-Rutishauser, and P. Gehr. 2007. Dendritic Cells and Macrophages Form a Transepithelial Network against Foreign Particulate Antigens. *American Journal of Respiratory Cell and Molecular Biology*. 36:669.

Blyth, D., M. Pedrick, T. Savage, E. Hessel, and D. Fattah. 1996. Lung inflammation and

epithelial changes in a murine model of atopic asthma. *American Journal of Respiratory Cell and Molecular Biology*. 14:425.

Boyce, J.A., and K.F. Austen. 2005. No audible wheezing: nuggets and conundrums from mouse asthma models. *J. Exp. Med.* 201:1869–1873.

Broug-Holub, E., G.B. Toews, J.F. van Iwaarden, R.M. Strieter, S.L. Kunkel, R. Paine, and T.J. Standiford. 1997. Alveolar macrophages are required for protective pulmonary defenses in murine Klebsiella pneumonia: elimination of alveolar macrophages increases neutrophil recruitment but decreases bacterial clearance and survival. *Infect. Immun.* 65:1139–1146.

Bullen, A., R.S. Friedman, and M.F. Krummel. 2009. Two-photon imaging of the immune system: a custom technology platform for high-speed, multicolor tissue imaging of immune responses. *Curr. Top. Microbiol. Immunol.* 334:1–29.

Burns, A.R., C.W. Smith, and D.C. Walker. 2003. Unique structural features that influence neutrophil emigration into the lung. *Physiol. Rev.* 83:309–336.

Byersdorfer, C.A., and D.D. Chaplin. 2001. Visualization of early APC/T cell interactions in the mouse lung following intranasal challenge. *J. Immunol.* 167:6756–6764.

Cahalan, M.D., and I. Parker. 2008. Choreography of cell motility and interaction dynamics imaged by two-photon microscopy in lymphoid organs. *Annu. Rev. Immunol.* 26:585–626.

Carragher, D.M., J. Rangel-Moreno, and T.D. Randall. 2008. Ectopic lymphoid tissues and local immunity. *Semin. Immunol.* 20:26–42.

Carvalho, T.C., J.I. Peters, and R.O. Williams. 2011. Influence of particle size on regional lung deposition--what evidence is there? *Int J Pharm*. 406:1–10.

Chapman, T.J., K. Lambert, and D.J. Topham. 2011. Rapid reactivation of extralymphoid CD4 T cells during secondary infection. *PLoS ONE*. 6:e20493.

Chieppa, M., M. Rescigno, A.Y.C. Huang, and R.N. Germain. 2006. Dynamic imaging of dendritic cell extension into the small bowel lumen in response to epithelial cell TLR engagement. *J. Exp. Med.* 203:2841–2852.

Corry, D.B., G. Grünig, H. Hadeiba, V.P. Kurup, M.L. Warnock, D. Sheppard, D.M. Rennick, and R.M. Locksley. 1998. Requirements for allergen-induced airway hyperreactivity in T and B cell-deficient mice. *Mol. Med.* 4:344–355.

Cowburn, A.S., A.M. Condliffe, N. Farahi, C. Summers, and E.R. Chilvers. 2008. Advances in neutrophil biology: clinical implications. *Chest*. 134:606–612.

Dandurand, R.J., C.G. Wang, N.C. Phillips, and D.H. Eidelman. 1993. Responsiveness of individual airways to methacholine in adult rat lung explants. *J. Appl. Physiol.* 75:364–372.

de Boer, W.I., J.K. Sont, A. van Schadewijk, J. Stolk, J.H. van Krieken, and P.S. Hiemstra. 2000. Monocyte chemoattractant protein 1, interleukin 8, and chronic airways inflammation in COPD. *J. Pathol.* 190:619–626.

Delmotte, P. 2006. Ciliary Beat Frequency Is Maintained at a Maximal Rate in the Small Airways of Mouse Lung Slices. *American Journal of Respiratory Cell and Molecular Biology*. 35:110–117.

Desch, A.N., G.J. Randolph, K. Murphy, E.L. Gautier, R.M. Kedl, M.H. Lahoud, I. Caminschi, K. Shortman, P.M. Henson, and C.V. Jakubzick. 2011. CD103+ pulmonary dendritic cells preferentially acquire and present apoptotic cell-associated antigen. *Journal of Experimental Medicine*. 208:1789–1797.

Elliot, J.G., C.M. Jensen, S. Mutavdzic, J.P. Lamb, N.G. Carroll, and A.L. James. 2004. Aggregations of lymphoid cells in the airways of nonsmokers, smokers, and subjects with asthma. *Am. J. Respir. Crit. Care Med.* 169:712–718.

Faust, N., F. Varas, L.M. Kelly, S. Heck, and T. Graf. 2000. Insertion of enhanced green fluorescent protein into the lysozyme gene creates mice with green fluorescent granulocytes and macrophages. *Blood*. 96:719–726.

Fernandez, M.-I., M.L. Heuzé, C. Martinez-Cingolani, E. Volpe, M.-H. Donnadieu, M. Piel, B. Homey, A.-M. Lennon-Duménil, and V. Soumelis. 2011. The human cytokine TSLP triggers a cell-autonomous dendritic cell migration in confined environments. *Blood*. 118:3862–3869.

Fleige, H., J.D. Haas, F.R. Stahl, S. Willenzon, I. Prinz, and R. Förster. 2011. Induction of BALT in the absence of IL-17. *Nat. Immunol.* 13:1.

Friedman, R.S., P. Beemiller, C.M. Sorensen, J. Jacobelli, and M.F. Krummel. 2010. Real-time analysis of T cell receptors in naive cells in vitro and in vivo reveals flexibility

in synapse and signaling dynamics. *Journal of Experimental Medicine*. 207:2733–2749.

Garnier, von, C., L. Filgueira, M. Wikstrom, M. Smith, J.A. Thomas, D.H. Strickland, P.G. Holt, and P.A. Stumbles. 2005. Anatomical location determines the distribution and function of dendritic cells and other APCs in the respiratory tract. *J. Immunol.* 175:1609–1618.

Gebb, S.A., J.A. Graham, C.C. Hanger, P.S. Godbey, R.L. Capen, C.M. Doerschuk, and W.W. Wagner. 1995. Sites of leukocyte sequestration in the pulmonary microcirculation. *J. Appl. Physiol.* 79:493–497.

Germain, R.N., M. Bajénoff, F. Castellino, M. Chieppa, J.G. Egen, A.Y.C. Huang, M. Ishii, L.Y. Koo, and H. Qi. 2008. Making friends in out-of-the-way places: how cells of the immune system get together and how they conduct their business as revealed by intravital imaging. *Immunol. Rev.* 221:163–181.

Germain, R.N., M.J. Miller, M.L. Dustin, and M.C. Nussenzweig. 2006. Dynamic imaging of the immune system: progress, pitfalls and promise. *Nat. Rev. Immunol.* 6:497–507.

Gordon, S. 2003. Alternative activation of macrophages. *Nat. Rev. Immunol.*

Grayson, M.H., M.S. Ramos, M.M. Rohlfing, R. Kitchens, H.D. Wang, A. Gould, E. Agapov, and M.J. Holtzman. 2007. Controls for lung dendritic cell maturation and migration during respiratory viral infection. *J. Immunol.* 179:1438–1448.

Hadjantonakis, A.-K., S. Macmaster, and A. Nagy. 2002. Embryonic stem cells and mice

expressing different GFP variants for multiple non-invasive reporter usage within a single animal. *BMC Biotechnol.* 2:11.

Halle, S., H.C. Dujardin, N. Bakocevic, H. Fleige, H. Danzer, S. Willenzon, Y. Suezer, G. Hammerling, N. Garbi, G. Sutter, T. Worbs, and R. Forster. 2009. Induced bronchus-associated lymphoid tissue serves as a general priming site for T cells and is maintained by dendritic cells. *Journal of Experimental Medicine*. 206:2593–2601.

Hamilton-Easton, A., and M. Eichelberger. 1995. Virus-specific antigen presentation by different subsets of cells from lung and mediastinal lymph node tissues of influenza virus-infected mice. *J. Virol.* 69:6359–6366.

Hammad, H., and B.N. Lambrecht. 2007. Lung dendritic cell migration. *Adv. Immunol.* 93:265–278.

Hammad, H., and B.N. Lambrecht. 2008. Dendritic cells and epithelial cells: linking innate and adaptive immunity in asthma. *Nat. Rev. Immunol.* 8:193–204.

Hammad, H., M. Chieppa, F. Perros, M.A. Willart, R.N. Germain, and B.N. Lambrecht. 2009. House dust mite allergen induces asthma via Toll-like receptor 4 triggering of airway structural cells. *Nat. Med.* 15:410–416.

Hammad, H., M. Plantinga, K. Deswarte, P. Pouliot, M.A.M. Willart, M. Kool, F. Muskens, and B.N. Lambrecht. 2010. Inflammatory dendritic cells--not basophils--are necessary and sufficient for induction of Th2 immunity to inhaled house dust mite allergen. *Journal of Experimental Medicine*. 207:2097–2111.

Hasegawa, A., K. Hayashi, H. Kishimoto, M. Yang, S. Tofukuji, K. Suzuki, H. Nakajima, R.M. Hoffman, M. Shirai, and T. Nakayama. 2010. Color-coded real-time cellular imaging of lung T-lymphocyte accumulation and focus formation in a mouse asthma model. *J. Allergy Clin. Immunol.* 125:461–468.e6.

Hoffman, A.M., A. Shifren, M.R. Mazan, A.M. Gruntman, K.M. Lascola, R.D. Nolen-Walston, C.F. Kim, L. Tsai, R.A. Pierce, R.P. Mecham, and E.P. Ingenito. 2010. Matrix modulation of compensatory lung regrowth and progenitor cell proliferation in mice. *Am. J. Physiol. Lung Cell Mol. Physiol.* 298:L158–68.

Holt, P.G. 2005. Pulmonary dendritic cells in local immunity to inert and pathogenic antigens in the respiratory tract. *Proc Am Thorac Soc*. 2:116–120.

Huh, J., D. Strickland, and F. Jahnsen. 2003. Bidirectional Interactions between Antigen-bearing Respiratory Tract Dendritic Cells (DCs) and T Cells Precede the Late Phase Reaction in Experimental Asthma. *... of experimental ...*.

Jackson, D.J., A. Sykes, P. Mallia, and S.L. Johnston. 2011. Asthma exacerbations: origin, effect, and prevention. *J. Allergy Clin. Immunol.* 128:1165–1174.

Jahnsen, F.L., D.H. Strickland, J.A. Thomas, I.T. Tobagus, S. Napoli, G.R. Zosky, D.J. Turner, P.D. Sly, P.A. Stumbles, and P.G. Holt. 2006. Accelerated antigen sampling and transport by airway mucosal dendritic cells following inhalation of a bacterial stimulus. *J. Immunol.* 177:5861–5867.

Jakubzick, C., F. Tacke, J. Llodra, N. van Rooijen, and G.J. Randolph. 2006. Modulation of dendritic cell trafficking to and from the airways. *J. Immunol.* 176:3578–3584.

Jakubzick, C., J. Helft, T.J. Kaplan, and G.J. Randolph. 2008a. Optimization of methods to study pulmonary dendritic cell migration reveals distinct capacities of DC subsets to acquire soluble versus particulate antigen. *J. Immunol. Methods*. 337:121–131.

Jakubzick, C., M. Bogunovic, A.J. Bonito, E.L. Kuan, M. Merad, and G.J. Randolph. 2008b. Lymph-migrating, tissue-derived dendritic cells are minor constituents within steady-state lymph nodes. *Journal of Experimental Medicine*. 205:2839–2850.

Jarman, E.R., K.A.L. Tan, and J.R. Lamb. 2005. Transgenic mice expressing the T cell antigen receptor specific for an immunodominant epitope of a major allergen of house dust mite develop an asthmatic phenotype on exposure of the airways to allergen. *Clin. Exp. Allergy*. 35:960–969.

Ji, N., D.E. Milkie, and E. Betzig. 2010. Adaptive optics via pupil segmentation for high-resolution imaging in biological tissues. *Nat. Methods*. 7:141–147.

Kiefmann, R., J.M. Rifkind, E. Nagababu, and J. Bhattacharya. 2008. Red blood cells induce hypoxic lung inflammation. *Blood*. 111:5205–5214.

Kraft, M., G.H. Cassell, J.E. Henson, H. Watson, J. Williamson, B.P. Marmion, C.A. Gaydos, and R.J. Martin. 1998. Detection of Mycoplasma pneumoniae in the airways of adults with chronic asthma. *Am. J. Respir. Crit. Care Med.* 158:998–1001.

Kreisel, D., R.G. Nava, W. Li, B.H. Zinselmeyer, B. Wang, J. Lai, R. Pless, A.E. Gelman, A.S. Krupnick, and M.J. Miller. 2010. In vivo two-photon imaging reveals monocyte-dependent neutrophil extravasation during pulmonary inflammation. *Proc. Natl. Acad. Sci. U.S.A.* 107:18073–18078.

Kuebler, W.M., X. Ying, B. Singh, A.C. Issekutz, and J. Bhattacharya. 1999. Pressure is proinflammatory in lung venular capillaries. *J. Clin. Invest.* 104:495–502.

Lambrecht, B.N., and H. Hammad. 2009. Biology of lung dendritic cells at the origin of asthma. *Immunity*. 31:412–424.

Lambrecht, B.N., B. Salomon, D. Klatzmann, and R.A. Pauwels. 1998. Dendritic cells are required for the development of chronic eosinophilic airway inflammation in response to inhaled antigen in sensitized mice. *J. Immunol.* 160:4090–4097.

Lamm, W.J.E., S.L. Bernard, W.W. Wagner, and R.W. Glenny. 2005. Intravital microscopic observations of 15-microm microspheres lodging in the pulmonary microcirculation. *J. Appl. Physiol.* 98:2242–2248.

Lindquist, R.L., G. Shakhar, D. Dudziak, H. Wardemann, T. Eisenreich, M.L. Dustin, and M.C. Nussenzweig. 2004. Visualizing dendritic cell networks in vivo. *Nat. Immunol.* 5:1243–1250.

Looney, M.R., E.E. Thornton, D. Sen, W.J. Lamm, R.W. Glenny, and M.F. Krummel. 2011. Stabilized imaging of immune surveillance in the mouse lung. *Nat. Methods*. 8:91–96.

Looney, M.R., X. Su, J.A. Van Ziffle, C.A. Lowell, and M.A. Matthay. 2006. Neutrophils and their Fc gamma receptors are essential in a mouse model of transfusion-related acute lung injury. *J. Clin. Invest.* 116:1615–1623.

Lukens, M.V., D. Kruijsen, F.E.J. Coenjaerts, J.L.L. Kimpen, and G.M. van Bleek. 2009.

Respiratory syncytial virus-induced activation and migration of respiratory dendritic cells and subsequent antigen presentation in the lung-draining lymph node. *J. Virol.* 83:7235–7243.

Martin, R.J., M. Kraft, H.W. Chu, E.A. Berns, and G.H. Cassell. 2001. A link between chronic asthma and chronic infection. *J. Allergy Clin. Immunol.* 107:595–601.

Martin, T.R., and C.W. Frevert. 2005. Innate Immunity in the Lungs. *Proc Am Thorac Soc*. 2:403.

Masoli, M., D. Fabian, S. Holt, R. Beasley, Global Initiative for Asthma (GINA) Program. 2004. The global burden of asthma: executive summary of the GINA Dissemination Committee report. *Allergy*. 59:469–478.

McWilliam, A.S., S. Napoli, A.M. Marsh, F.L. Pemper, D.J. Nelson, C.L. Pimm, P.A. Stumbles, T.N. Wells, and P.G. Holt. 1996. Dendritic cells are recruited into the airway epithelium during the inflammatory response to a broad spectrum of stimuli. *J. Exp. Med.* 184:2429–2432.

Medoff, B.D., E. Seung, S. Hong, S.Y. Thomas, B.P. Sandall, J.S. Duffield, D.A. Kuperman, D.J. Erle, and A.D. Luster. 2009. CD11b+ myeloid cells are the key mediators of Th2 cell homing into the airway in allergic inflammation. *J. Immunol.* 182:623–635.

Medoff, B.D., S.Y. Thomas, and A.D. Luster. 2008. T cell trafficking in allergic asthma: the ins and outs. *Annu. Rev. Immunol.* 26:205–232.

Mikhak, Z., M. Fukui, A. Farsidjani, B.D. Medoff, A.M. Tager, and A.D. Luster. 2009. Contribution of CCR4 and CCR8 to antigen-specific T(H)2 cell trafficking in allergic pulmonary inflammation. *J. Allergy Clin. Immunol.* 123:67–73.e3.

Miller, M.J., S.H. Wei, I. Parker, and M.D. Cahalan. 2002. Two-photon imaging of lymphocyte motility and antigen response in intact lymph node. *Science*. 296:1869–1873.

Miller, M.J., S.H. Wei, M.D. Cahalan, and I. Parker. 2003. Autonomous T cell trafficking examined in vivo with intravital two-photon microscopy. *Proc. Natl. Acad. Sci. U.S.A.* 100:2604–2609.

Minor, T.E., E.C. Dick, A.N. DeMeo, J.J. Ouellette, M. Cohen, and C.E. Reed. 1974. Viruses as precipitants of asthmatic attacks in children. *JAMA*. 227:292–298.

Moyron-Quiroz, J.E., J. Rangel-Moreno, K. Kusser, L. Hartson, F. Sprague, S. Goodrich, D.L. Woodland, F.E. Lund, and T.D. Randall. 2004. Role of inducible bronchus associated lymphoid tissue (iBALT) in respiratory immunity. *Nat. Med.* 10:927–934.

Nakano, H., M.E. Free, G.S. Whitehead, S. Maruoka, R.H. Wilson, K. Nakano, and D.N. Cook. 2012. Pulmonary CD103(+) dendritic cells prime Th2 responses to inhaled allergens. *Mucosal Immunol*. 5:53–65.

Nguyen, Q.T., N. Callamaras, C. Hsieh, and I. Parker. 2001. Construction of a two-photon microscope for video-rate Ca(2+) imaging. *Cell Calcium*. 30:383–393.

Nials, A.T., and S. Uddin. 2008. Mouse models of allergic asthma: acute and chronic allergen challenge. *Dis Model Mech*. 1:213–220.

Oba, Y., and G.A. Salzman. 2000. Ventilation with lower tidal volumes as compared with traditional tidal volumes for acute lung injury. *N. Engl. J. Med.* 343:813; author reply 813–4.

Pedroza-González, A., G.S. García-Romo, D. Aguilar-León, J. Calderon-Amador, R. Hurtado-Ortiz, H. Orozco-Estevez, B.N. Lambrecht, I. Estrada-García, R. Hernández-Pando, and L. Flores-Romo. 2004. In situ analysis of lung antigen-presenting cells during murine pulmonary infection with virulent Mycobacterium tuberculosis. *Int J Exp Pathol*. 85:135–145.

Perrigoue, J.G., S.A. Saenz, M.C. Siracusa, E.J. Allenspach, B.C. Taylor, P.R. Giacomin, M.G. Nair, Y. Du, C. Zaph, N. van Rooijen, M.R. Comeau, E.J. Pearce, T.M. Laufer, and D. Artis. 2009. MHC class II-dependent basophil-CD4+ T cell interactions promote T(H)2 cytokine-dependent immunity. *Nat. Immunol.* 10:697–705.

Podsypanina, K., Y.-C.N. Du, M. Jechlinger, L.J. Beverly, D. Hambardzumyan, and H. Varmus. 2008. Seeding and propagation of untransformed mouse mammary cells in the lung. *Science*. 321:1841–1844.

Popel, A.S., and P.C. Johnson. 2005. Microcirculation and Hemorheology. *Annu Rev Fluid Mech*. 37:43–69.

Presson, R.G., W.A. Baumgartner, A.J. Peterson, R.W. Glenny, and W.W. Wagner. 2002. Pulmonary capillaries are recruited during pulsatile flow. *J. Appl. Physiol.* 92:1183–1190.

Proceedings of the ATS workshop on refractory asthma: current understanding, recommendations, and unanswered questions. American Thoracic Society. 2000.

Proceedings of the ATS workshop on refractory asthma: current understanding, recommendations, and unanswered questions. American Thoracic Society. *In* American journal of respiratory and critical care medicine. 2341–2351.

Randolph, G.J., J. Ochando, and S. Partida-Sánchez. 2008. Migration of dendritic cell subsets and their precursors. *Annu. Rev. Immunol.* 26:293–316.

Rangel-Moreno, J., D.M. Carragher, M. de la Luz Garcia-Hernandez, J.Y. Hwang, K. Kusser, L. Hartson, J.K. Kolls, S.A. Khader, and T.D. Randall. 2011. The development of inducible bronchus-associated lymphoid tissue depends on IL-17. *Nat. Immunol.* 12:639–646.

Reese, T.A., H.-E. Liang, A.M. Tager, A.D. Luster, N. van Rooijen, D. Voehringer, and R.M. Locksley. 2007. Chitin induces accumulation in tissue of innate immune cells associated with allergy. *Nature*. 447:92–96.

Rescigno, M., M. Urbano, B. Valzasina, M. Francolini, G. Rotta, R. Bonasio, F. Granucci, J.P. Kraehenbuhl, and P. Ricciardi-Castagnoli. 2001. Dendritic cells express tight junction proteins and penetrate gut epithelial monolayers to sample bacteria. *Nat. Immunol.* 2:361–367.

Robertson, D.G., A.T. Kerigan, F.E. Hargreave, R. Chalmers, and J. Dolovich. 1974. Late asthmatic responses induced by ragweed pollen allergen. *J. Allergy Clin. Immunol.* 54:244–254.

Robinson, D.S., Q. Hamid, S. Ying, A. Tsicopoulos, J. Barkans, A.M. Bentley, C. Corrigan, S.R. Durham, and A.B. Kay. 1992. Predominant TH2-like bronchoalveolar T-

lymphocyte population in atopic asthma. *N. Engl. J. Med.* 326:298–304.

Sasmono, R.T., D. Oceandy, J.W. Pollard, W. Tong, P. Pavli, B.J. Wainwright, M.C. Ostrowski, S.R. Himes, and D.A. Hume. 2003. A macrophage colony-stimulating factor receptor-green fluorescent protein transgene is expressed throughout the mononuclear phagocyte system of the mouse. *Blood*. 101:1155–1163.

Sen, D., L. Forrest, T.B. Kepler, I. Parker, and M.D. Cahalan. 2010. Selective and site-specific mobilization of dermal dendritic cells and Langerhans cells by Th1- and Th2-polarizing adjuvants. *Proc. Natl. Acad. Sci. U.S.A.* 107:8334–8339.

Sheridan, B.S., and L. Lefrançois. 2011. Regional and mucosal memory T cells. *Nat. Immunol.* 12:485–491.

Short, A.C., M.L. Montoya, S.A. Gebb, R.G. Presson, W.W. Wagner, and R.L. Capen. 1996. Pulmonary capillary diameters and recruitment characteristics in subpleural and interior networks. *J. Appl. Physiol.* 80:1568–1573.

Sokol, C.L., N.-Q. Chu, S. Yu, S.A. Nish, T.M. Laufer, and R. Medzhitov. 2009. Basophils function as antigen-presenting cells for an allergen-induced T helper type 2 response. *Nat. Immunol.* 10:713–720.

Soumelis, V., P.A. Reche, H. Kanzler, W. Yuan, G. Edward, B. Homey, M. Gilliet, S. Ho, S. Antonenko, A. Lauerma, K. Smith, D. Gorman, S. Zurawski, J. Abrams, S. Menon, T. McClanahan, R. de Waal-Malefyt Rd, F. Bazan, R.A. Kastelein, and Y.-J. Liu. 2002. Human epithelial cells trigger dendritic cell mediated allergic inflammation by producing TSLP. *Nat. Immunol.* 3:673–680.

Sullivan, B.M., H.-E. Liang, J.K. Bando, D. Wu, L.E. Cheng, J.K. McKerrow, C.D.C. Allen, and R.M. Locksley. 2011a. Genetic analysis of basophil function in vivo. *Nat. Immunol.* 12:527–535.

Sullivan, P.W., V.H. Ghushchyan, J.F. Slejko, V. Belozeroff, D.R. Globe, and S.-L. Lin. 2011b. The burden of adult asthma in the United States: evidence from the Medical Expenditure Panel Survey. *J. Allergy Clin. Immunol.* 127:363–369.e1–3.

Sung, S.-S.J., S.M. Fu, C.E. Rose, F. Gaskin, S.-T. Ju, and S.R. Beaty. 2006. A major lung CD103 (alphaE)-beta7 integrin-positive epithelial dendritic cell population expressing Langerin and tight junction proteins. *J. Immunol.* 176:2161–2172.

Sutherland, E.R., and R.J. Martin. 2007. Asthma and atypical bacterial infection. *Chest*. 132:1962–1966.

Tabuchi, A., M. Mertens, H. Kuppe, A.R. Pries, and W.M. Kuebler. 2008. Intravital microscopy of the murine pulmonary microcirculation. *J. Appl. Physiol.* 104:338–346.

Takano, K.-I., T. Kojima, M. Go, M. Murata, S. Ichimiya, T. Himi, and N. Sawada. 2005. HLA-DR- and CD11c-positive dendritic cells penetrate beyond well-developed epithelial tight junctions in human nasal mucosa of allergic rhinitis. *J. Histochem. Cytochem.* 53:611–619.

Tan, W.C. 2005. Viruses in asthma exacerbations. *Current Opinion in Pulmonary Medicine*. 11:21.

Tang, Q., J.Y. Adams, A.J. Tooley, M. Bi, B.T. Fife, P. Serra, P. Santamaria, R.M.

Locksley, M.F. Krummel, and J.A. Bluestone. 2006. Visualizing regulatory T cell control of autoimmune responses in nonobese diabetic mice. *Nat. Immunol.* 7:83–92.

Tregoning, J.S., and J. Schwarze. 2010. Respiratory viral infections in infants: causes, clinical symptoms, virology, and immunology. *Clin. Microbiol. Rev.* 23:74–98.

van Rijt, L.S. 2002. Allergen-induced accumulation of airway dendritic cells is supported by an increase in CD31hiLy-6Cneg bone marrow precursors in a mouse model of asthma. *Blood*. 100:3663–3671.

van Rijt, L.S., S. Jung, A. Kleinjan, N. Vos, M. Willart, C. Duez, H.C. Hoogsteden, and B.N. Lambrecht. 2005. In vivo depletion of lung CD11c+ dendritic cells during allergen challenge abrogates the characteristic features of asthma. *J. Exp. Med.* 201:981–991.

Veiga-Fernandes, H., M.C. Coles, K.E. Foster, A. Patel, A. Williams, D. Natarajan, A. Barlow, V. Pachnis, and D. Kioussis. 2007. Tyrosine kinase receptor RET is a key regulator of Peyer's Patch organogenesis. *Nature*. 446:547–551.

Vermaelen, K.Y., I. Carro-Muino, B.N. Lambrecht, and R.A. Pauwels. 2001. Specific migratory dendritic cells rapidly transport antigen from the airways to the thoracic lymph nodes. *J. Exp. Med.* 193:51–60.

Voehringer, D. 2011. Basophils in allergic immune responses. *Curr. Opin. Immunol.* 23:789–793.

Voehringer, D., T.A. Reese, X. Huang, K. Shinkai, and R.M. Locksley. 2006. Type 2 immunity is controlled by IL-4/IL-13 expression in hematopoietic non-eosinophil cells of

the innate immune system. *J. Exp. Med.* 203:1435–1446.

Wagner, W.W. 1969. Pulmonary microcirculatory observations in vivo under physiological conditions. *J. Appl. Physiol.* 26:375–377.

Waisman, D., A. Abramovich, V. Brod, O. Lavon, S. Nurkin, F. Popovski, A. Rotschild, and H. Bitterman. 2006. Subpleural microvascular flow velocities and shear rates in normal and septic mechanically ventilated rats. *Shock*. 26:87–94.

Wenzel, S., D. Wilbraham, R. Fuller, E.B. Getz, and M. Longphre. 2007. Effect of an interleukin-4 variant on late phase asthmatic response to allergen challenge in asthmatic patients: results of two phase 2a studies. *Lancet*. 370:1422–1431.

Wiggs, B.R., D. English, W.M. Quinlan, N.A. Doyle, J.C. Hogg, and C.M. Doerschuk. 1994. Contributions of capillary pathway size and neutrophil deformability to neutrophil transit through rabbit lungs. *J. Appl. Physiol.* 77:463–470.

Wikstrom, M.E., and P.A. Stumbles. 2007. Mouse respiratory tract dendritic cell subsets and the immunological fate of inhaled antigens. *Immunol. Cell Biol.* 85:182–188.

Wilson, R.H., G.S. Whitehead, H. Nakano, M.E. Free, J.K. Kolls, and D.N. Cook. 2009. Allergic sensitization through the airway primes Th17-dependent neutrophilia and airway hyperresponsiveness. *Am. J. Respir. Crit. Care Med.* 180:720–730.

Woodruff, P.G., B. Modrek, D.F. Choy, G. Jia, A.R. Abbas, A. Ellwanger, L.L. Koth, J.R. Arron, and J.V. Fahy. 2009. T-helper type 2-driven inflammation defines major subphenotypes of asthma. *Am. J. Respir. Crit. Care Med.* 180:388–395.

Xia, W., C.E. Pinto, and R.L. Kradin. 1995. The antigen-presenting activities of Ia+ dendritic cells shift dynamically from lung to lymph node after an airway challenge with soluble antigen. *J. Exp. Med.* 181:1275–1283.

Yoshimoto, T., K. Yasuda, H. Tanaka, M. Nakahira, Y. Imai, Y. Fujimori, and K. Nakanishi. 2009. Basophils contribute to T(H)2-IgE responses in vivo via IL-4 production and presentation of peptide-MHC class II complexes to CD4+ T cells. *Nat. Immunol.* 10:706–712.

Zarbock, A., and K. Ley. 2009. New insights into leukocyte recruitment by intravital microscopy. *Curr. Top. Microbiol. Immunol.* 334:129–152.

Publishing Agreement

It is the policy of the University to encourage the distribution of all theses, dissertations, and manuscripts. Copies of all UCSF theses, dissertations, and manuscripts will be routed to the library via the Graduate Division. The library will make all theses, dissertations, and manuscripts accessible to the public and will preserve these to the best of their abilities, in perpetuity.

I hereby grant permission to the Graduate Division of the University of California, San Francisco to release copies of my thesis, dissertation, or manuscript to the Campus Library to provide access and preservation, in whole or in part, in perpetuity.

Emily E Thornton — Author Signature

3/22/2012 — Date